An Adaptive Protocol for Use Over Meteor Scatter Channels

by

Michael Dwight Spann

DECEMBER 1987

Submitted in partial fulfillment of the requirements for the degree of Doctor of Philosophy in the Department of Electronic Engineering, University of Natal

An Adaptive Protocol for Use Over Meteor Scatter Channels

by

Michael Spann

Abstract

Modern technology has revived interest in the once popular area of meteor scatter communications. Meteor scatter systems offer reliable communications in the 500 to 2000 km range all day, every day. Recent advances in microprocessor technology have made meteor scatter communications a viable and cost effective method of providing modest data rate communications. A return to the basic fundamentals has revealed characteristics of meteor scatter propagation that can be used to optimize the protocols for a meteor scatter link.

The duration of an underdense trail is bounded when its initial amplitude is known. The upper bound of the duration is determined by maximizing the classical underdense model. The lower bound is determined by considering the volume of sky utilized. The duration distribution between these bounds is computed and compared to measured values.

The duration distribution is then used to specify a fixed data rate, frame adaptive protocol which more efficaciously utilizes underdense trails, in the half duplex environment, than a non-adaptive protocol. The performance of these protocols is verified by modeling.

Preface

The authors involvement in meteor scatter communications began in 1985 when he joined the meteor scatter project at the University of Natal. Designing efficient data communication protocols for use over a novel channel seemed an interesting topic for a person whose background was in computer science. After becoming familiar with the field, much time was spent developing specialized measurement equipment to verify the theoretical predictions. This work culminated in August 1987 when a set of experiments were conducted between Pretoria and Arniston which provided the measured data used in this thesis. With this, and subsequently gathered data as supporting evidence, the author is proud to present this dissertation.

This thesis will show that the usable duration of a meteor reflection can be predicted when the initial amplitude is known. After the relation between initial amplitude, time constant and usable duration is presented, a theoretical model is developed for determining the time constant distribution of a meteor scatter link. An experimental link was established to verify the time constant distribution and a measurement system constructed. The predicted time constant distribution is compared to the measured distribution and conclusions are presented.

Knowing the expected duration of a trail can be used to adapt a block adaptive protocol to achieve more throughput with better efficiency than a non-adaptive protocol. A throughput model will be developed to demonstrate the improvements achievable by a block adaptive protocol. These models can be applied to predicted or measured distributions.

This entire thesis, unless specifically indicated to the contrary, represents the authors own original work.

Acknowledgments

This thesis is dedicated to Angela, my wife, for her support during trying times, and my mother and father for teaching me the importance of an education.

The author gratefully acknowledges the assistance of Salbu (PTY) Ltd and especially D.V. Larsen for their contributions towards the experimental phase of this work. The author would also like to thank Professor A.D. Broadhurst for his caring supervision and assistance in the preparation of this thesis. Special thanks go to J.D. Larsen and R.S. Mawrey for their valuable assistance in developing the measurement system and performing the experimental work.

Table of Contents

List of Figures

List of Tables

Chapter 1

Introduction

Modern technology has revived interest in the once popular subject of meteor scatter communications. Meteor scatter systems, which transmit data at VHF frequencies using ionized meteor trails in the earths upper atmosphere, offer reliable communications in the 500 to 2000 km range all day, every day. Recent advances in microprocessor technology have made meteor scatter communications a viable and cost effective method of providing modest data rate communications [Day, 1982]. A return to the basic fundamentals has revealed characteristics of meteor scatter propagation that can be used to optimize the protocols for a meteor scatter link.

During the late 1970's and early 1980's, microprocessor technology blossomed thus opening avenues of research previously blocked by slow and expensive data gathering techniques. Along with the microprocessor development, storage costs using semiconductor memories plummeted. These two factors combined to make meteor scatter communications not only a viable method of communications, but also a cost effective method [Bokhari *et al*, 1975].

Improved protocols are needed to make use of the meteor scatter medium now that the technology exists to implement more efficient meteor scatter systems. The development of such a protocol requires a knowledge of digital communications as well as a knowledge of meteor scatter propagation. A study of the fundamentals of meteor scatter propagation reveals that underdense trails are more common than overdense trails, however overdense trails are capable of providing the majority of the throughput [Weitzen, 1983]. If the objective of the system is to maximize throughput, the system must be designed to use overdense trails efficiently. The system must make optimum use of underdense trails when rapid delivery of short messages is required and the volume of information to be transmitted is relatively small in comparison to the maximum capacity of the meteor scatter channel.

It is convenient to specify a typical system configuration in order to evaluate the properties of a particular type of link. One possible system configuration using meteor scatter links is shown in figure 1-1 and consists of a high power, full duplex master

station in a central location connected to the public carrier network. This high power, full duplex master station would be able to forward telex, digital facsimile and other data to and from low complexity outstations over meteor scatter links. The types of data processing required at the outstations could easily be performed by low cost, general purpose, personal computers.

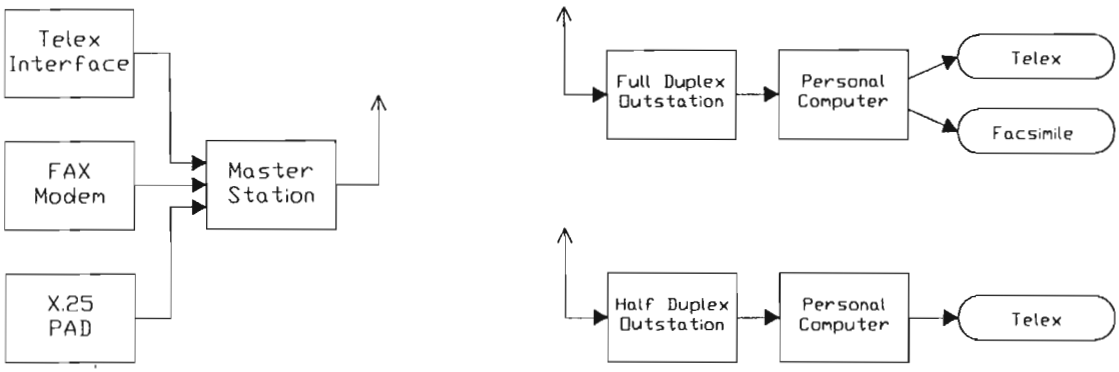

Figure 1-1. Typical System Configuration for a Meteor Scatter Network.

Communication systems using meteor scatter links have the potential to offer reliable, low data rate communications in the difficult 500 to 2000 km range. This is especially true in third world countries, sparsely populated areas or in areas of rugged terrain when data requirements are modest and other communication systems are not cost effective [Meyer, 1980].

In this thesis, an efficient protocol is described to operate in the low power, fixed data rate, half duplex, meteor scatter environment where short waiting times for message delivery are crucial and the volume of data is modest. These criterion require efficient use to be made of the underdense type reflections.

Chapter three of this thesis will show that the duration of underdense trails are predictable and can be bounded if certain system parameters are known. This bound on the duration of a trail can be used to develop an adaptive protocol to make more effective use of a meteor scatter channel than a non-adaptive protocol.

Much interest has been expressed in adaptive protocols. Adaptive protocols change some of their parameters to accommodate changes in the communication channel. Modification of the data rate has been suggested [Weitzen, 1983; Weitzen *et al*, 1984], but in many applications, data rate adaptive systems are not a cost effective solution. The throughput improvement gained from a data rate adaptive system over a system operating at the optimum fixed data rate is only 2 to 3 times for an idealized meteor scatter link [Abel, 1986]. In addition, waiting times are often increased rather than

being reduced. Further, the bandwidth required for such data rates exceeds what is realistically available in the frequency range for which meteor scatter is well suited. Hence it became apparent that there was much room for research in the field of fixed data rate, adaptive protocol design.

On first glance there might appear little that can be adapted in a meteor scatter protocol without changing the data rate. However, the distribution of the duration of usable meteor reflections makes the selection of the block size for a block protocol critical. By using the simple, fixed block, stop and wait protocols presently used by commercially available meteor scatter systems [Day, 1982], the maximum link utilization that can be achieved for a typical link configuration is approximately 33%. Clearly this is not ideal. This thesis shows that by using a sliding window protocol to send more than one frame at a time before waiting for an acknowledgment, the link utilization can be increased to almost 50%. Further, in chapter five, it will be shown that by adapting the block size on a trail by trail basis based on the initial signal received, a link utilization of 68% can be achieved. This two times improvement in link utilization is achieved without any increase in waiting times. To the contrary, the average waiting time between usable trails is reduced by 28%.

In chapter two, a brief introduction of the fundamentals of digital communications is presented. This is followed in chapter three by an introduction to meteor scatter communications and the specification and derivation of the peak signal to duration distribution on which the protocol developed for this thesis is based. This peak signal to duration distribution is then verified experimentally for a 500 km and 1300 km link.

Chapter four introduces adaptive protocols and chapter five covers the modeling of protocols which give the basis for selecting the protocol characteristics that will be used in the adaptive protocol specified in chapter six. Finally, chapter seven concludes the thesis and suggests areas for future research.

Chapter 2

Fundamentals of Digital Communication

Digital communications form the heart of most modern communication systems. Applications that have previously used analog communication systems are now using digital techniques. Telephone systems, once a maze of cross-bar switches and analog repeaters are being up-graded to packet switches. It is now more cost effective to transmit a half a page of text as a facsimile rather than send it as a telex. Both audio and video information are being stored and transmitted digitally. This tendency towards digital processing requires a well known, reliable communications channel.

The first digital networks used the existing communications channels provided by the telephone and point to point radio. As the power of digital communications became understood, digital networks started to look different from their analog counterparts. The Aloha Network [Abramson, 1975] demonstrated the ability of a radio network to link remote sites and ARPANET demonstrated how a network of non-homogeneous computers could be linked using an existing public carrier. Out of this, packet switching was derived as a logical extension of the general concept of time division multiplexing. Once the concept of storing up a 'packet' of information and transmitting the complete packet as one indivisible entity was accepted, new types of digital networks emerged [Roberts, 1978].

These digital networks utilized different types of communications channels and often radically different protocols. The differences between the characteristics of point to point wiring, shared cable, public carrier, point to point radio, and satellites caused much variation in the appearance of these networks. This variation caused problems when applications tried to utilize several networks to improve the class of service offered. These complications prompted the International Standards Organization to form a committee to look into a standard network architecture where the details of the various physical communications channels were isolated to a communications subnet so a network could be constructed to make efficient use of all channels available.

This chapter reviews the fundamentals of digital communications within the structure of the ISO-OSI reference model. This chapter is intentionally brief. Detailed references are given for important concepts. The general theory of data communication networks can be found in Tanenbaum [Tanenbaum, 1981] and Green [Green, 1980], while the theory of the electronics of digital communications can be found in Schwartz [Schwartz, 1980] and Lathi [Lathi, 1965].

2.1 Organization of a Digital Communications Protocol

In 1979 the International Standards Organization formed a special group to look into the organization for data communication networks. The result of this investigation is a layered model called the Reference Model of Open Systems Interconnection (OSI) [Zimmermann, 1980]. Some of the key concepts used to define the seven layers in the ISO-OSI reference model are:

1. Each layer should perform a well defined function.
2. New layers should be created when a new level of abstraction is required
3. The number of layers should be kept to a minimum to reduce interactions.

The seven layers of the OSI reference model are:

1. The Physical Layer.

The physical layer is concerned with the raw transmission of bits over the communication channel. Choice of modulation technique, bit synchronization, timing, channel contention and direction of data flow must be made at the physical layer.

2. The Data Link Layer.

The data link layer is concerned with providing reliable point-to-point communications. Choice of frame synchronization, error detection, error correction, retransmission and flow control must be made at the data link layer.

3. The Network Layer.

The network layer, or communication subnet layer, controls the routine of information within the communication subnet. The network layer is primarily concerned with ensuring packets get delivered to the proper destination. This usually entails selecting the optimum path to avoid congestion or out of service links. In addition, some accounting is often incorporated at the network layer.

4. The Transport Layer.

The transport layer is the first end-to-end layer of the OSI reference model and is responsible for packaging the data received from the session layer and passing this on

to the network layer in the most efficient manner. The transport layer is the first layer that is not concerned with the details of the point-to-point communications, but is merely concerned with providing the class of service requested at the lowest cost.

5. The Session Layer.

The session layer provides the connection between two users with the desired class of service. The primary functions of the session layer include the negotiation of costs for the desired class of service and the establishment of the connection between the two users.

6. The Presentation Layer.

The presentation layer provides functions to the applications layer that are so commonly requested that they are included in the model. Such functions include file transfer, character set conversion, data compression and data encryption.

7. The Application Layer.

The application layer performs the actual user applications. The functions performed at the application layer are not specified in the ISO-OSI reference model.

2.2 Physical Layer Considerations

The physical layer considers the raw transmission of bits from one point to another. The considerations include gaining access to the channel, coordination the direction of data flow, assigning electrical waveforms to represent the different symbols and possibly establishing symbol synchronization. Other considerations are transmitter power, duty cycle limitations, propagation characteristics, line equalization and receiver sensitivity.

2.2.1 Channel Contention

Channel contention techniques are concerned with assuring that all users of a channel get fair access to the channel and that the channel is efficiently utilized. Channel contention techniques can be classified as either reservation techniques or dynamic allocation techniques. Channels can be shared in time (TDM), frequency (FDM) or both (spread spectrum code). Dynamic allocation techniques range from the simple Aloha technique [Abramson, 1975] through CSMA [Kleinrock and Tobagi, 1975] to more sophisticated techniques such as generalized TDMA [Capetanakis, 1979]. Most dynamic allocation techniques have difficulty when all stations can not receive each others signals [Tobagi and Kleinrock, 1975].

2.2.2 Direction Of Data Flow

The limited time and bandwidth available on any communication system require some decisions to be made as to how much time and bandwidth is to be used for each direction of data flow. In *simplex* communications, all the time and bandwidth are allocated to one direction of data flow. No data flows in the reverse direction. Simplex communications make optimum use of both time and bandwidth for data flow in one direction in the absence of errors.

Half duplex communications is also known as two way alternating and allocates all the bandwidth to data flow in one direction at a time. Half duplex communications make efficient use of bandwidth and can be efficient in the use of time if changes in the direction of data flow are infrequent and well defined.

Full duplex, or two way simultaneous communications allocates all the time to both directions by sharing the bandwidth. Full duplex communications are inherently inefficient in their use of bandwidth due to the necessity of guard bands and can be

inefficient in their use of time unless the bandwidth allocations are well matched to the supply of data. Full duplex systems do not require any 'turn around' procedures and therefore minimize waiting times when the data is infrequent.

2.2.3 Modulation

Because most communication channels are analog channels with poor DC characteristics, it is usually necessary to modulate the baseband binary signal. A modulated signal can be expressed as $A\cos(\omega_c t + \theta)$ where A represents the amplitude, ω_c the carrier frequency, θ the phase shift and t is time. All modulation techniques alter some combination of A, ω_c and θ. In amplitude shift keying (ASK or OOK), the amplitude is changed, in frequency shift keying (FSK), the frequency is changed and in phase shift keying (PSK), the phase is changed. Modulation techniques are further described by the number of unique values a parameter may have. In binary modulation techniques a parameter must be one of two possible values.

If a coherent reference signal is available, coherent demodulation can take place. Coherent demodulation has better error characteristics than non-coherent demodulation but may require additional bandwidth to transmit the coherent reference.

Modulation techniques can be evaluated by comparing their error characteristics in the presence of noise and the length of time the demodulator requires to 'lock' onto the received signal [Bylanski and Ingram, 1976].

2.3 Data Link Layer Considerations

The data link layer of the ISO-OSI reference model provides an error free point to point communications channel from the error prone physical channel utilized by the physical layer. To provide this error free point to point channel, the data link layer must apply the error detection or error correction, blocking, retransmission and flow control techniques appropriate to the physical channel. Although the data link layer is not concerned with the details of how the raw data is transmitted over the physical channel, it is concerned with the overall properties of error rate and delay times.

2.3.1 Frame Synchronization

It is important that both ends of the communication link be in synchronization. This allows the receiving station to know when a bit time is starting, when to sample the signal and when the next bit time is to occur. Two things are required for this synchronization to take place. First of all, both stations must agree to the interval between bit times. With the accuracy of modern oscillators, there is no problem in staying in synchronization over a modest block length once synchronization has been established. The second requirement for synchronization is to determine when the beginning of the first bit time takes place. There are two methods of assuring that both ends of the communication link are in synchronization. These are synchronous communications and asynchronous communications.

For asynchronous communications, each datum is sent independently of any others. They may start and stop at any time irrespective of any previous or succeeding datum. Because synchronization is established on a datum by datum basis, there must be some sort of synchronizing information sent with each datum. Also, the datum are usually fixed size.

These characteristics are independent of any higher level protocol features which do not depend on the low level synchronization method. Because of the high overhead incurred on asynchronous protocols just to establish the beginning and ending of a datum (20% or more for most asynchronous protocols), another method of establishing basic synchronization has been defined.

In synchronous communications, synchronization is established for a block of data known as a *frame*. Once synchronization has been established for a frame, datum must follow immediately after the preceding datum with no intervening delay.

In a synchronous protocol, the frames may be any number of bits in length. To maintain synchronization a unique sequence known as the end of frame sequence must be defined that never occurs in the data stream. There are several common methods of preventing this unique end of frame sequence from occurring in the data stream. Both methods involve replacing every occurrence of this (and other unique sequences defined in the protocol) with other sequences. The two major families of doing this are the bit synchronous protocols and the byte synchronous protocols. In a bit synchronous protocol, if a sequence is detected in the data stream that looks like the end of frame sequence, an extra bit is automatically inserted in the data stream to change it. Of course when this modified sequence is detected at the receiver, the extra bit is removed. This method is known as *bit-stuffing* and is used in such protocols as X.25. In byte synchronous protocols, the end of frame sequence, like all other sequences in the protocol, is an eight bit byte. When the end of frame sequence is detected in the data stream, it is replaced by a different sequence. When the receiver detects this new sequence, it is changed back to its original form.

There are some disadvantages of synchronous protocols over asynchronous protocols. Firstly, until the frame size becomes large enough that the start of frame sequence and end of frame sequence are less than 20% of the data stream size, asynchronous protocols are more efficient. Secondly, if synchronization is lost at any time during a frame, the entire frame is usually lost. It is often impossible to recover synchronization until a new frame starts.

2.3.2 Error Detection

Errors occur in varying degrees with all communication channels. Data may be received incorrectly in time (a phase error) or the levels may be incorrectly detected. Errors frequently occur together as burst errors and therefore the probability of an error occurring may not be independent of other errors. When this happens, the simple gaussian noise models of errors are then inaccurate and more sophisticated error models must be used.

In many circumstances, it is undesirable for errors to be passed undetected through the channel. Therefore some method must be devised for detecting when an error has occurred. All methods of error detection send extra information along with the data to check the validity of the data bits sent. These error detection algorithms apply a mathematical formula to the data bits and send the result of the computation along with

the data. The proportion of extra information to data varies from method to method. The extra information is either sent separately or intermixed with the data. The simplest error detection method consists of a modulus two addition of all the data bits with a single parity bit appended to the end of the data stream. A parity check will detect all errors with an odd number of bits in error. If errors are considered rare and independent of each other, then a simple parity check is often adequate. Most of the other error detection methods consist of calculating an eight or sixteen bit quantity and sending it after the data stream for verification. The CRCC-16 or CCITT polynomials will detect all single or double errors. They will also detect all errors with an even number of bits in error and all burst errors with a length less than 15 [Lin and Costello, 1983].

Once an error has been detected, it is the function of the protocol either to accept the data knowing it is in error, or to request the remote station to re-transmit the data in error.

2.3.3 Error Correction

Often it is either not possible to request retransmission of the data when an error is detected or it is too inefficient due to turn around delays and propagation delays. In this case it is desirable to ensure that the data is sent correctly even in the presence of noise and other error generation sources. To facilitate this, error correction codes have been devised. Error correction codes work by sending the information redundantly. The simplest error correction method is to retransmit the same data over and over again until the confidence that the data has been successfully received is high enough. This is known as broadcasting and is often used in simplex communications. When the probability of an error is high and burst-like in nature, the chances of any single message getting through correctly is still very low. If this is the case, a more sophisticated algorithm must be used. In the more sophisticated algorithms, check digits are intermixed with the data to provide the redundancy. These check digits are usually related to more than one of the data bits and each data bit is checked by more than one check digit. By providing this multiple redundancy, the chances of getting the data through correctly increases in the presence of both random gaussian noise and burst type noise [Ples, 1982].

As with error detection codes, the confidence in the information increases with the number of extra check digits sent. Typical error correction codes use a ratio of 1/2. This means that for every data digit, there is a single check digit sent. Therefore, one half of the raw data bits received are information, and the other half are check digits. Different error correction codes are designed for particular types of errors. Some work best in the

presence of random Gaussian noise, others in the presence of burst noise where the channel is clean for long periods of time followed by brief periods of total disruption. Some are designed to work in the presence of predictable fading where the channel is relatively free from errors but with periodic fading. This makes it essential that the noise characteristics of the channel be well understood.

2.3.4 Blocking

There are several reasons to group data into blocks for transmission. With a synchronous protocol using some form of block error detection or correction, the data must be sent in a block. The choice of block size is an important factor in determining system performance. Because the protocol overhead (synchronization bits plus error detection code) is usually fixed, short blocks are inefficient. On the other hand, large blocks increase the delay between the time data is offered to the transmitter and the time the data is delivered by the receiver. Larger blocks also require more buffer space at the transmitter and the receiver. More importantly, larger blocks stand a greater change of being corrupted by errors than a shorter block. When the channel bit error rate is constant, the probability a block being received correctly is $(1\text{-}e_b)^n$ where e_b is the bit error rate and n is the number of bit in the block. Chapter five shows that the situation is more difficult when the bit error rate is not constant.

The trade-off can be seen by examining the efficiency of various blocking factors. The efficiency (E_F) of a blocking factor can be defined as the ratio of the number of data bits (n_d) received to the total number of bits sent (n). Excluding errors,

$$E_F = \frac{n_d}{n} \tag{2.1}$$

To include the influence of errors, but ignoring the overhead of requesting retransmission, it is necessary to accept the average throughput (N_B) in bits per block as:

$$N_B = n_d \cdot (1 - e_b)^n \tag{2.2}$$

where e_b is the bit error rate. The efficiency then becomes

$$E_F = \frac{n_d \cdot (1 - e_b)^n}{n} \tag{2.3}$$

As can be seen in figure 2-1, the protocol efficiency is highly dependent on the block size, and this effect is stronger at the higher bit error rates.

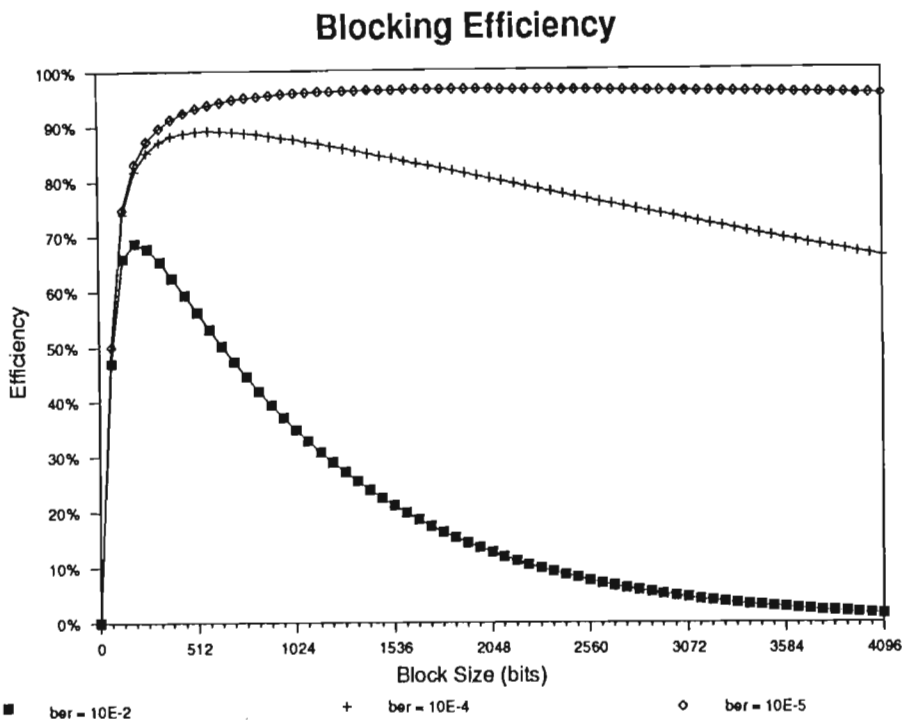

Figure 2-1. Variation in Efficiency as A Function of Block Size And Bit Error Rate (Ber) with a protocol overhead of 48 bits per block

2.3.5 Retransmission

When an uncorrectable error is detected, the invalid data must be discarded, used with errors or retransmitted. The simplest error control scheme is known as stop and wait. In a stop and wait protocol, the transmitter stops after every frame and waits for a positive acknowledgment (ACK) or a negative acknowledgment (NAK). Most stop and wait protocols employ a timeout scheme in case an acknowledgment is lost. An extension to the stop and wait protocol called stutter stop and wait is discussed by Townsley [Townsley, 1978] involves continuously repeating a frame until a positive acknowledgment is received. In a stop and wait protocol, much time is spent waiting for acknowledgments. This time can be large if the propagation delay is long as in satellite communications or when turnaround times are long as in some half duplex channels. To reduce this waiting time, some protocols send more than one frame at a time without waiting for an acknowledgment. These protocols are known as sliding window protocols and the maximum number of frames that may be transmitted without being acknowledged is called the window size. If more than the window size frames are unacknowledged, the transmitter must stop and await an acknowledgment. When an error is detected, there are two common techniques of retransmission. In the simplest

scheme, the frame in error and all succeeding frames are retransmitted. This technique is called 'go back N' and is the most common. An alternate technique uses selective retransmission and only retransmits the frames in error.

2.3.6 Flow Control

At the data link layer, flow control is used to regulate the volume of data sent over the channel so that buffer space is not exhausted. Should all the buffer space become used, congestion occurs and deadlocks are possible. Some protocols combine flow control with error control and perform pacing by delaying the transmission of acknowledgments or controlling the window size. Other protocols have functions specifically for flow control such as issuing credits for each frame to be transmitted.

Chapter 3

Characterization of Meteor Trails

The foundation of this thesis is based on the presumption that the duration of an underdense trail is bounded once its initial amplitude is known. The basis for this presumption is shown theoretically and demonstrated experimentally. The upper bound of the duration can be determined by maximizing the classical underdense equation. This upper bound has been used by many authors as a representative value of the duration of a reflection even though the average duration is significantly less. The lower bound of the duration, and the distribution between the limits, can be determined by examining the contributions of the various sky regions.

In this chapter, the background material essential to the derivation of the duration distribution is presented. Dissertations on the fundamentals of meteor scatter communications can be found in Weitzen [Weitzen, 1983], Rudie [Rudie, 1967], James [James, 1958] and Sites [Sites, 1978]. An excellent reference for many topics in the science of meteor scatter is the book by McKinley [McKinley, 1961]. The background information presented in this chapter is followed by the derivation of the initial amplitude to duration distribution. In order to verify the validity of the derivation, a measurement system is specified and implemented. The results of this measurement system are compared to the predicted values.

3.1 General Theory of Meteor Reflections

Billions of meteors enter the earth's atmosphere everyday varying in size from tiny particles of dust to giant chunks of rock. As they hit the dense atmosphere about 100 km above earth, most burn up leaving a trail of ionized particles. If these ionization trails are oriented to produce a specular reflection, as three to five percent are, they can be used to propagate radio waves as shown in figure 3-1. This type of communications is known as forward scatter.

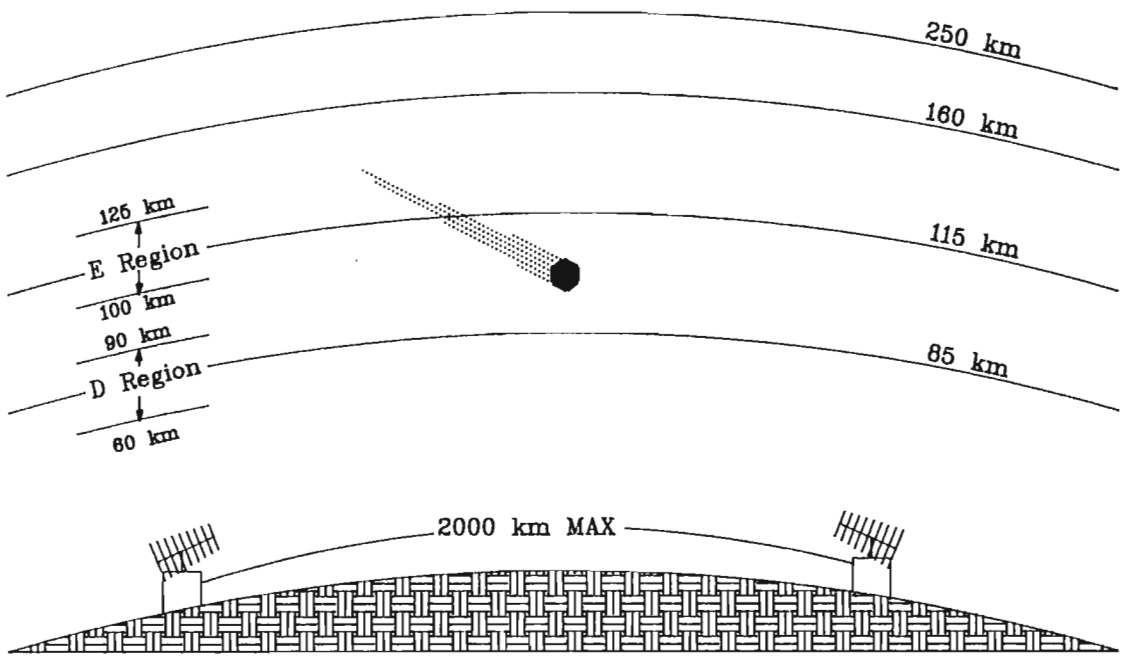

Figure 3-1. Geometry of Meteor Scatter Communication.

The number of meteors entering the atmosphere is inversely related to their size. Far more smaller meteors are observed than larger ones. Table 3-1 shows the estimated number of meteors verses their size and mass [Sites, 1978]. Meteor trails of electron line density greater than 10^{13} electrons per meter produce usable radio reflections. This electron line density is produced by a speck of dust with a mass less than a milligram and having a diameter less than half a millimeter. According to table 3-1, approximately one hundred million of these meteors enter the earth's atmosphere each day.

The meteors velocity relative to the earth is bounded by the escape velocity of the earth and the escape velocity of the solar system. The escape velocity at the earth's distance from the sun is 42 km/sec and the speed of the earth is 30 km/sec. These combine to give a maximum relative velocity of up to 72 km/sec. This is the maximum speed a

Table 3-1. Size vs number of meteors [Sites, 1978].

	Mass (grams)	Radius	Number of this mass or greater swept up by the earth each day	Electron line density (electrons per meter of trail length)
Particles pass through the atmosphere and fall to the ground	10^{4}			
Particles totally disintegrated in the upper atmosphere	10^{3} 10^{2} 10^{1} 1 10^{-1} 10^{-2} 10^{-3} 10^{-4}	4.0 cm 2.0 cm 0.8 cm 0.4 cm 0.2 cm 0.08 cm 0.04 cm 0.02 cm	10^{2} 10^{3} 10^{4} 10^{5} 10^{6} 10^{7} 10^{8} 10^{9}	-- -- 10^{18} 10^{17} 10^{16} 10^{15} 10^{14} 10^{13}
Limit of Radar Measurements	10^{-9}	to 8.0 microns	10^{13}	$> 10^{9}$
Micro-Meteorites (particles float down, changed by atmospheric collisions)	10^{-9} to 10^{-12}	4.0 to 0.4 microns	Total as high as 10^{20}	Practically none
Particles Removed from the Solar System by Radiation Pressure	10^{-13}	0.2 microns	--	--

meteor striking the earth can have if the meteor was originally in solar orbit. The escape velocity of a particle leaving the earth is 11.3 km/sec which corresponds to the smallest speed a meteor can have if it started at infinite distance with zero velocity relative to the earth and was attracted by earth's gravity alone.

Particles larger than a half a millimeter in diameter will typically produce overdense type reflections whilst particles smaller than half a millimeter will produce underdense type reflections. Underdense reflections are produced by sparse ionization trails with an electron line density of less than 10^{14} electrons/meter where each ion acts independently of others, is excited and re-radiates the signal. Overdense trails act as solid column reflectors [Sugar, 1964]. The envelope of power received from signals reflected by meteor trails is shown in figure 3-2 for both the underdense case and the overdense case. It should be noted that the power is shown on a log scale and the straight

line decay for the underdense trails corresponds to an exponential decay. This property of underdense trails has led many researchers to define the time constant of trails in much the same way as time constants are defined for R-C circuits. Most trails are underdense and therefore must be used in order to make efficient use of the medium. Overdense trails on the other hand provide long, strong reflections.

The power received as a function of time for an underdense type reflection is given by [Weitzen *et al*, 1984] when the electron line density q is less than 10^{14} electrons/meter:

$$P_R(t) = \frac{P_T G_T G_R \sigma_e \lambda^3 q^2 S^2}{(4\pi)^3 R_T R_R (R_T + R_R) \cdot (1 - \sin^2\phi \cos^2\beta)} \cdot \exp\left(-\frac{8\pi^2 r_0^2}{\lambda^2 \sec^2\phi}\right) \cdot \exp\left(-\frac{32\pi^2 D t}{\lambda^2 \sec^2\phi}\right) \tag{3.1}$$

The power received as a function of time for an overdense type reflection is given by [Weitzen *et al*, 1984] when the electron line density q is greater than 10^{14} electrons/meter:

$$P_R(t) = \frac{P_T G_T G_R \lambda^2}{32\pi^2 R_T R_R (R_T + R_R)(1 - \sin^2\phi \cos^2\beta)} \cdot \sqrt{\frac{4Dt}{\sec^2\phi} \cdot \ln\left(\frac{\sigma_e q \lambda^2 \sec^2\phi}{\sqrt{1 + 0.16 t^2 \pi^2 4Dt}}\right)} \tag{3.2}$$

where all symbols are defined in section 3.3 or the glossary.

There are two major sources of meteors, sporadic meteors and shower meteors. The meteors that comprise a shower are believed to come from debris moving together in the orbits of comets [Sites, 1978]. These orbits are well defined. Meteor showers occur when the earth intersects these orbit at specific times of the year. Because all the particles are moving together with similar velocities, the meteors in a shower all seem to originate from the same location in the sky and produce similar reflections. For meteor scatter to be more than just a once and a while form of communication, a more regular source of meteors must be used. The only other source of meteors are the sporadic meteors.

Sporadic meteors are believed to be random particles in solar orbit. Arrival rates of sporadic meteors are dependent on many factors including time of day, day of year, location on earth and path orientation. The diurnal cycle is strong with at least a four to one difference between morning and evening. The yearly cycle is also strong having to due with the position of the earth around the sun as well as the tilt of the earth.

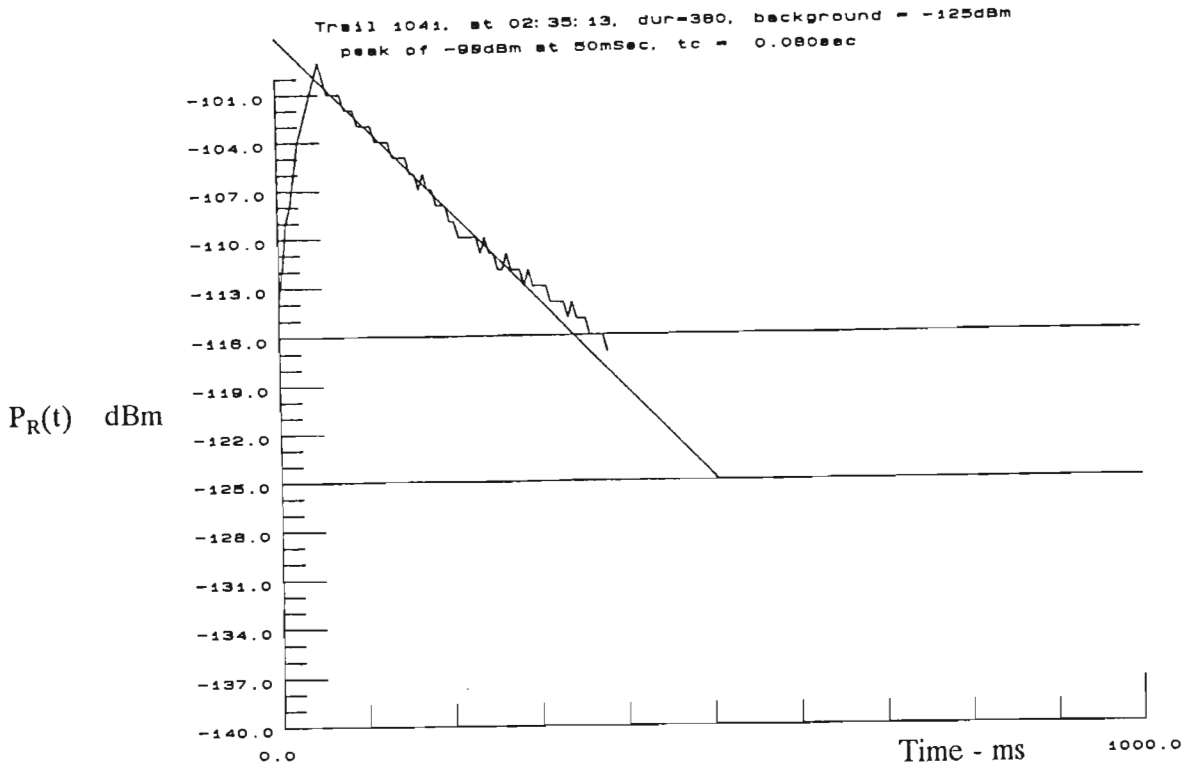

(a) Underdense trail.

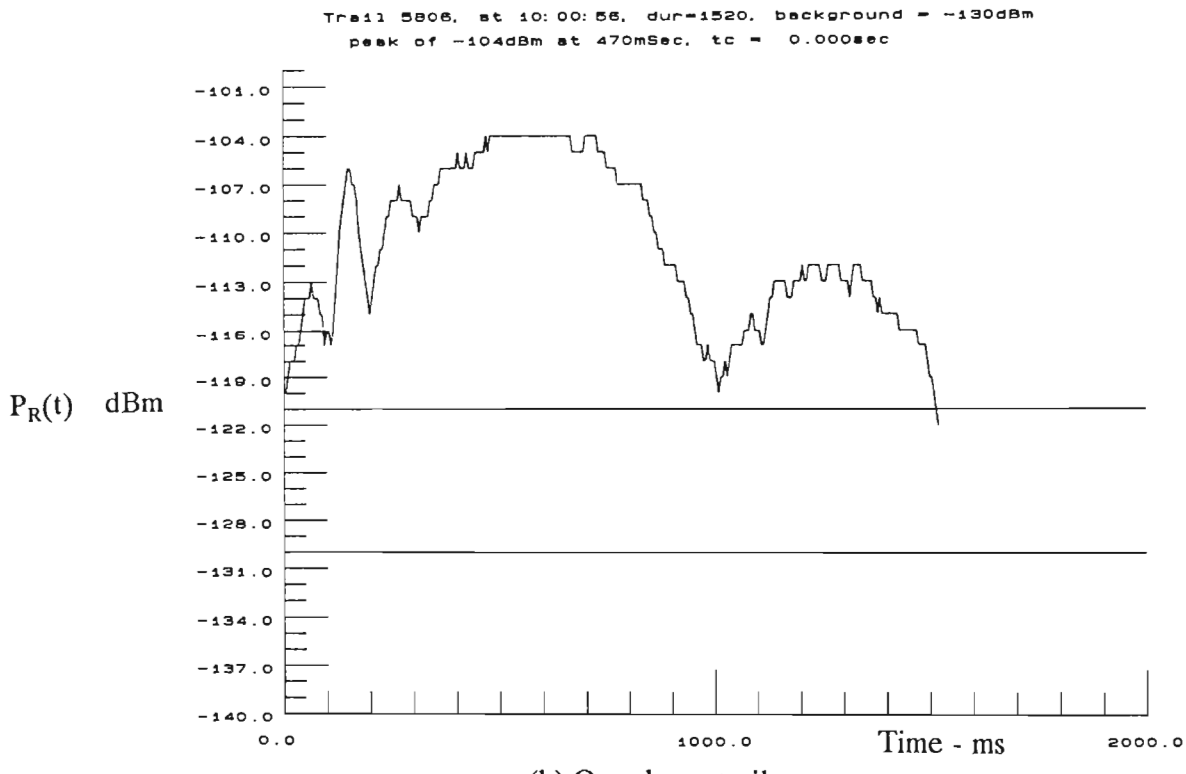

(b) Overdense trail.

Figure 3-2. Envelope of Typical Signals Received From Meteor Scatter Reflections.

The duration and signal strength distributions are dependent on frequency. The duration for underdense trails has been shown proportional to the wavelength squared whereas the signal strength has been shown proportional to the wavelength cubed [Brown and Williams, 1978].

3.2 Specification of Reference System

The propagation equations contain several system dependent parameters that need to be specified or normalized out. Throughout this dissertation, unless otherwise noted, the reference system used will be the following:

Table 3-2. Reference System Specification

	Location of Transmitter Station	Lat 25.54 East Long 28.16 South
P_T	Transmitter Power	500 W (56 dBm)
	Location of Durban Monitoring Station	Lat 29.51 East Long 31.02 South
	Great Circle Distance Between Transmitter And Durban Monitoring Station	520 km
G_T	Gain of Transmitter Antenna to Durban Station	14 dBi
G_R	Gain of Durban Receiver Antenna	14 dBi
	Location of Remote Monitoring Station	Lat 20.05 East Long 34.40 South
	Great Circle Distance Between Transmitter And Remote Monitoring Station	1300 km
G_T	Gain of Transmitter Antenna to Remote Station	17 dBi
G_R	Gain of Remote Receiver Antenna	17 dBi
f	Frequency	50.050 MHz
B	Half Power Bandwidth of Receiver	1.7 kHz
F	Noise Figure of Receiver	6 dB

3.3 Coordinate System and Definition of Symbols

The coordinate system and symbols are adopted from the literature [Eshleman and Manning, 1954; James, 1958; Weitzen, 1986]. The reference system shown in figure 3-3 is a cartesian coordinate system with its origin at the midpoint of the straight line between the transmitter and the receiver. The X axis is along the line through the transmitter and the receiver while the Z axis is vertical through the center of the earth. Given the great circle distance between the transmitter and the receiver (s), the coordinates of the transmitter is defined to be T_x = (+d,0,0) and the coordinates of the receiver to be R_x = (-d,0,0) where

$$d = R_E \sin\frac{s}{2R_E} \tag{3.3}$$

is one half the straight line distance from the transmitter to the receiver and R_E is the radius of the earth.

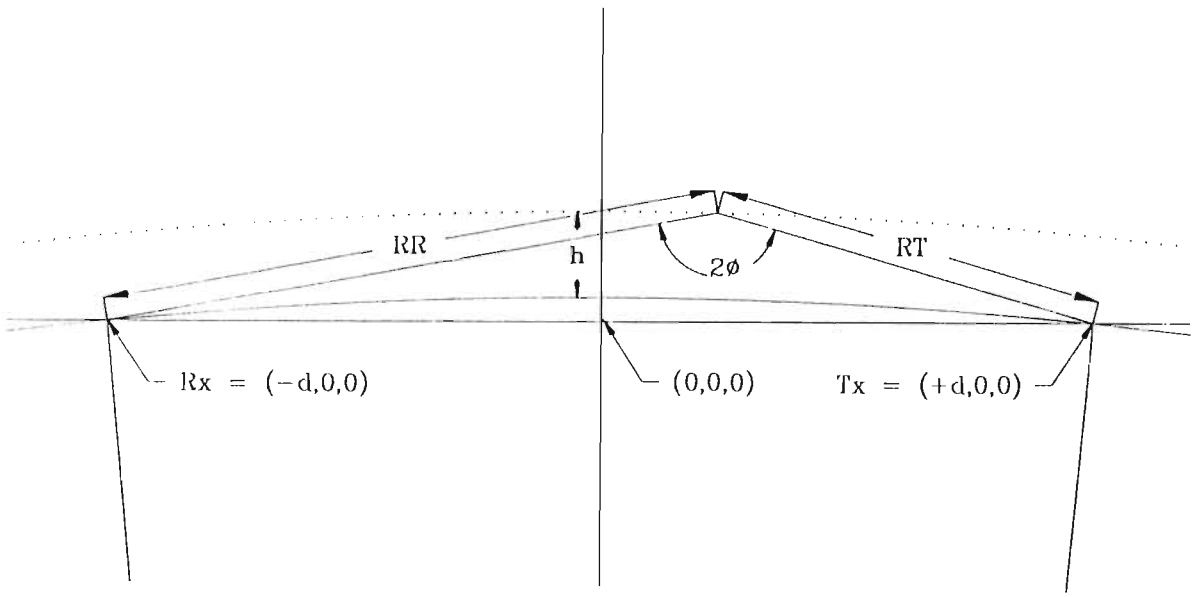

Figure 3-3. Coordinate System.

For a point on the sphere a distance h above the surface of the earth, the Z axis coordinate for any (x,y) pair can be computed as

$$z(x,y,h) = \sqrt{(R_E+h)^2 - x^2 - y^2} - R_E \cdot \cos\left(\frac{s}{2R_E}\right) \tag{3.4}$$

The distance from the transmitter to any point in the reference system is

$$R_T = |\overrightarrow{R_T}| = \sqrt{(x+d)^2 + y^2 + z^2} \tag{3.5}$$

The distance from the receiver to any point in the reference system is

$$R_R = |\overrightarrow{R_R}| = \sqrt{(x-d)^2 + y^2 + z^2} \tag{3.6}$$

whilst half the angle between the two vectors is

$$\phi = \frac{1}{2}\cos^{-1}\left[\frac{\overrightarrow{R_T}\cdot\overrightarrow{R_R}}{|\overrightarrow{R_T}|\,|\overrightarrow{R_R}|}\right] = \frac{1}{2}\cos^{-1}\left[\frac{x^2+y^2+z^2-d^2}{R_T R_R}\right] \tag{3.7}$$

The use of a flat earth model as proposed by some authors yields modest errors in the computation of the station separation, however this assumption can yield significant errors in the values of ϕ.

The celestial sphere is the sphere above the earth that the stars appear to be moving on. The coordinates of the point on the celestial sphere where the meteor appears is called the meteor radiant [James, 1958].

A presentation format was adopted that will be used extensively for describing the various position dependent features of meteor scatter communications. This format is called a sky contour map. The sky contour format was chosen to display the desired attributes for ease of interpretation. An example of a sky contour map is shown in figure 3-4 for the expected time constant for the reference system at a height of 95 km.

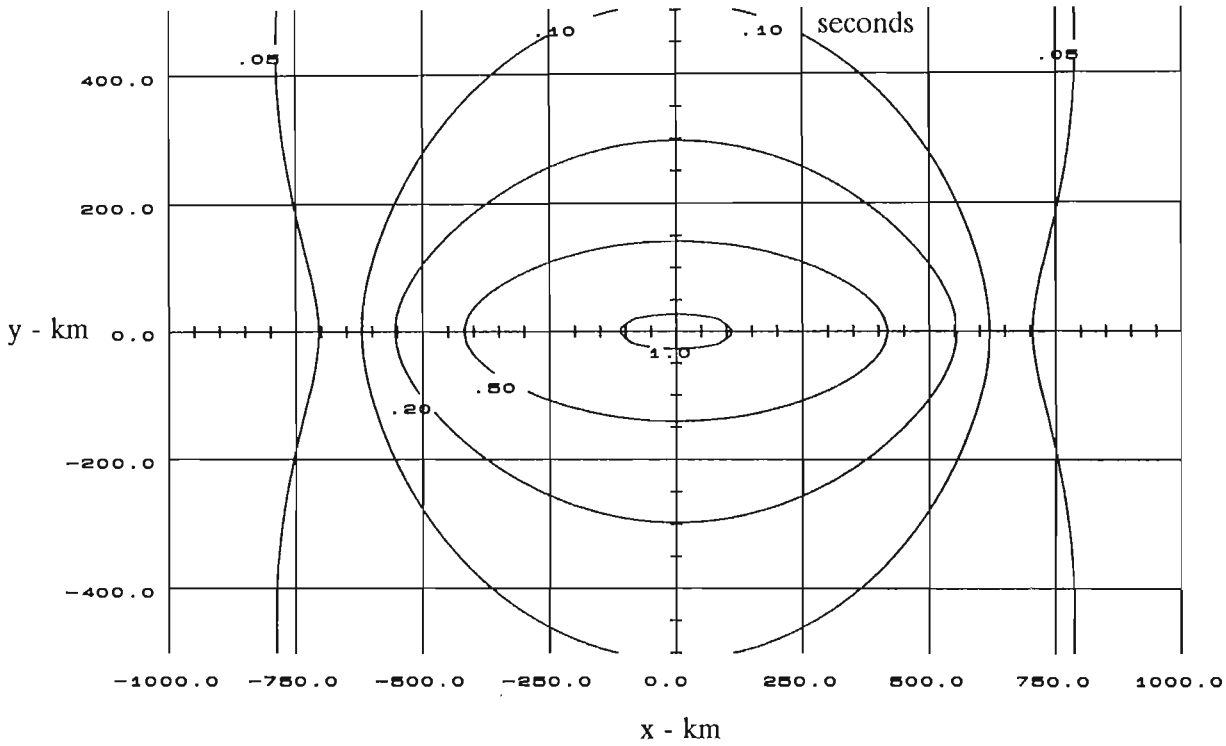

Figure 3-4. Expected Time Constant Over Sky Region at 95 km.

3.4 Theoretical Analysis of The Expected Duration of Underdense Trails

In this section, the factors affecting the duration of underdense trails are examined. These factors include the initial amplitude of the trail, the geometry of the reflection and the ambipolar diffusion coefficient. After determining a method for predicting the duration for any given trail, a probabilistic model is developed to predict the duration distribution for different system configurations.

Using equation (3.1), the power received as a function of time for an underdense trail can be written as

$$P_R(t) = P_{max} \exp \frac{-2t}{\tau} \tag{3.8}$$

where P_{max} is the initial peak signal at time $t=t_0$ and τ is the time for the power signal to drop to $1/e^2$ of its initial amplitude

$$\tau = \frac{\lambda^2 \sec^2 \phi}{16\pi^2 D} \tag{3.9}$$

The time constant τ is given in terms of ϕ, λ and D. To convert to the coordinate system of our reference system, we use the identities

$$\sec^2 \phi = \frac{1}{\cos^2 \phi} = \frac{1}{\frac{1+\cos 2\phi}{2}} = \frac{2}{1+\cos 2\phi} \tag{3.10}$$

which is in a form convenient for combined with equation [3.7] to derive τ as a function of (x,y,h).

$$\tau(x,y,h) = \frac{\lambda^2}{16\pi^2 D(h)} \cdot \frac{2}{1+\frac{x^2+y^2+z(x,y,h)^2-d^2}{R_T R_R}} \tag{3.11}$$

Given a trail with initial amplitude P_{max}, the time constant can be determined by knowing the frequency, diffusion coefficient and location of the trail [Keary and Wirth, 1960]. The usable duration of a trail (T_u) is related to the time constant, initial amplitude (P_{max}) and minimal usable signal (P_{min}) by:

$$T_u = \frac{\tau}{2} \ln\left(\frac{P_{max}}{P_{min}}\right) \tag{3.12}$$

The time constant will be used for the remainder of this section to remove unnecessary computational complications. The duration can be computed from the time constant when the initial amplitude is known using equation (3.12).

3.4.1 Diffusion Coefficient

As a meteor burns up in the earth's upper atmosphere, it leaves a trail of ionized particles. These free ions expand due to ordinary diffusion and form a conical trail. The factor which describes the rate of diffusion is called the diffusion coefficient (D) and is expressed in meters^2 per second. In an iosothermic atmosphere, log D is linearly related to height [Greenhow and Hall, 1960]. Although considerable dispersion exists in the measured data of the height to diffusion coefficient data [Baggaley and Webb, 1980], the following empirical relationship will be used in this thesis [Greenhow and Nufield, 1959].

$$\log_{10} D = 6.7*10^{-5} h - 5.6 \tag{3.13}$$

3.4.2 Height Distribution

The height distribution of meteors has been determined experimentally. For this thesis, the height distribution of meteors will be assumed to follow a normal distribution with a mean of 94.4 km and a standard deviation of 5.4 km [Baggaley and Webb, 1980].

3.4.3 Probability of Detection

It is necessary to determine the probability of a usable trail forming at all (x,y,h) locations to derive the time constant distribution for a given system. Although meteors produce trails of ionization 15 to 30 km long [Eshleman and Manning, 1954], the center of the first Fresnel zone producing a specular reflection is called the (x,y,h) location of the trail. To be a usable trail, the trail must be oriented to produce a specular reflection, the amplitude of the received signal must exceed some arbitrary minimum signal P_{min} and

the time constant must be greater than some arbitrary time constant τ_{min}. Specular reflection occurs when the bisector of the angle between the incident wave from the transmitter and the reflected wave to the receiver is perpendicular to the trail axis.

One factor that has an effect on the time constant distribution is the probability of a usable trail occurring in some incremental sky region $(x+\Delta x, y+\Delta y, h+\Delta h)$. This probability function is based on an assumed knowledge of the origin and trajectory of the meteor. Early work by Eshleman [Eshleman and Manning, 1954] developed a probability density of detection based on an isotropic radiant distribution. Eshleman's work was re-written by James [James and Meeks, 1956] as a n-factor to indicate the relative number of usable trails per unit time. This n-factor was shown to be the same as Eshleman's probability density of detection. James continued to develop a radiant distribution assuming all meteors originated on the ecliptic plane and compared the results to the isotropic distribution. In a subsequent report, James [James, 1958] continued his work by developing a model for a single point radiant such as would be found in a meteor shower. This was extended to a three point radiant distribution by considering Hawkins [Hawkins, 1956] empirical model for radiant distributions. The most complete work on radiant distributions was done by Rudie [Rudie, 1967] who computed the relative number of observable trails per differential area per second for a geocentric radiant distribution. This work differs from all previous work by considering meteors as objects in orbit around the sun and computing their intersection with the earth as opposed to the other models which maintain an earth based reference. A similar, but less complicated radiant distribution was first proposed by Weiss [Weiss, 1958] and uses a uniform heliocentric radiant distribution with uniform heliocentric velocities.

One measure of the accuracy of a radiant distribution model is its ability to follow measured diurnal and seasonal cycles. The isotropic radiant distribution does not consider diurnal and seasonal cycles. The ecliptic radiant distribution was not successful in predicting the diurnal and seasonal cycles, however the three point radiant distribution appears to be very close [James, 1958]. The geocentric radiant distribution developed by Rudie should produce even better results if his assumptions on meteoric orbits is correct, however the model Rudie implemented failed to produce a smooth, continuous diurnal cycle and could not be fairly compared. A subsequent analysis [Weitzen, 1986] did produce a smooth, continuous diurnal cycle that followed measured data. Further Weitzen's new model produced the same azimuth distribution of meteor radiants as

measured data [Hawkins, 1956] to further reinforce its validity. The heliocentric radiant distribution was also able to predict the diurnal and seasonal variations and has been used in computer models [Felber *et al*, 1985].

Because of the scope and goals of this investigation, the isotropic radiant distribution will be used. The isotropic radiant distribution is believed to be a long term average of the true radiant distribution. Predictions using the isotropic radiant distribution should produce accurate results for long term averaged data. Short term comparisons are likely to disagree. The advantages of the isotropic radiant distribution for the specification of protocols is that time, date and path location do not affect the predictions. Using the other models, a complicated calculation could have to take place each time a trail occurs. This level of computation is unacceptable in low complexity mobile or portable stations.

All probability of detection models agree that the region of longest time constant and often largest antenna gain is unlikely to provide any usable reflections. The center of the path, mid point between the two stations is often used as a typical trail location due to the simplifications this assumption enables in the calculations [Abel, 1986]. Regrettably, both theory and experimental analysis show this region to be unproductive.

The derivation of the probability of detection will follow the derivation used by James [James, 1958] in his thesis with minor changes in nomenclature. James work is an extension of Eshleman's [Eshleman and Manning, 1954] earlier work with fewer assumption. Refer to James [James, 1958] for the complete derivation including derivation of all terms presented in the glossary. James [James, 1958] defines the relative number of useful meteors per unit area of sky at a given height to be

$$p_T(x, y \mid h) \propto \int N(q_0) \cos\zeta \, d\zeta \tag{3.14}$$

where $N(q_0)$ is the number of meteors with electron line density greater than or equal to q_0 which pass through a unit area at position x, y and height h, q_0 is the electron line density a trail must have to produce a usable reflection and ζ is the angle between the zenith and the trail axis. Eshleman states that the region of sky that produces useful reflections can be approximated by a narrow band of width $2\,\psi_m$ where

$$\psi_m = \frac{L(R_T + R_R)}{4R_T R_R \cos\phi}(1 - \sin^2\phi\cos^2\beta) \tag{3.15}$$

Following James [James, 1958], the surface integral of N (q_0) cos ζ over the relatively narrow band of width 2 ψ_m will be replaced with a line integral along the center line of the band. Thus

$$p_T(x,y \mid h) \propto \int_{-\epsilon}^{\pi-\epsilon} 2\psi_m N(q_0)\cos\zeta \, d\beta \tag{3.16}$$

To solve this, we use

$$\cos\zeta = \cos\gamma \sin(\beta+\varepsilon) \tag{3.17}$$

where

$$\gamma = \sin^{-1}\sqrt{\frac{z(x,y,h)^2(R_T+R_R)^2}{R_TR_R(R_T+R_R)^2 - 4R_TR_RD^2}} \tag{3.18}$$

$$\varepsilon = \cos^{-1}\left[\frac{y}{\sqrt{y^2+z^2(x,y,h)\sin^2\left(\phi-\cos^{-1}\left(\sqrt{\frac{z^2(x,y,h)-y^2}{R_R}}\right)\right)}}\right] \tag{3.19}$$

as derived by James [James, 1958].

Finally, to derive N(q_0), we assume N(q) = K / q^k as given by Eshleman [Eshleman and Manning, 1954] and k and K are constant. q_0 can be found by solving equation (3.1) for q after setting t = 0 and $P_{rec}(0) = P_{min}$. This yields

$$q_0 = Q\cdot\sqrt{1-\sin^2\phi\cos^2\beta} \tag{3.20}$$

where

$$Q = \sqrt{\frac{P_{min}}{P_T}\frac{(4\pi)^3R_TR_R(R_T+R_R)}{G_TG_R\sigma_e\lambda^3S^2\exp\left[\frac{-8\pi r_0^2}{\lambda^2\sec^2\phi}\right]}} \tag{3.21}$$

substituting into equation (3.16) we get

$$p_T(x,y \mid h) \propto \frac{2\cdot L\cdot K\cdot(R_T+R_R)\cos\gamma}{4R_TR_RQ^k\cos\phi}\cdot \int_{-\epsilon}^{\pi-\epsilon}(1-\sin^2\phi\cos^2\beta)^{-k/2}\sin(\beta+\varepsilon)d\beta \tag{3.22}$$

To determine the probability of occurrence at any (x,y,h) location, equation (3.22) must be combined with the height distribution. Hence:

$$p_T(x,y,h) = p_T(x,y \mid h) \cdot p_H(h) \tag{3.23}$$

3.4.4 Derivation of Time Constant Distribution

In a communication system, we are more interested in how long a trail will last and what its reflection envelope will be than in the location of the trail. This section will derive the time constant density function, that is the probability that a trail will have the time constant τ given that the trail has occurred.

Given the probability of a usable trail forming in the incremental region of sky ($p_T(x,y,h)$) and the time constant a trail would have if it were to occur in that incremental region of sky ($\tau(x,y,h)$), calculating the probability of a trail occurring with a time constant equal to τ ($p(\tau)$) may be derived using a transformation of one function of three random variables.

This transformation will follow the derivation by Papoulis [Papoulis, 1984], section 6-2 extended to three variables. The density function of τ can be determined by finding the regions ΔD_τ such that $\tau < \tau(x,y,h) < \tau + d\tau$ and integrating the probability of occurrence over these regions.

$$p(\tau)d\tau = \iiint_{\Delta D_\tau} p_T(x,y,h)dx\,dy\,dh \tag{3.24}$$

In other words, the probability of a trail having a time constant between τ and $\tau + \Delta\tau$ is the probability of a trail occurring in any of the regions of the sky where a trail would have a time constant between τ and $\tau + \Delta\tau$. These regions of the sky where a trail would have a time constant between τ and $\tau + \Delta\tau$ (ΔD_τ) may be determined explicitly or numerically.

3.4.5 Derivation of Duration Distribution

Knowledge of the expected usable duration of a trail is important for determining how long to transmit data. The initial amplitude and noise levels are easily measured in practical communication systems. Equation (3.12) relates the usable duration to the time constant and the initial amplitude to noise ratio. The time constant distribution can be

transformed into a duration distribution when the initial amplitude and noise levels are known. This assumes the time constant is independant of the initial amplitude. This independance will be shown in section 3.7.1.

Following the method given by Papoulis [Papoulis, 1984] for determining the distribution function for a function of a random variable, we rewrite equation (3.12) to be the function of transformation

$$g(D) = \frac{\ln\left(\frac{P_{max}}{P_{min}}\right)}{2}\tau \tag{3.25}$$

which is in the same form as his example 1 on page 96. From this we find the duration distribution to be

$$p_T(D \mid P_{max}) = \frac{1}{|a|} p_\tau\left(\frac{\tau}{a}\right) \tag{3.26}$$

where

$$a = \frac{\ln\left(\frac{P_{max}}{P_{min}}\right)}{2} \tag{3.27}$$

3.5 Predicted Underdense Duration Distribution

Following the theoretical derivations in the previous section, the time constant distribution for underdense trails will be computed for the reference system. This computation will involve determining the polar patterns for the transmitter and receiver antenna, mapping the polar patterns onto the sky regions, adopting a probability of detection model, computing the time constant at each point in the sky region, then computing a weighted average of the time constants over the sky volume. This time constant distribution can be mapped into a duration distribution for any given initial amplitude and threshold as described in section 3.4.5.

These computations take place on a high speed digital computer. A block diagram of the steps involved and the intermediate results is shown in figure 3-5. Each step was performed by a separate program to allow verification of the intermediate results.

The polar pattern information was stored with a resolution of one degree and the sky region information was stored with a resolution of 15 km in the x and y directions and a resolution of 2 km in height.

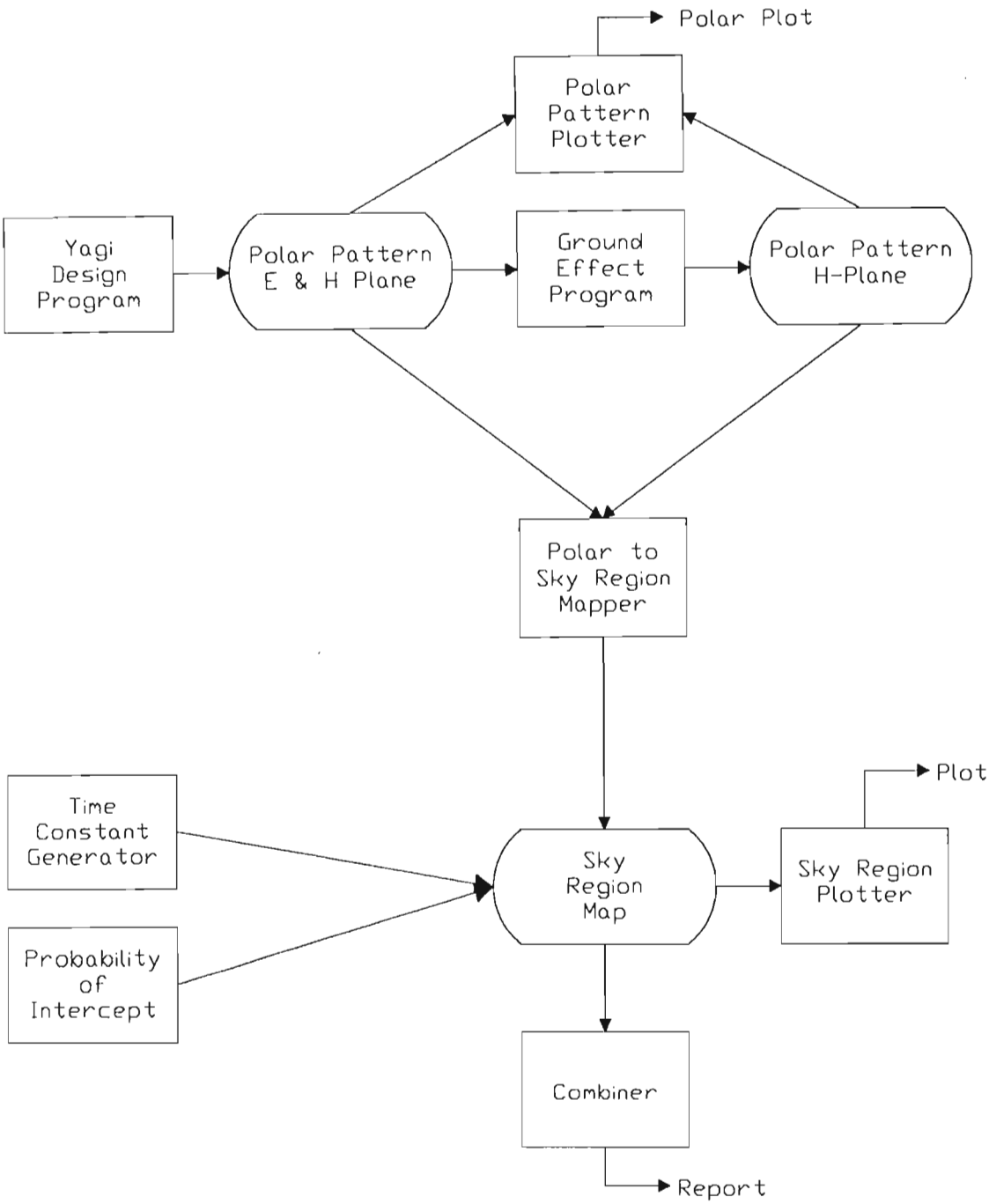

Figure 3-5. Block Diagram of Computer Model.

3.5.1 Yagi Antenna Predictions

The polar patterns for commercial Yagi antennas are usually supplied by the manufacturer. Algorithms for computing Yagi antenna polar patterns exist although many manufacturers still use measurement procedures. As the design and modeling of

Yagi antennas exceed the scope of this investigation, an existing Yagi design program was used to predict the polar patterns of the antennas used [Lawson, 1986; Larsen]. The output of the Yagi design program consists of the E- and H-plane polar patterns.

Two different antennas were used extensively in this investigation. The first antenna is a five element antenna manufactured by Meteor Communications Corporation specifically for meteor burst communications. The other antenna is an eleven element KLM Yagi. The dimensions for the five element MCC Yagi and the eleven element KLM Yagi are shown in tables 3-3 and 3-4. The free space polar patterns for the five element MCC Yagi and the eleven element KLM Yagi as predicted by the Yagi design program are shown in figure 3-6 and 3-7.

Table 3-3. Dimensions of the Five Element MCC Yagi.

F = 50 MHz Forward Gain = 9.14 dB F/B = 16.56 dB **Length - inches**			
ELE. #1	LENGTH = 128.00	SPACE = .000λ(0.00)	
ELE. #2	LENGTH = 118.50	SPACE = .180λ(42.50)	Phase = 0
ELE. #3	LENGTH = 112.50	SPACE = .294λ(69.50)	
ELE. #4	LENGTH = 108.50	SPACE = .408λ(96.50)	
ELE. #5	LENGTH = 106.25	SPACE = .523λ(123.50)	

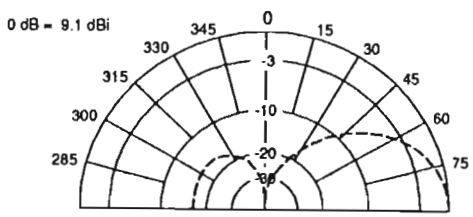

a. E-Plane polar plot

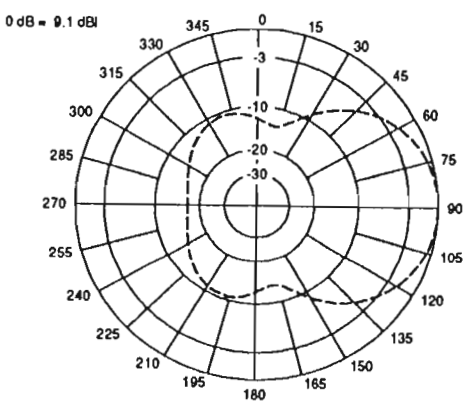

b. H-Plane polar plot

Figure 3-6. Free Space Polar Patterns For Five Element MCC Yagi.

Table 3-4. Dimensions of the Eleven Element KLM Yagi.

F = 50 MHz Forward Gain = 12.42 dB F/B = 17.84 dB **Length - inches**			
ELE. #1	LENGTH = 118.00	SPACE = .000λ(0.00)	
ELE. #2	LENGTH = 108.00	SPACE = .084λ(20.00)	Phase =180
ELE. #3	LENGTH = 107.00	SPACE = .165λ(39.00)	Phase = 0
ELE. #4	LENGTH = 104.00	SPACE = .241λ(57.00)	Phase =180
ELE. #5	LENGTH = 99.00	SPACE = .313λ(74.00)	Phase = 0
ELE. #6	LENGTH = 102.00	SPACE = .421λ(99.50)	
ELE. #7	LENGTH = 101.00	SPACE = .696λ(164.50)	
ELE. #8	LENGTH = 101.00	SPACE = .937λ(221.25)	
ELE. #9	LENGTH = 100.25	SPACE = 1.217λ(287.50)	
ELE. #10	LENGTH = 100.25	SPACE = 1.361λ(321.50)	
ELE. #11	LENGTH = 96.50	SPACE = 1.518λ(358.50)	

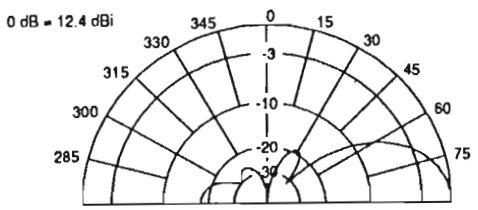

a. E-Plane polar plot.

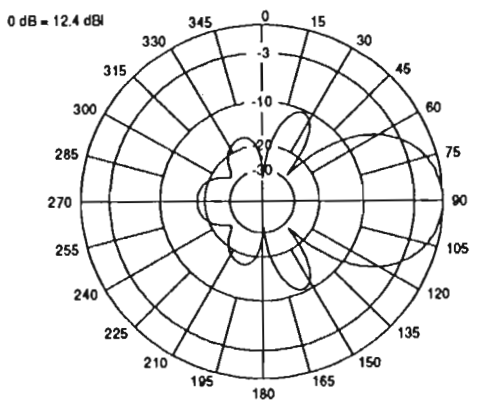

b. H-Plane polar plot.

Figure 3-7. Free Space Polar Patterns For Eleven Element KLM Yagi.

3.5.2 Ground Reflection and Stacking

Both the effects of stacking and ground reflection are considered together. If the stacked antennas are mounted sufficiently apart that they do not directly interact, the effect can be modeled by summing the wave from the two antennas. Likewise, the effect of ground reflections can be modeled by considering an antenna mirrored by the ground with the appropriate attenuation and diffraction factors [Larsen, to be published]. Only the plane perpendicular to the ground is affected by ground reflections and vertical stacking. Figure 3-8 shows the configuration for two stacked antennas with ground reflection.

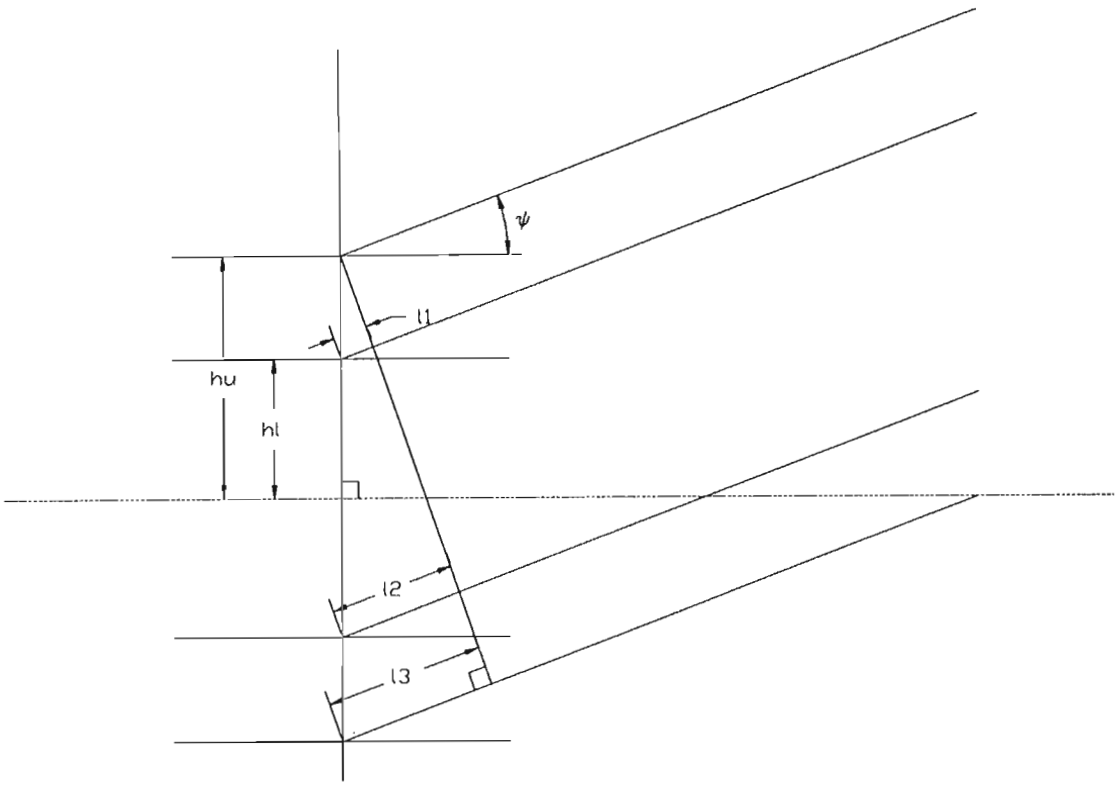

Figure 3-8. Stacked Antenna Configuration.

The voltage gain of the stacked antenna configuration is:

$$G = \left| \frac{\sqrt{2}}{2} G_1(\psi) + \frac{\sqrt{2}}{2} G_2(\psi) e^{j2\pi \frac{l1}{\lambda}} + \frac{\sqrt{2}}{2} G_2(-\psi) e^{j2\pi \frac{l2}{\lambda}} \rho e^{j\theta} + \frac{\sqrt{2}}{2} G_1(-\psi) e^{j2\pi \frac{l3}{\lambda}} \rho e^{j\theta} \right| \tag{3.28}$$

where

$$\begin{aligned} l1 &= \cos(90-\psi)(hu-hl) = \sin(\psi)(hu-hl) \\ l2 &= \cos(90-\psi)(hu+hl) = \sin(\psi)(hu+hl) \\ l3 &= \cos(90-\psi)(hu+hu) = \sin(\psi)(hu+hu) \end{aligned} \tag{3.29}$$

and

G_1 is the voltage gain of antenna 1

G_2 is the voltage gain of antenna 2

For a single antenna, omit the G_2 terms.

The Fresnel reflection coefficients depend on the ground conductivity (σ), permittivity ($K\epsilon_0$), frequency (f), angle of incidence (ψ), and the type of polarization involved [Collin, 1985]. For a perfectly reflecting ground

$$\rho e^{j\theta} = -1 \tag{3.30}$$

However for a non perfectly reflecting ground

$$\rho e^{j\theta} = \frac{(K - j\chi)\sin\psi - \sqrt{(K - j\chi) - \cos^2\psi}}{(K - j\chi)\sin\psi + \sqrt{(K - j\chi) - \cos^2\psi}} \tag{3.31}$$

for vertical polarization, and

$$\rho e^{j\theta} = \frac{\sin\psi - \sqrt{(K - j\chi) - \cos^2\psi}}{\sin\psi + \sqrt{(K - j\chi) - \cos^2\psi}} \tag{3.32}$$

for horizontal polarization, where:

$$\chi = \frac{\sigma}{2\pi f \epsilon_0} \tag{3.33}$$

The conductivity of soil can range from about 10^{-3} S/m for reasonably dry soil to about 1 S/m or more for wet soil near a beach due to the moisture and salt content of the soil. A typical ground conductivity for flat prairie land is 10^{-2} S/m.

The moisture content of soil has an effect on the dielectric constant of the ground. Dry soil, sand and rock have dielectric constants ranging from about 4 to 7, whilst the dielectric constant of normal moist soil varies between 10 and 30.

Only the H-plane is affected by ground reflection and vertical stacking for horizontally polarized antennas. The H-plane polar plot for two five element MCC Yagi antennas stacked 12 and 16.5 meters above the ground is shown in figure 3-9 assuming a ground conductivity of 10^{-2} S/m and a dielectric constant (K) of 15 at a frequency of 50 MHz[1]. The H-plane polar plot for a single eleven element KLM Yagi mounted three meters above the ground is shown in figure 3-10 with the same assumptions.

---

1 The values selected for ground conductivity and dielectric constant are typical for the experimental area. The effect of variations in ground conductivity and dielectric constant on the polar patterns is reported by Larsen [Larsen].

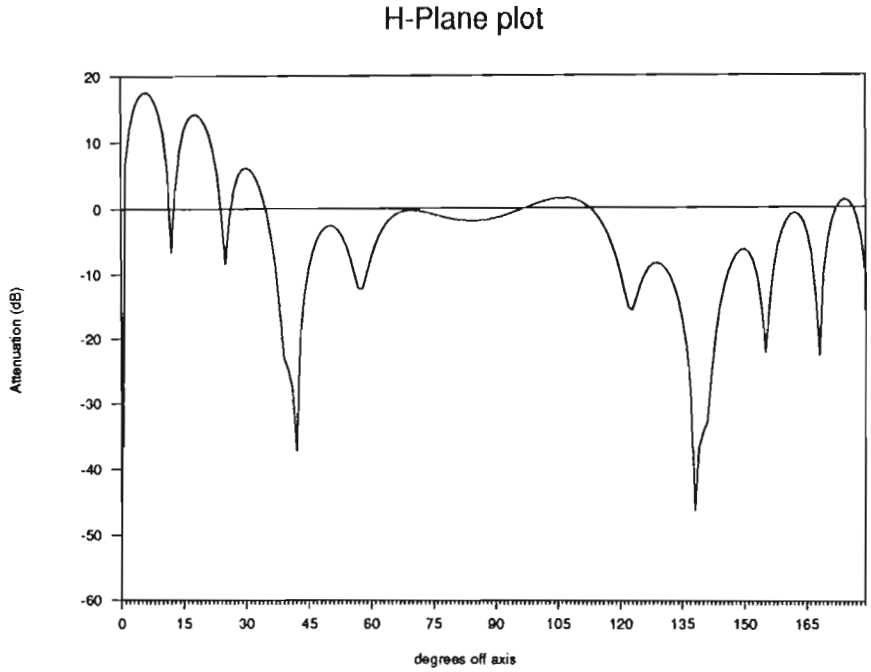

Figure 3-9. H-Plane Polar Pattern For Stacked MCC Yagis at 12 And 16.5 Meters Above The Ground.

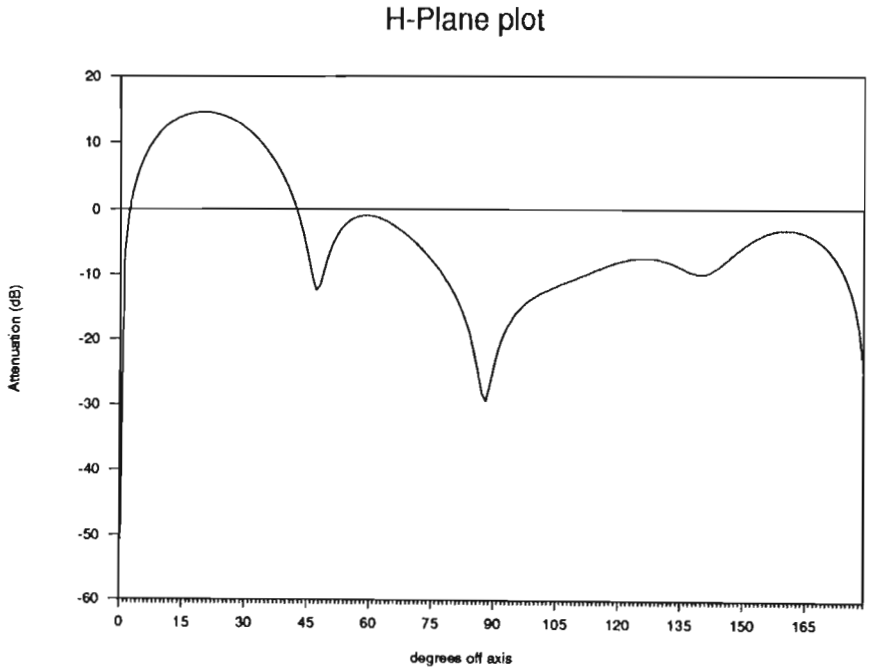

Figure 3-10. H-Plane Polar Pattern For Eleven Element KLM Yagi at 3 Meters Above The Ground.

3.5.3 Mapping Polar Patterns to Sky Regions

The polar patterns predicted by the Yagi design and ground reflection programs can be mapped to sky region plots by a straight forward geometric procedure. The antenna gain patterns are given in terms of θ, the angle off the main beam of the antenna and ψ, the elevation angle. The normalized gain G(x,y,h) for a horizontally polarized antenna is

$$G(x,y,h) = \frac{G_E(\theta)G_H(\psi)}{G_{max}} \tag{3.34}$$

where

$$\theta = \sin^{-1}\frac{y}{\sqrt{x^2+y^2}} \tag{3.35}$$

$$\psi = \sin^{-1}\frac{z(x,y,h)}{\sqrt{x^2+z^2(x,y,h)}} \tag{3.36}$$

The sky contour plots showing the region of sky illuminated by the receiver antenna array for a path distance of 1300 km is shown in figure 3-11. The sky contour plot showing the common region of sky illuminated by both the transmitter and the receiver array is shown in figure 3-12.

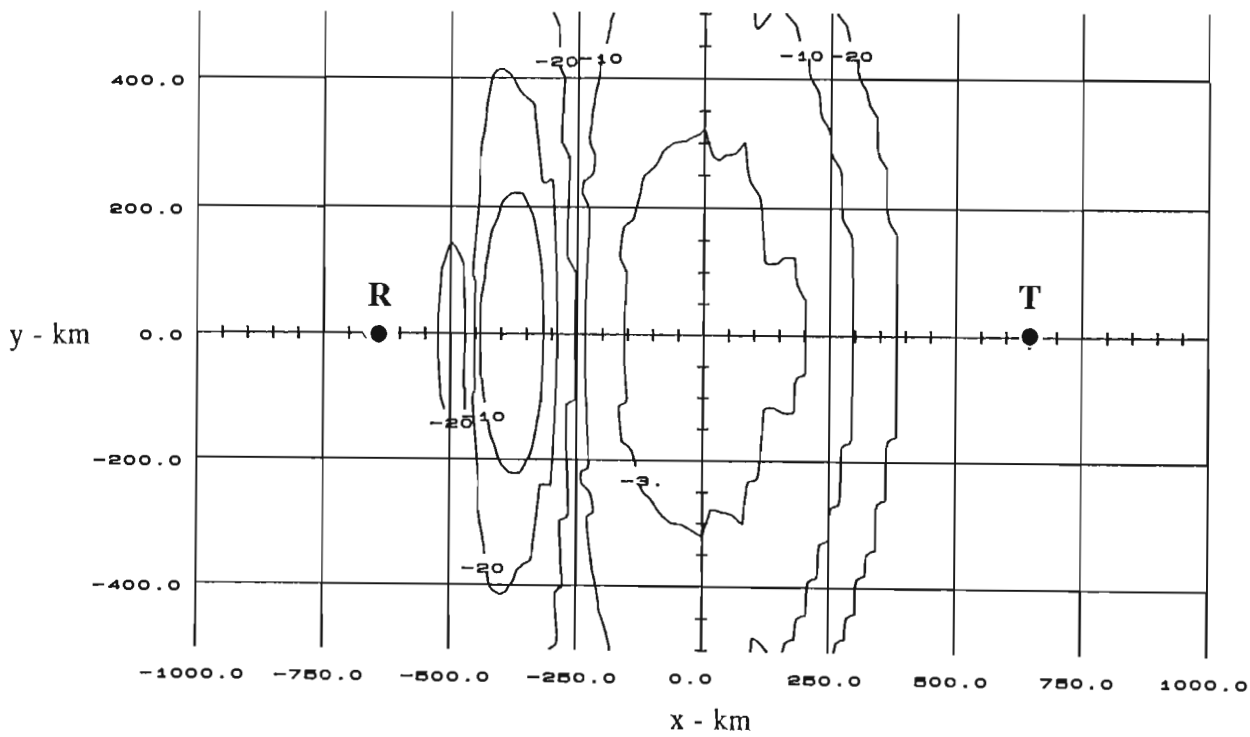

Figure 3-11. Sky Region for Receive Antenna for the 1300 km path.

Contours in dB, T and R mark transmitter and receiver positions.

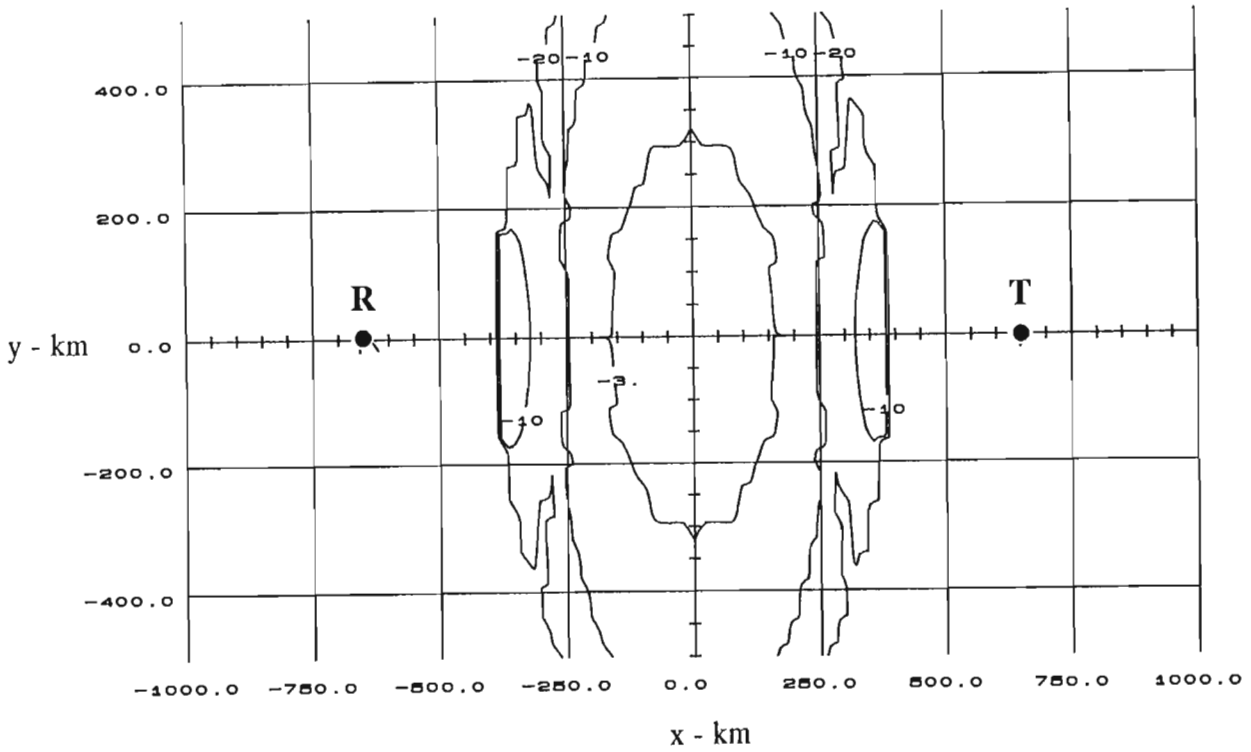

Figure 3-12. Common Antenna Illumination Pattern for the 1300 km path.

The sky contours for the eleven element KLM antennas for a 500 km path are shown in figures 3-13 and 3-14.

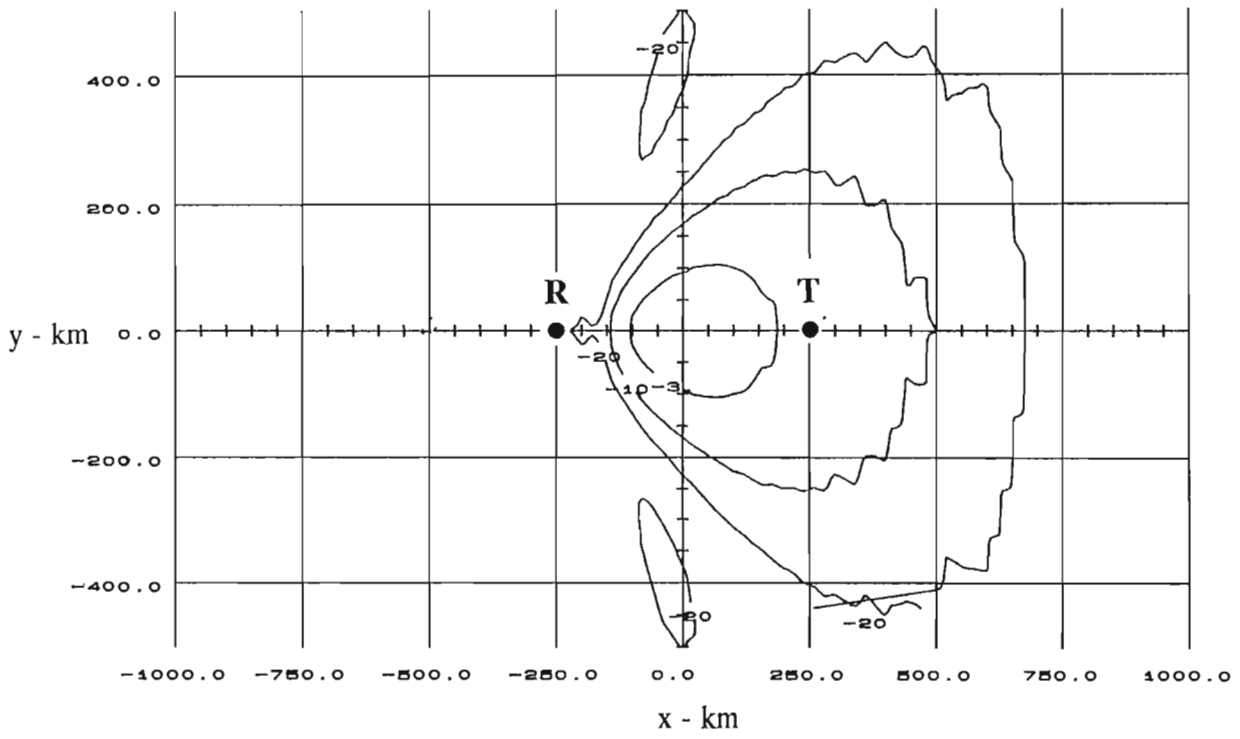

Figure 3-13. Sky Region for Receive Antenna for the 500 km path.

Contours in dB, T and R mark transmitter and receiver positions.

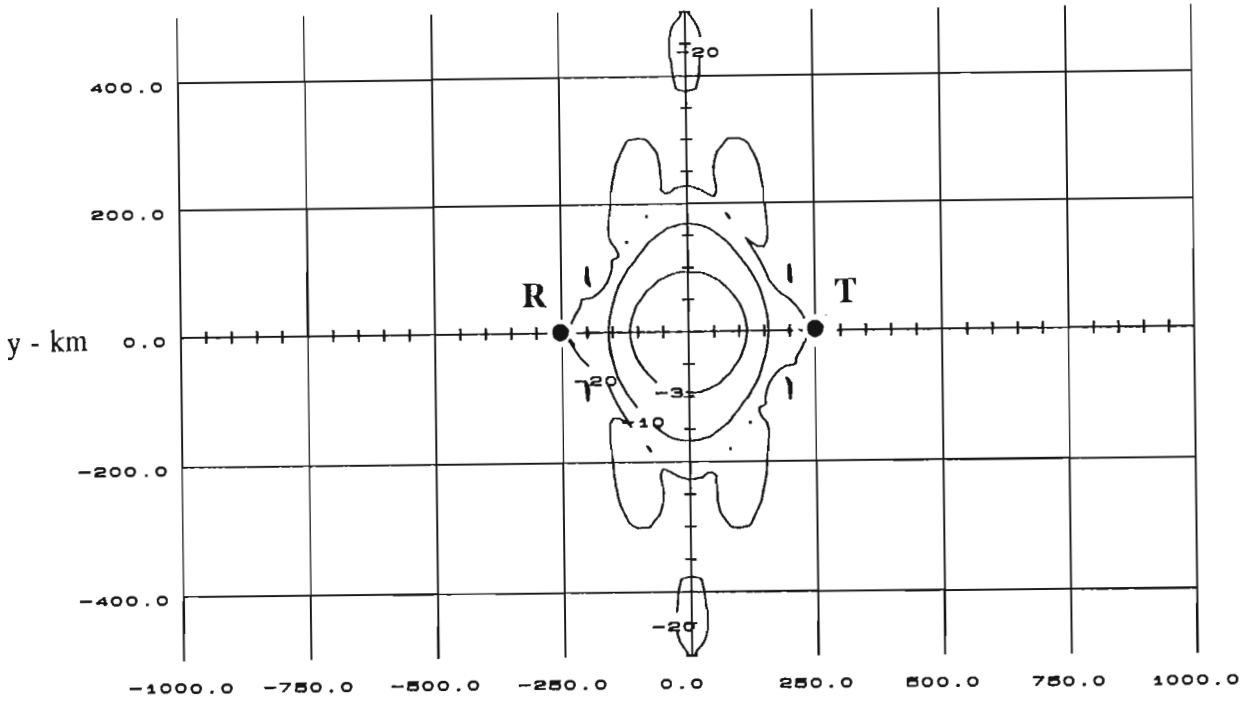

Figure 3-14. Common Antenna Illumination Pattern for the 500 km path.
Contours in dB, T and R mark transmitter and receiver positions.

3.5.4 Probability of Detection Model

The probability of detection model derived in section 3.4.3 for an isotropic radiant distribution was implemented. The probability of detection for a 250 km path assuming horizontal polarization but excluding antenna gain is shown in figure 3-15 for comparison with James [James, 1958] figure 4. The probability of detection for a 1300 km path assuming a trail height of 95 km is shown in figure 3-16 and for a 500 km path in figure 3-17. The exact value of the coutour lines are arbitrary although the relative numbers are consistent.

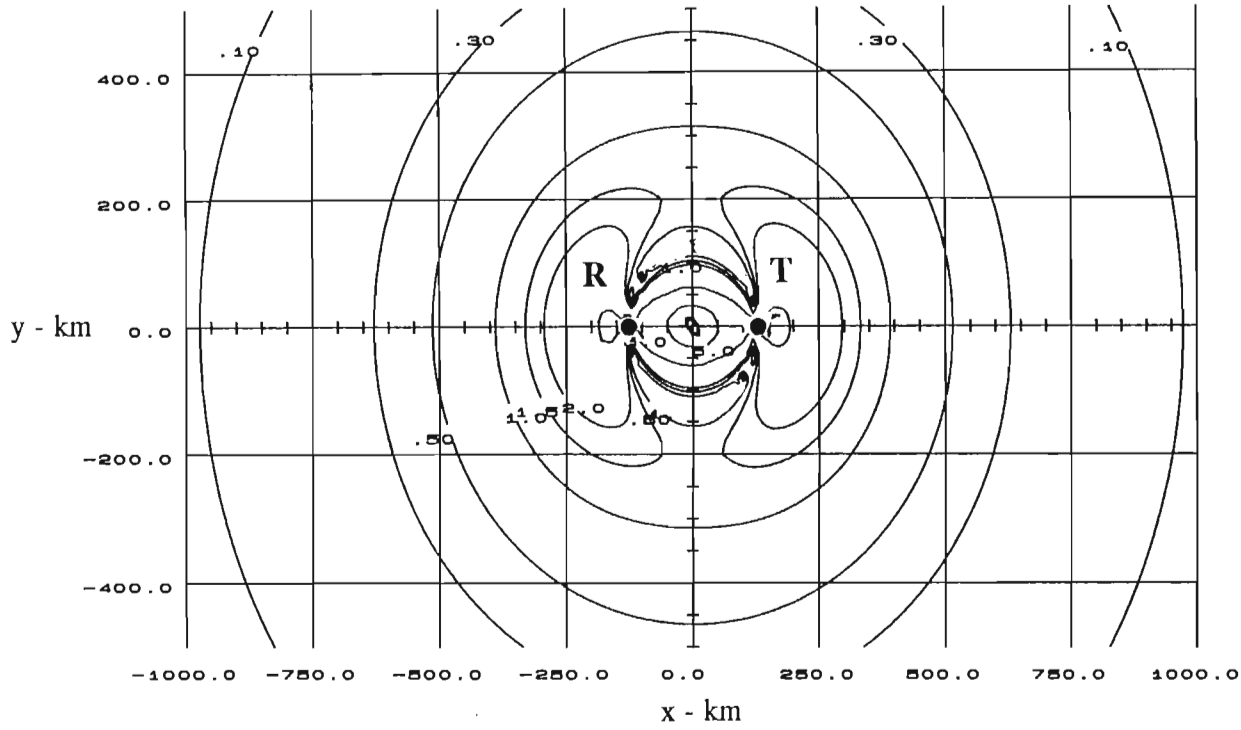

Figure 3-15. Relative Number Of Usable Trails For a 250 Km Path With Both Antennas Horizontally Polarized.

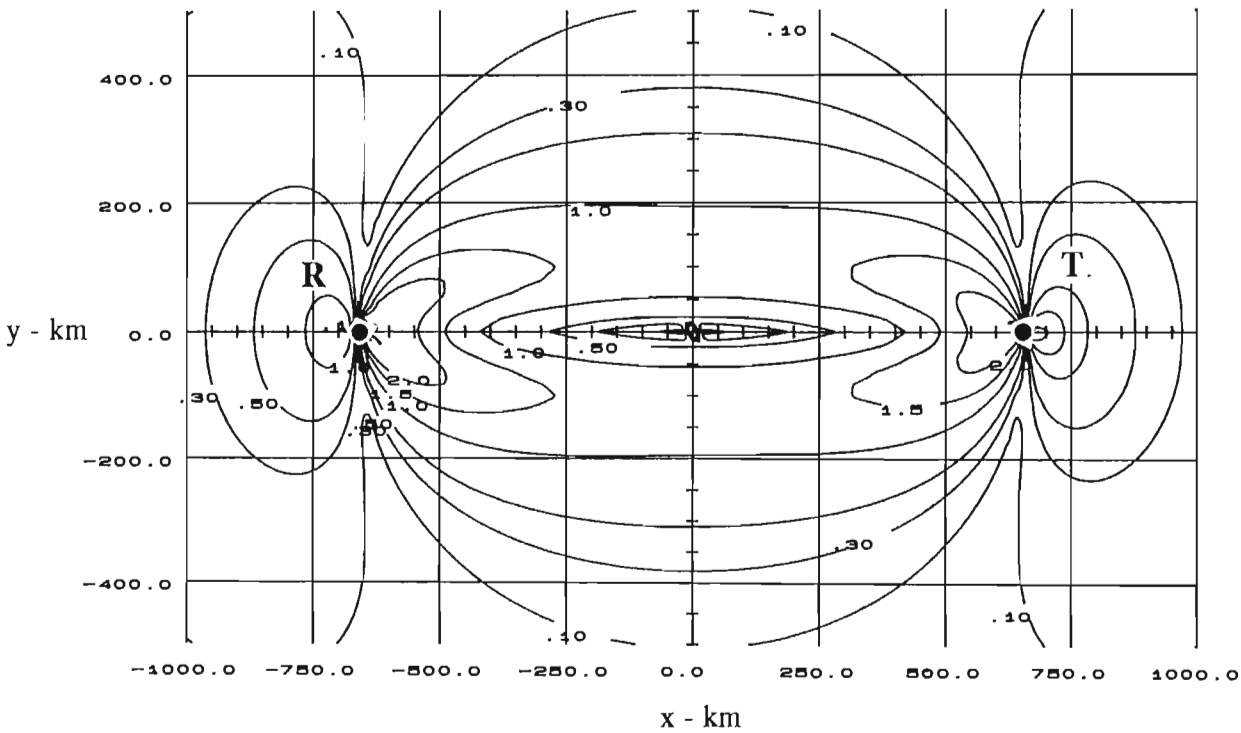

Figure 3-16. Relative Number of Usable Trails For The 1300 Km Path.
T and R mark transmitter and receiver positions.

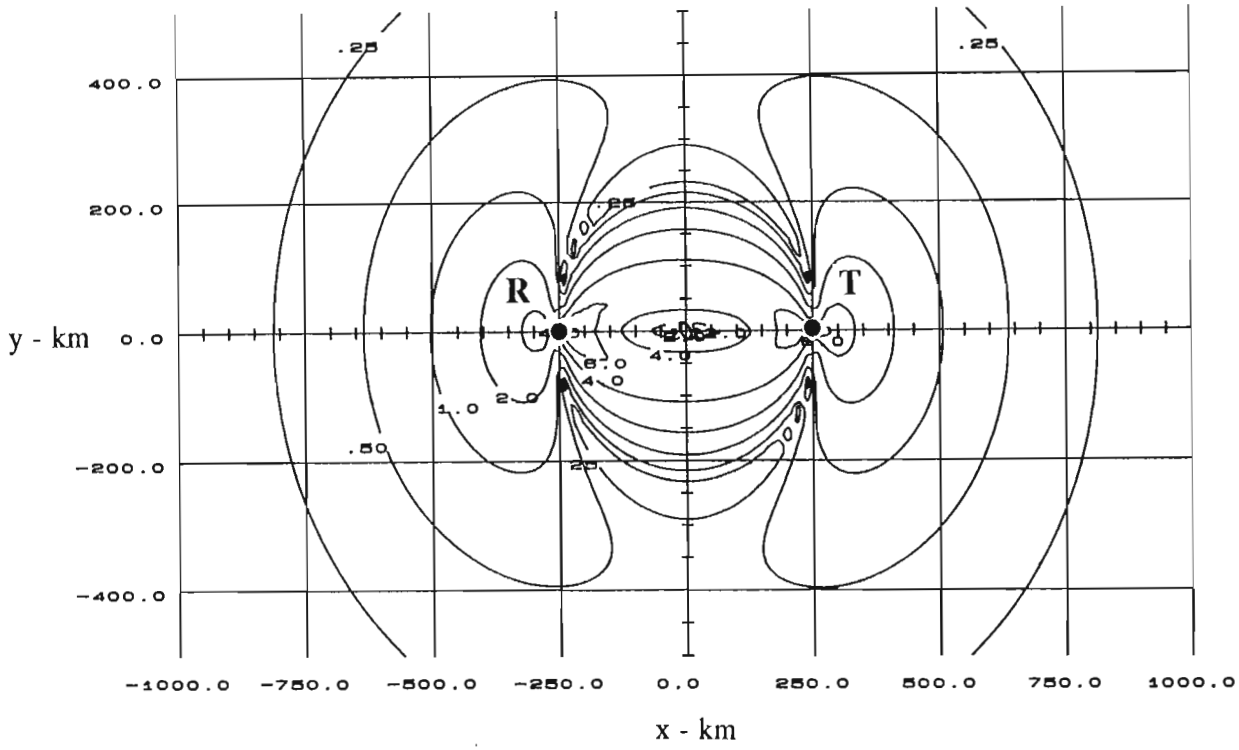

Figure 3-17. Relative Number of Usable Trails For The 500 Km Path.

T and R mark transmitter and receiver positions.

By including the gain factors of the antennas as computed in section 3.5.3, the regions of interest become clearly defined. Figure 3-18 shows the sky regions of interest for the 1300 km path with stacked five element MCC yagis at both ends of the path. Figure 3-19 shows the sky regions of interest for the 500 km path with single eleven element KLM yagis at each end.

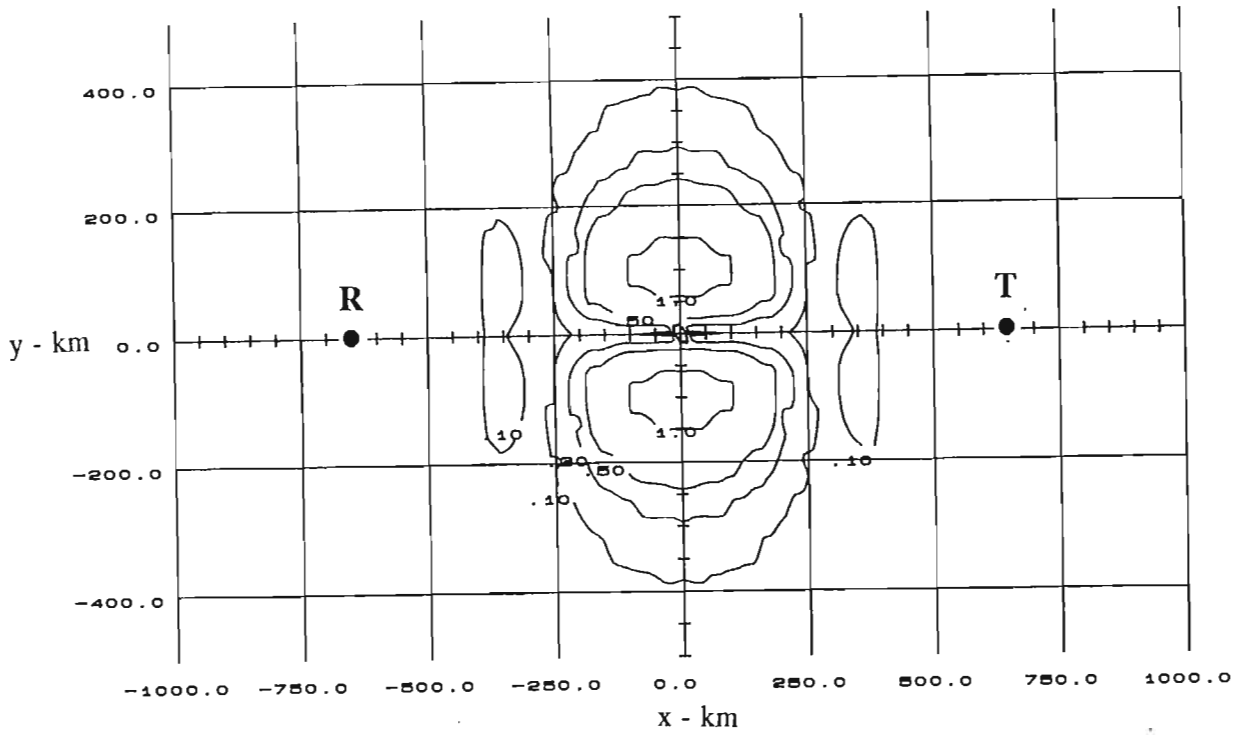

Figure 3-18. Relative Productive Sky Regions For The 1300 Km Path Including Antenna Gain.

T and R mark transmitter and receiver positions.

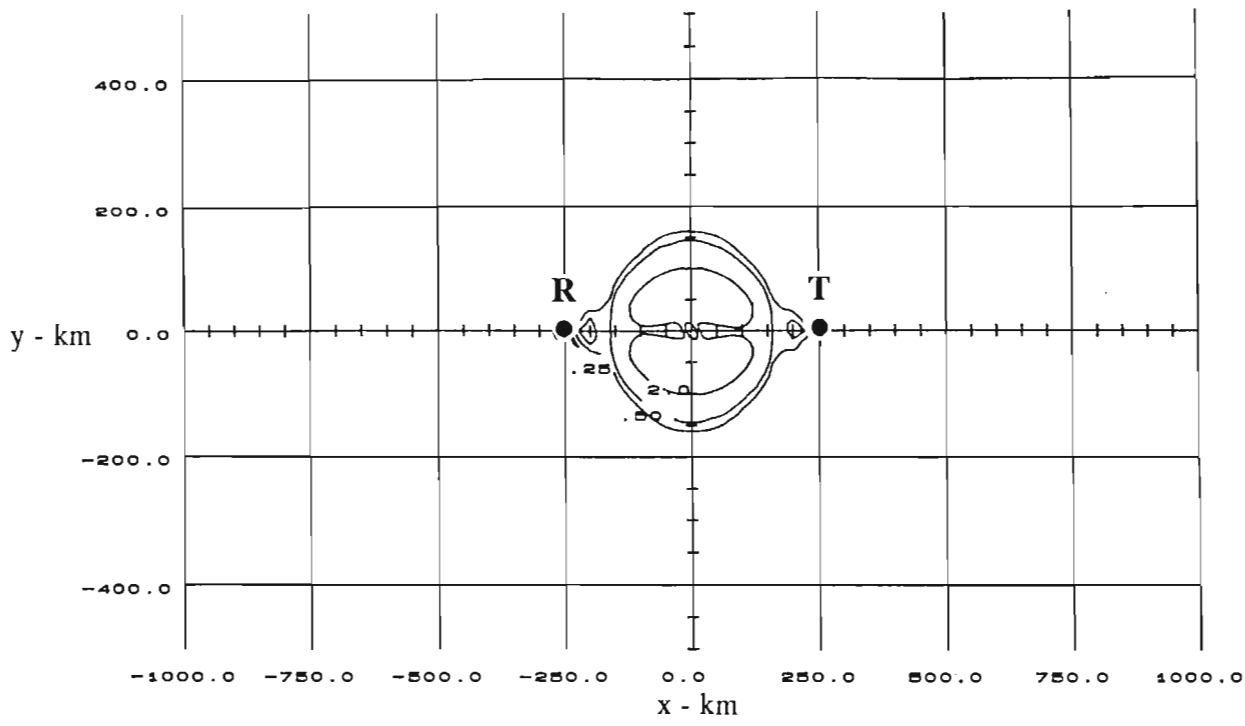

Figure 3-19. Relative Productive Sky Regions For The 500 Km Path Including Antenna Gain.

T and R mark transmitter and receiver positions.

3.5.5 Computing Time Constant

The time constant was defined in section 3.4, the diffusion coefficient discussed in section 3.4.1. The expected time constant sky region plot is shown in figure 3-20 at various heights for the 1300 km path and in figure 3-21 for the 500 km path.

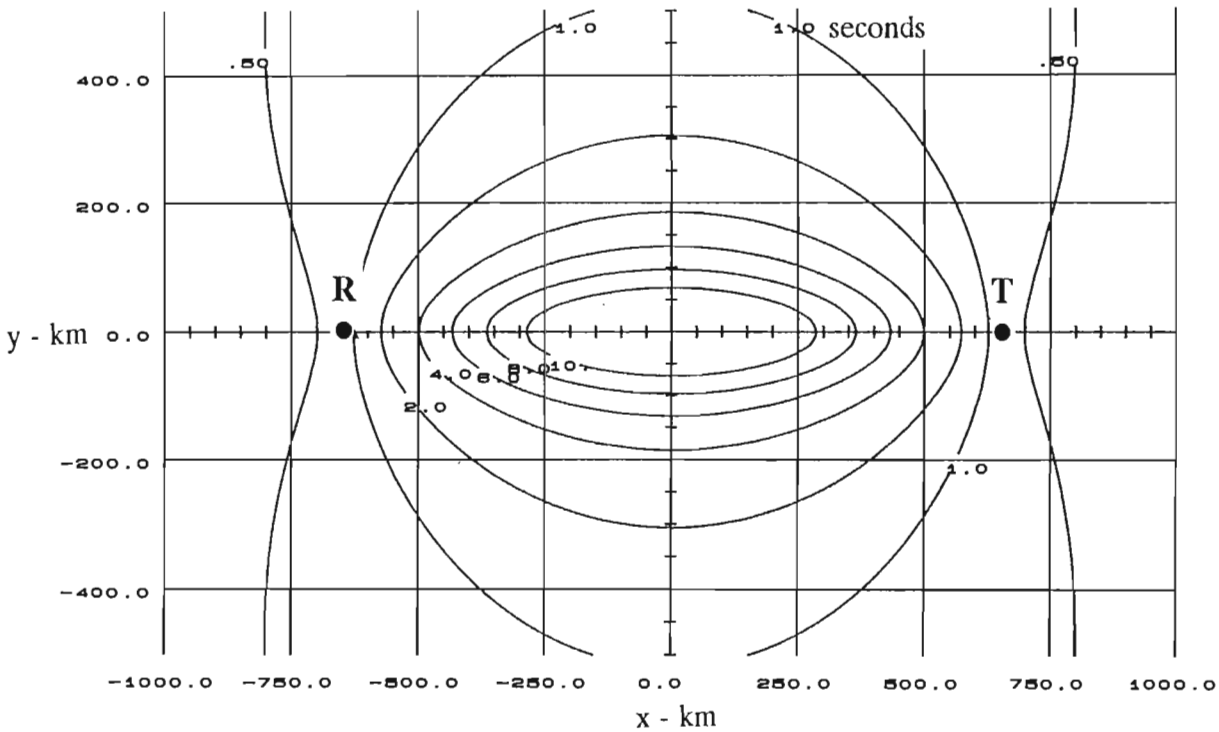

a. Height = 80 km.

Figure 3-20. Time Constant at Different Heights for a 1300 Km Path.

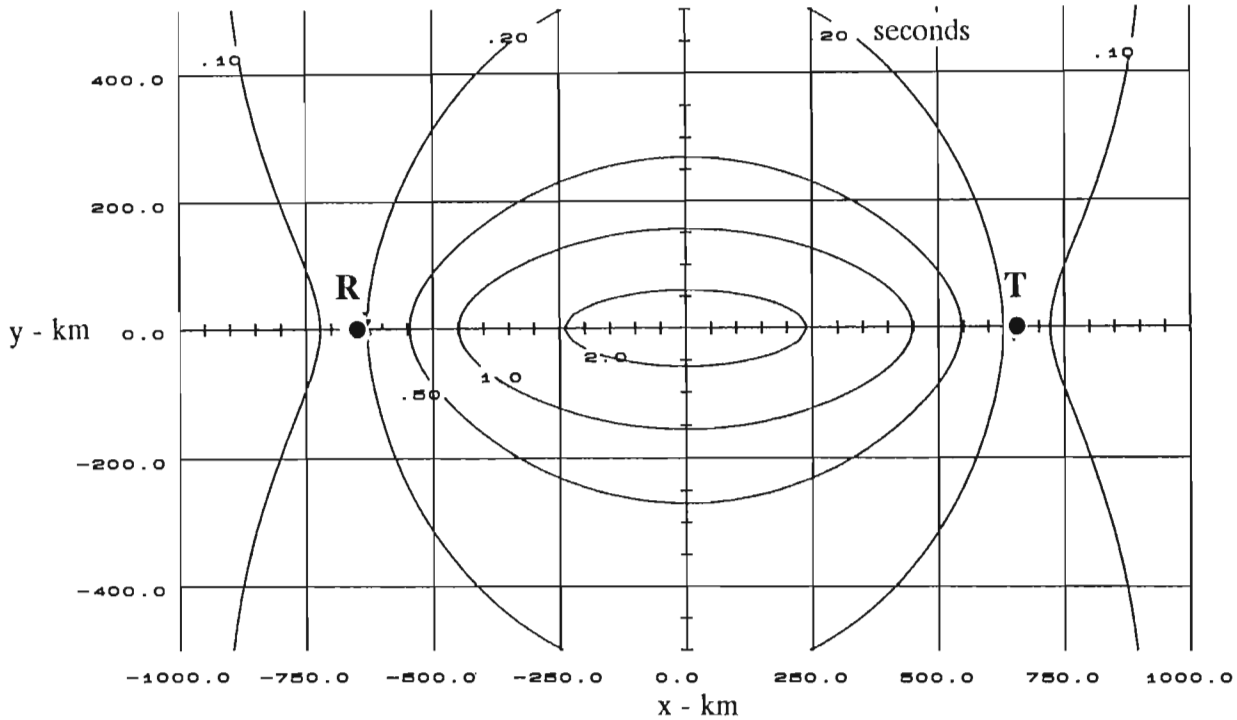

b. Height = 90 km.

Figure 3-20. Time Constant at Different Heights for a 1300 Km Path.

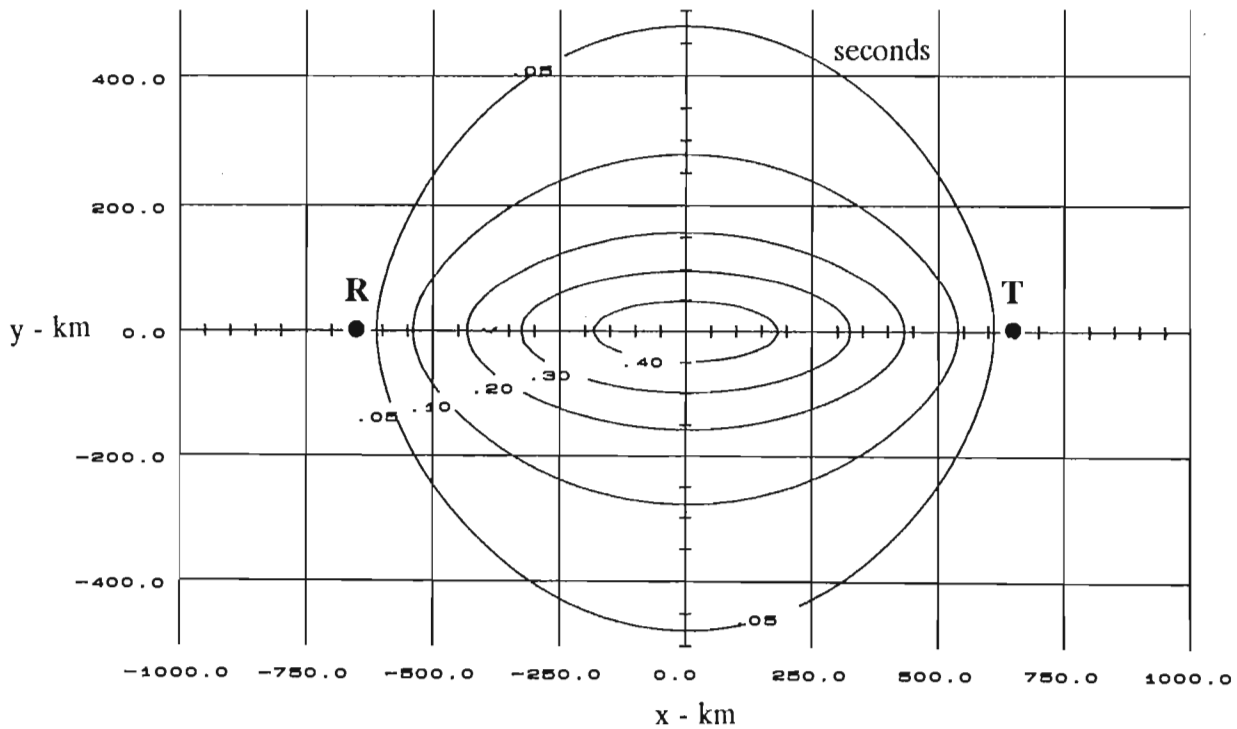

c. Height = 100 km.

Figure 3-20. Time Constant at Different Heights for a 1300 Km Path.

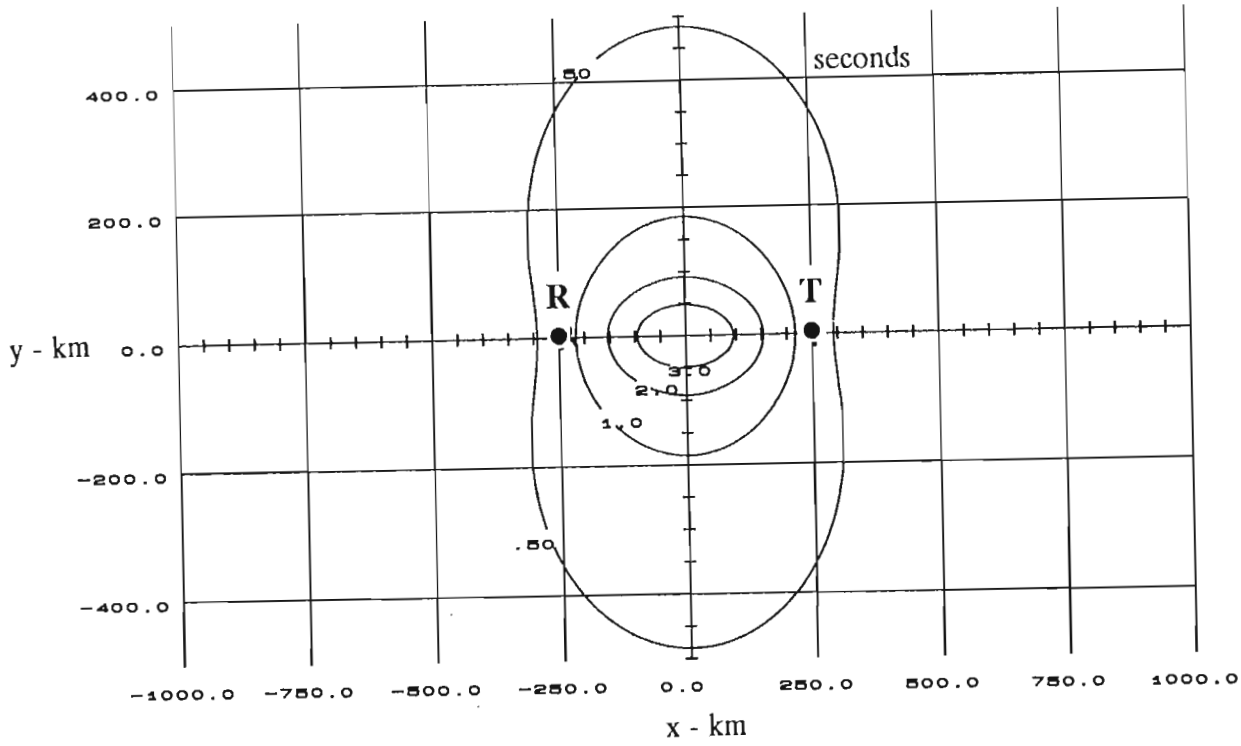

a. Height = 80 km.

Figure 3-21. Time Constant at Different Heights for a 500 Km Path.

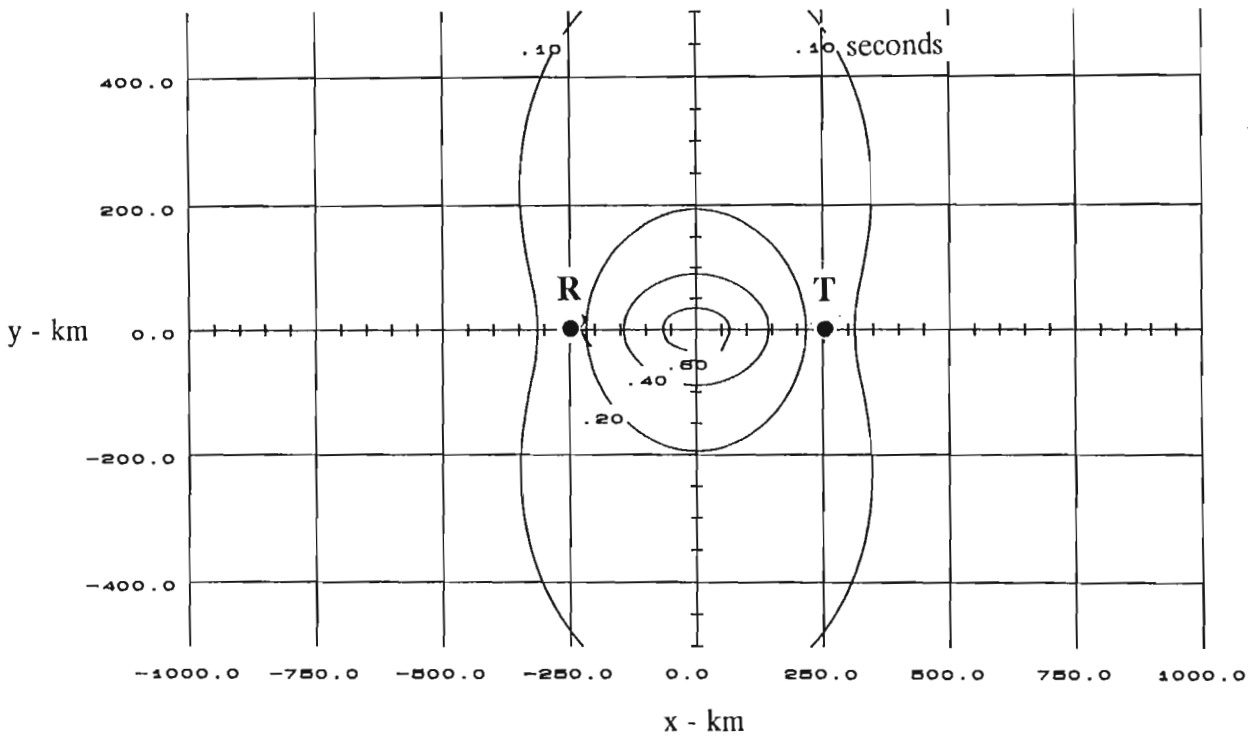

b. Height = 90 km.

Figure 3-21. Time Constant at Different Heights for a 500 Km Path.

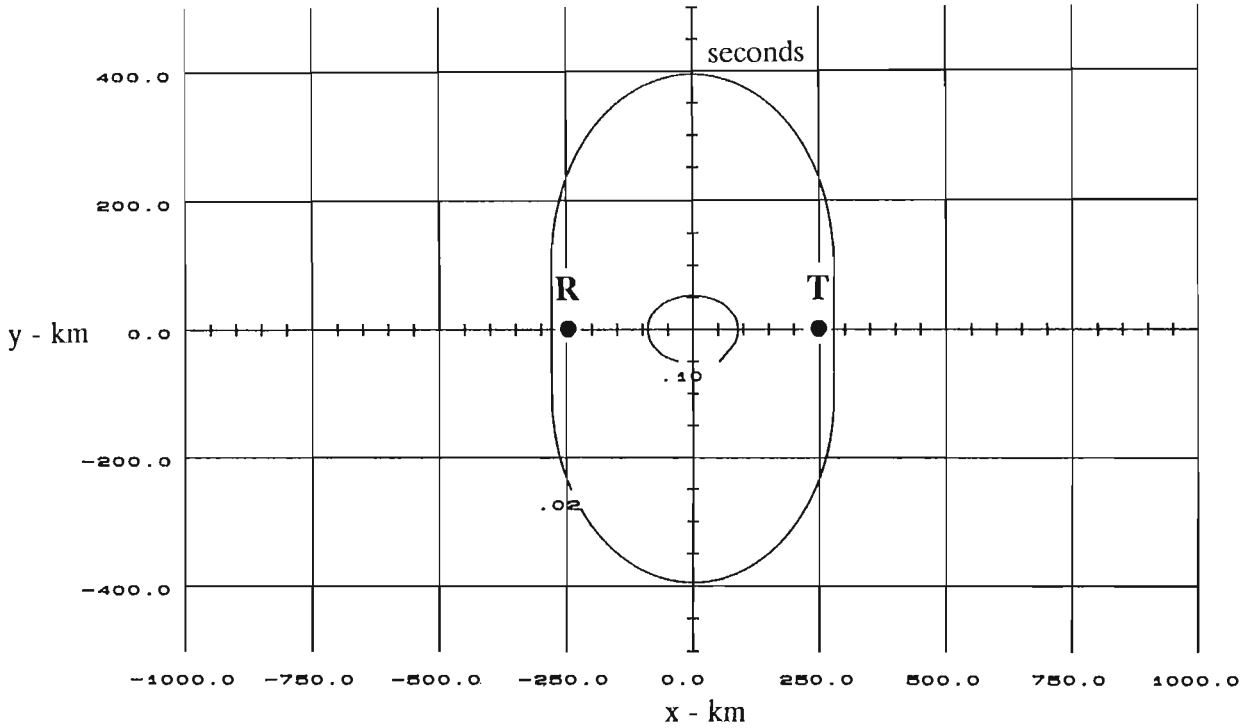

c. Height = 100 km.

Figure 3-21. Time Constant at Different Heights for a 500 Km Path.

Examining the effect of the various contributors to the expected theoretical duration, the diffusion coefficient has as much as a 10:1 effect on the time constant which is entirely due to height variations.

For a 1300 km path with typical antennas, the $\sec^2\phi$ term has a 5:1 effect on the time constant within the antennas beamwidth primarily due to the (x,y) position of the trail. The height variation only has a 5-10% effect in the $\sec^2\phi$ term.

3.5.6 Computing Time Constant Distribution

The time constant distribution was approximated numerically. A frequency histogram was computed for each time constant value by accumulating the probability of detection $p_t(x,y,h)$ over the region where $\tau \le \tau(x,y,h) \le \tau + \Delta\tau$ for each τ. The time constant distribution for heights 90, 96 and 100 km for the 1300 km path reference system are shown in figure 3-22. The time constant distribution for the 1300 km path reference system assuming the normal height distribution given in section 3.4.2 is shown in figure 3-23. For the 500 km path, the predicted time constant distribution at different heights is shown in figure 3-24 and with the normal height distribution in figure 3-25.

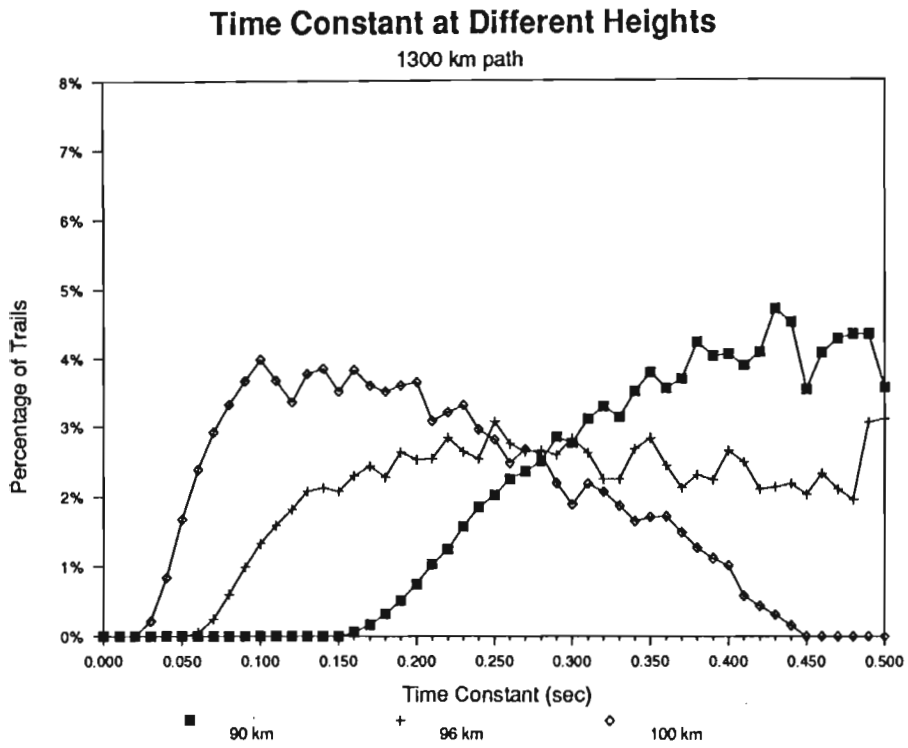

Figure 3-22. Predicted Time Constant Distribution For A 1300 km Path At Different Heights.

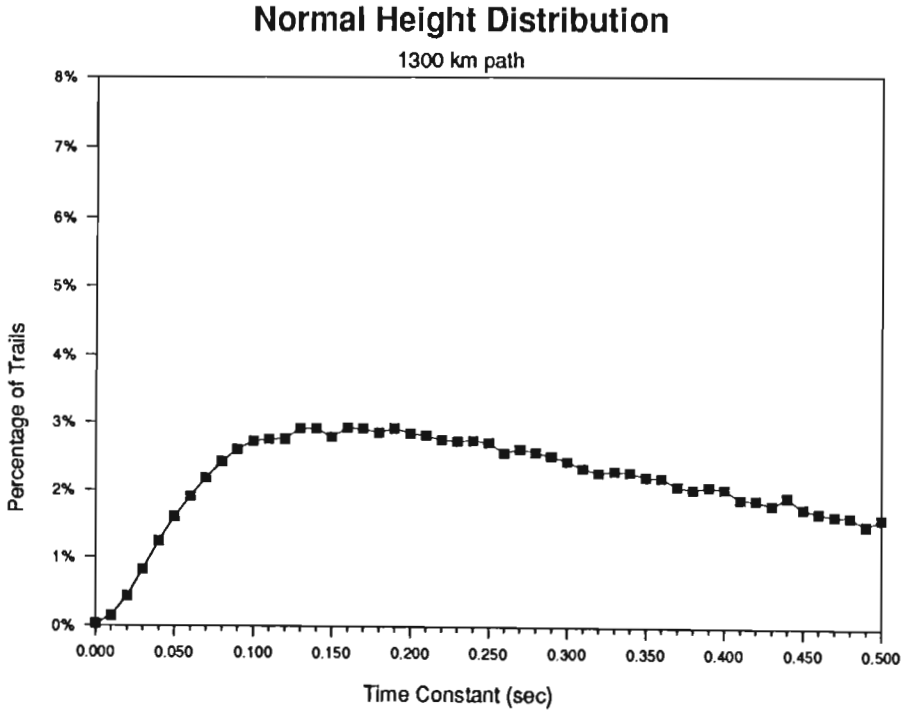

Figure 3-23. Predicted Time Constant Distribution For A 1300 km Path With The Normal Height Distribution.

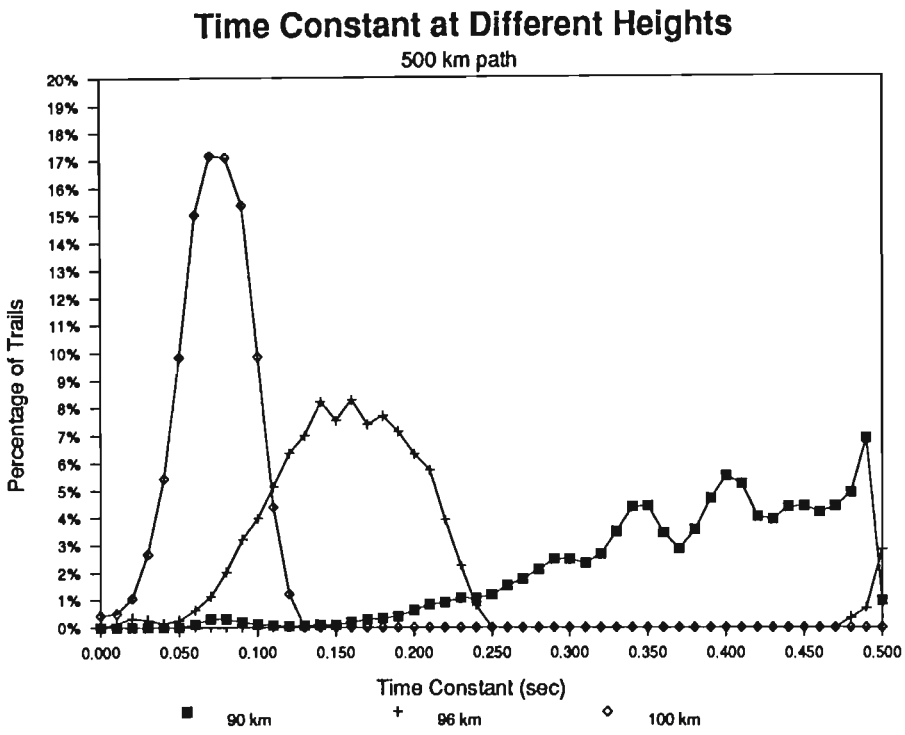

Figure 3-24. Predicted Time Constant Distribution For A 500 km Path At Different Heights.

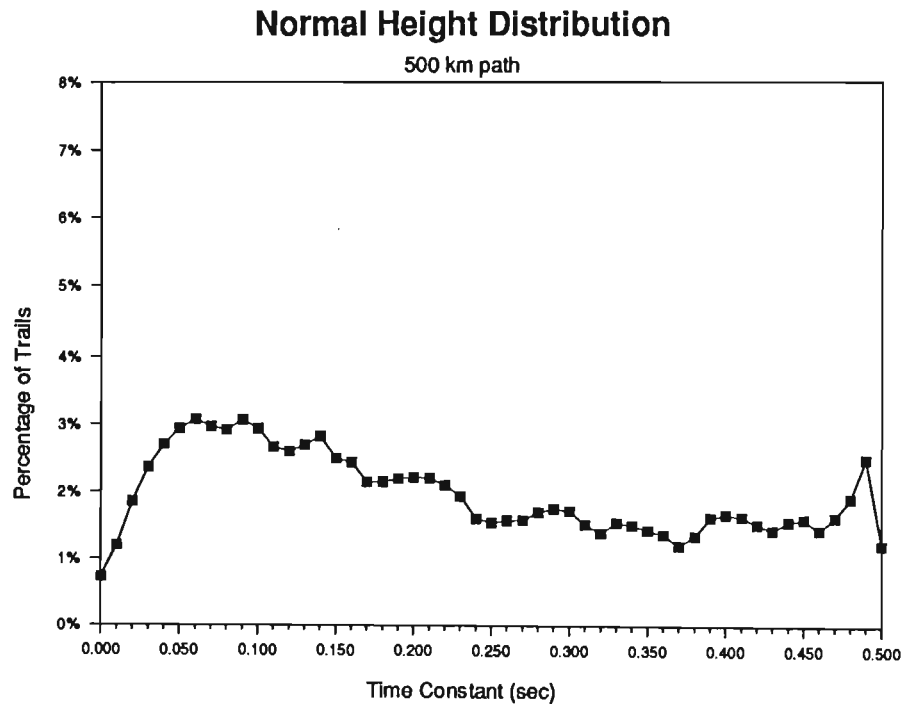

Figure 3-25. Predicted Time Constant Distribution For A 500 km Path With The Normal Height Distribution.

3.6 Measurement of the Duration of Underdense Trails

To verify the predicted duration distribution for underdense trails, the peak signal to duration distribution of the meteor scatter link defined in section 3.2 was measured. A sensitive receiving station and a method for recording and analyzing the signals received was needed.

Because the models used in this thesis only apply to underdense trails, some method of classifying the trails was required. This classification could either take place in real time, or could take place later if sufficient detail was recorded on each trail. The requirement that the full amplitude-time envelope of each meteor trail be recorded for the protocol simulator described in chapter five allows off line classification as well as additional off line processing. A completely analog recording system was rejected because of the large volume of data required as well as the difficulty in processing. Therefore, a high speed digital acquisition and analysis system was used to digitize the envelope of the signal received, analyze the envelope and store it away for future processing. This method had the additional advantage of being able to produce periodic, short term statistics which were useful for observing long term trends such as diurnal and yearly cycles without having to process a huge data base on a trail by trail basis.

3.6.1 Measurement Procedure

With the overall requirements of the measurement system specified, a procedure for measuring the duration distribution can be defined. The design requirements are best met with a high speed digital measurement system augmented with analog front end processing. A system block diagram for the measurement system is shown in figure 3-26. The analog front end processor converts the signal from a linear power scale to a decibel power scale with a log converter. This log output is then filtered to prevent aliasing due to sampling and level adjusted before being presented to the analog to digital converter. Details of the analog and RF sections are reported by Mawrey [Mawrey, 1988].

The digital measurement system is required to digitize the signal level presented by the receiver to determine the instantaneous signal to noise ratio. The current background noise level must therefore be measured to determine the signal to noise ratio. Analog methods of measuring the signal to noise ratio were investigated. Methods such as a dual bandwidth receiver which compared a signal channel to a noise channel were

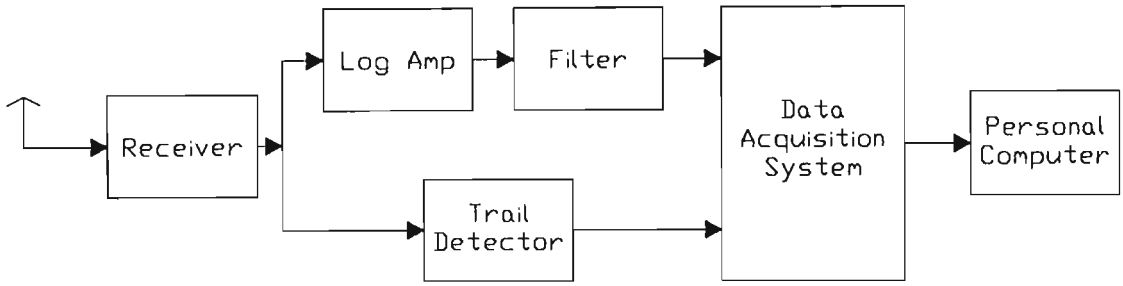

Figure 3-26. Measurement System Component Block Diagram.

discarded due to equipment complexity. Simple analog techniques involving long term averaging of the background noise were rejected because the digital section could perform the same task without adding any additional equipment.

An additional component that was added as the experiment progressed was a valid signal detector. A valid signal detector became necessary when the measurement system became plagued with noise from a local sports field lighting system and from interference during lightning storms. The signal detector worked by sensing the presence of a 1500 Hz tone on the receiver which was tuned 1500 Hz away from the carrier frequency of the transmitter. Whilst this valid signal detector was not able to differentiate between propagation due to meteoric reflections and other forms of propagation, it did allow the rejection of noise spikes.

Once the signal to noise ratio exceeded the minimum usable signal level, the envelope of the trail was captured. Data collection continued until the signal drops below the minimum usable signal level for a predetermined time. The data collection could not be stopped immediately when the signal faded below the minimum usable signal level because of the rapid fading common to non-spectral overdense trails. Once the true end of the trail had been determined, the trail was then analyzed, categorized and stored. This processing took place in the background while the regular sampling of the receiver level continued without interruption. This feature is an improvement over other measurement systems where sampling was disabled during data analysis and storage [Weitzen, 1987].

The background processing for each trail involved measuring the following information:

Table 3-5. Data Measured for Each Trail.

1.	The maximum amplitude.
2.	The total duration.
3.	The waiting time between trails.
4.	The slope of the rising edge of the envelope.
5.	The slope of the decay if the trail is underdense.

The maximum amplitude, total duration, time constant, background noise and waiting time were categorized and stored in histogram form. The maximum amplitude and total duration were cross correlated in a two dimensional histogram. Finally, the trail envelopes are compressed using data compression techniques and stored on disc on the host computer for future processing.

The short term statistics were printed at regular intervals to give a paper record of the measured results and to assist system verification.

3.6.2 Measurement Apparatus

The measurement system used in this thesis was constructed as a team effort. The transmitter was supplied and maintained by the sponsoring company. The antennas were specified by Larsen. The radio receiver and analog systems were developed by Larsen [Larsen] and Mawrey [Mawrey, 1988]. The digital acquisition system, data logging and data processing techniques were developed by the author.

Because no commercial data acquisition and analysis equipment was available to perform the required functions, a custom system was constructed. The Meteor Monitor Unit consists of a Z80 microprocessor with 64K bytes of memory, two serial ports, one parallel printer port, a real time clock and an analog to digital converter as shown in figure 3-27. Initial development started on a STD-BUS based portable computer and resulted in the stand-alone unit shown in figure 3-28. The software for the Meteor Monitor Units was developed using a high level language to implement the real-time multi-tasking operating system, the device I/O drivers, the command interpreter, the data capture task, the data analysis task and the report generating task as shown in figure 3-29. Storage of the envelopes of the trails was produced by connecting a personal computer to the Meteor Monitor Units to save the data to a disc file. Software was developed to change disc

files every hour to reduce the loss of data in case of system failure or the disc becoming full. Additional software was developed to graphically display each trail as it was stored. A sample of the trail by trail data displayed by the Meteor Monitor Unit is shown in table 3-6 and an hourly statistics report shown in table 3-7.

Figure 3-27. Standalone Meteor Monitor Unit.

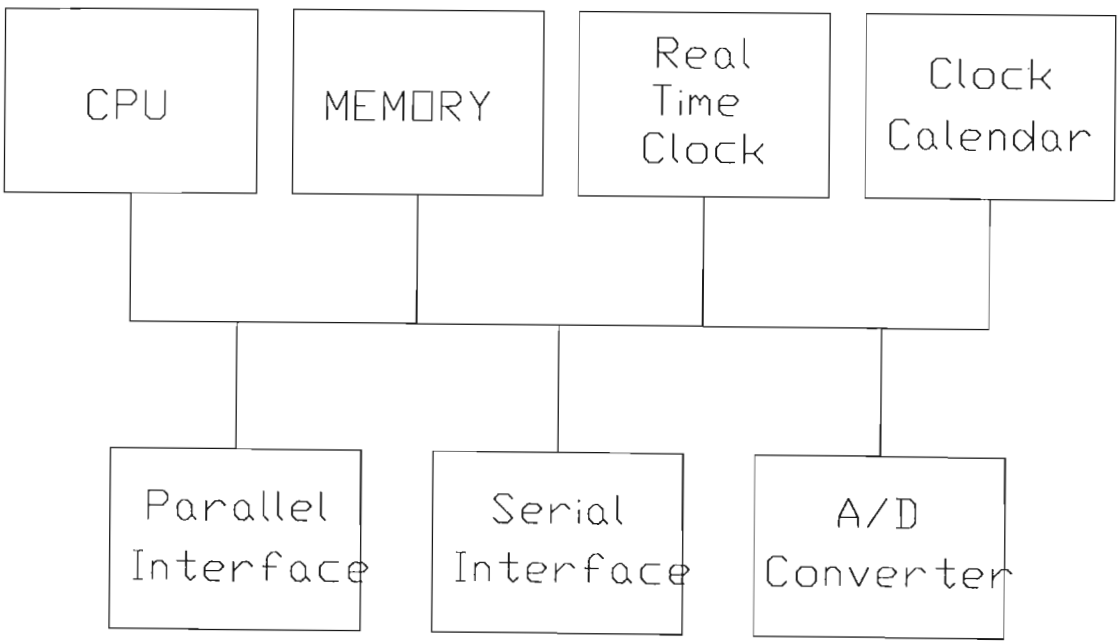

Figure 3-28. Hardware Block Diagram of the Meteor Monitor Unit.

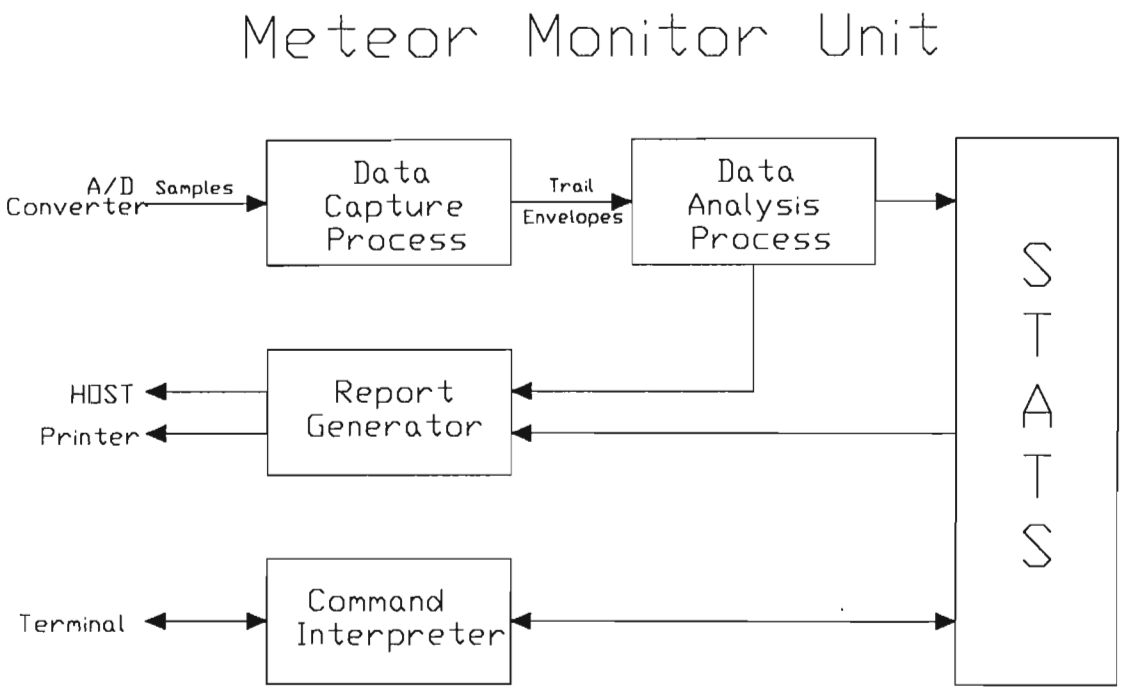

Figure 3-29. Software Block Diagram of the Meteor Monitor Unit.

Table 3-6. Sample Trail by Trail Output from the Meteor Monitor Unit.

Time	Trail id	Duration (sec)	Trail Detect	Peak Signal (dBm)	Time Constant
02:01:19	#707	0.250	0.250	-107(bg+18)	0.076
02:01:30	#708	0.310	0.310	-103(bg+22)	0.095
02:01:40	#709	0.260	0.260	-113(bg+12)	0.706
02:01:45	#710	0.040	0.040	-115(bg+10)	0.031
02:01:48	#711	0.685	0.550	-107(bg+18)	0.031
02:02:00	#712	0.115	0.115	-112(bg+13)	0.122
02:02:03	#713	0.145	0.145	-113(bg+12)	0.086
02:02:07	#714	0.385	0.385	-106(bg+19)	0.125
02:02:09	#715	0.090	0.090	-112(bg+13)	0.083
02:02:14	#716	0.055	0.050	-111(bg+14)	0.083
02:02:32	#717	0.210	0.210	-108(bg+17)	0.107
02:02:41	#718	0.555	0.555	-109(bg+16)	0.107
02:02:42	#719	1.225	1.225	-111(bg+14)	0.107
02:02:46	#720	0.215	0.215	-107(bg+18)	0.084
02:02:53	#721	0.165	0.160	-101(bg+24)	0.035
02:02:59	#722	0.095	0.095	-114(bg+11)	0.136
02:03:03	#723	0.130	0.130	-111(bg+14)	0.109
02:03:05	#724	0.135	0.135	-108(bg+17)	0.073
02:03:09	#725	0.030	0.025	-112(bg+13)	0.073
02:03:23	#726	0.090	0.090	-112(bg+13)	0.036
02:03:32	#727	0.090	0.090	-112(bg+13)	0.077
02:03:39	#728	0.130	0.130	-112(bg+13)	0.147
02:03:44	#729	0.115	0.115	-109(bg+16)	0.050
02:03:47	#730	0.040	0.040	-113(bg+12)	0.050
02:03:50	#731	0.110	0.110	-109(bg+16)	0.057
02:03:55	#732	0.110	0.110	-110(bg+15)	0.086
02:04:14	#733	0.175	0.175	-111(bg+14)	0.126
02:04:27	#734	0.365	0.365	-104(bg+21)	0.149
02:04:39	#735	0.695	0.685	-95(bg+30)	0.056
02:04:41	#736	0.050	0.050	-114(bg+11)	0.056
02:04:46	#737	0.395	0.395	-108(bg+17)	0.148
02:04:55	#738	0.435	0.435	-99(bg+26)	0.084
02:05:13	#739	0.320	0.320	-111(bg+14)	0.463

Table 3-7. Sample Hourly Statistics from Meteor Monitor Unit.

Meteor summary for file cmd248.02
Number of trails = 564 with 0 noise spikes, bg = -125.
Trail duration = 232.720 sec of which 229.510 sec had trail detect.

Usable time distribution is:

bg+6	bg+9	bg+12	bg+15
231.	214.	142.	85.3

Number qualified = 132 with average tc = 109.013 mSec.

10	20	30	40	50	60	70	80	90	100	110	120	130	140	150
1	3	4	7	14	9	15	8	12	7	8	9	4	6	25

Average duration = 412.6 mSec, distribution is:

0.05	0.10	0.15	0.2	0.3	0.4	0.5	0.6	0.7	0.8	0.9	1	2.5	5	10
188	81	54	57	43	20	23	16	11	9	9	42	8	2	1

Average signal = -109.0 dBm , distribution is:

-124	-121	-118	-115	-112	-109	-106	-103	-100	-97	-94	-91	-85	-80	-70
0	0	10	222	143	77	45	38	13	9	4	3	0	0	0

Average wait time = 6.5 Sec, distribution is:

0.1	0.5	1	2	5	10	20	40	60	120	240	360
1	66	94	166	119	95	20	2	0	0	0	0

Average noise = -125 dBm , distribution is:

5	6	7	8	9	10	11	12	13	14	15	16	17	18	19
0	0	0	0	0	0	0	0	0	0	564	0	0	0	0

	0.05	0.10	0.15	0.2	0.3	0.4	0.5	0.6	0.7	0.8	0.9	1	2.5	5	10
>-124(0):	0	0	0	0	0	0	0	0	0	0	0	0	0	0	0
>-121(0):	0	0	0	0	0	0	0	0	0	0	0	0	0	0	0
>-118(10):	10	0	0	0	0	0	0	0	0	0	0	0	0	0	0
>-115(222):	135	40	15	13	9	5	1	1	0	0	1	2	0	0	0
>-112(143):	38	31	15	22	9	4	8	3	0	2	2	9	0	0	0
>-109(77):	5	7	14	17	8	7	2	6	5	3	1	2	0	0	0
>-106(45):	0	2	4	3	10	1	2	3	2	1	3	12	2	0	0
>-103(38):	0	1	5	2	5	1	7	2	3	2	1	6	3	0	0
>-100(13):	0	0	1	0	2	2	0	0	1	1	0	4	1	1	0
>-97 (9):	0	0	0	0	0	0	3	1	0	0	0	4	1	0	0
>-94 (4):	0	0	0	0	0	0	0	0	0	0	1	2	1	0	0
>-91 (3):	0	0	0	0	0	0	0	0	0	0	0	1	0	1	1
>-85 (0):	0	0	0	0	0	0	0	0	0	0	0	0	0	0	0
>-80 (0):	0	0	0	0	0	0	0	0	0	0	0	0	0	0	0
>-70 (0):	0	0	0	0	0	0	0	0	0	0	0	0	0	0	0

3.6.3 Measurement Results

Initial equipment verification took place with a 500 watt transmitter in Pretoria and the monitoring equipment in a converted shipping container in Durban. The Durban monitoring site suffered from severe man made noise interference and lacked an adequate Fresnel zone for ground reflection prediction. It was used for initial development and verification for convenience. Once the equipment was verified, an alternate site was desired approximately 1000 km from the transmitter.

A portable monitoring system was assembled in a converted caravan and a mobile fifty foot crank up tower was borrowed. A site was selected as far away from the transmit site as was conveniently possible on the southern tip of Africa. The site was selected for a flat first Fresnel zone, low horizon and low man made noise levels. The site selected has a clear first Fresnel zone, a one degree horizon and was galactic noise limited for most of the experiment duration[1]. Photographs of the site, the portable monitoring station, the assembled equipment and the receiving antenna are shown in figures 3-31 through 3-33.

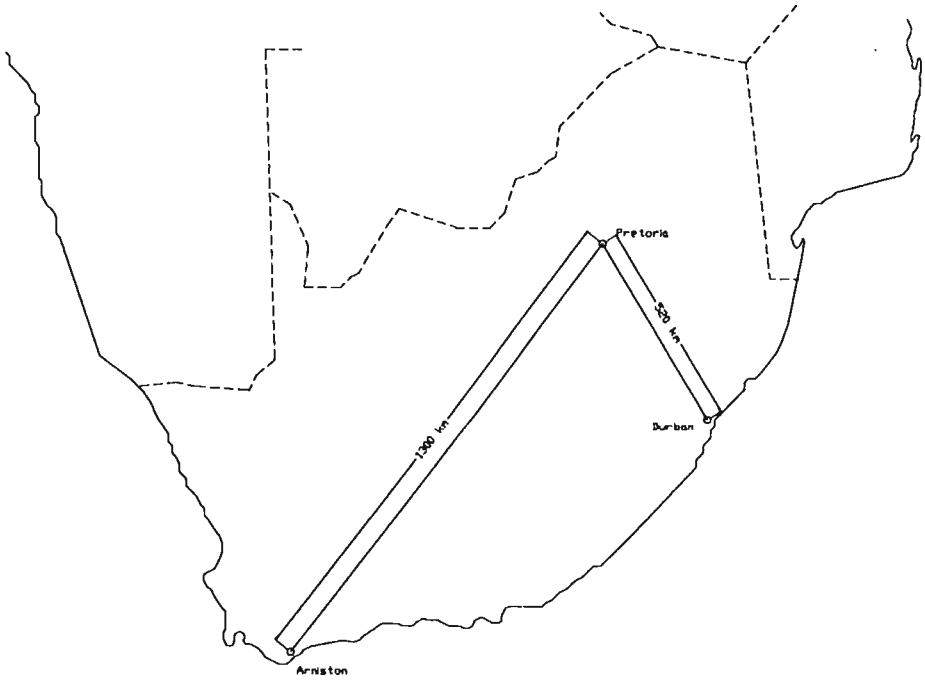

Figure 3-30. Map of Experiment Region.

1 A change in weather caused power line noise to develop during one part of the experiment.

Figure 3-31. Photograph of Remote Monitoring Site.

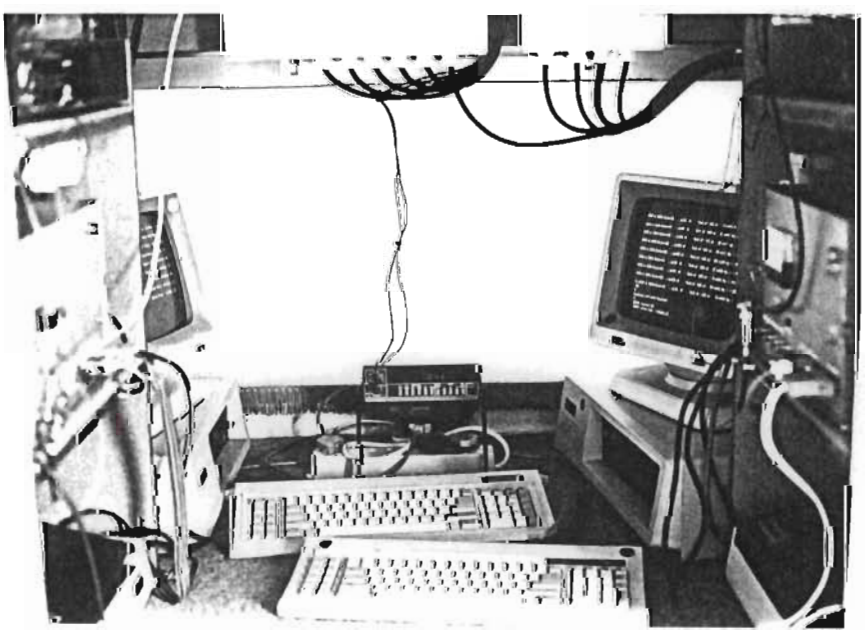

Figure 3-32. Photograph of Portable Monitoring Station.

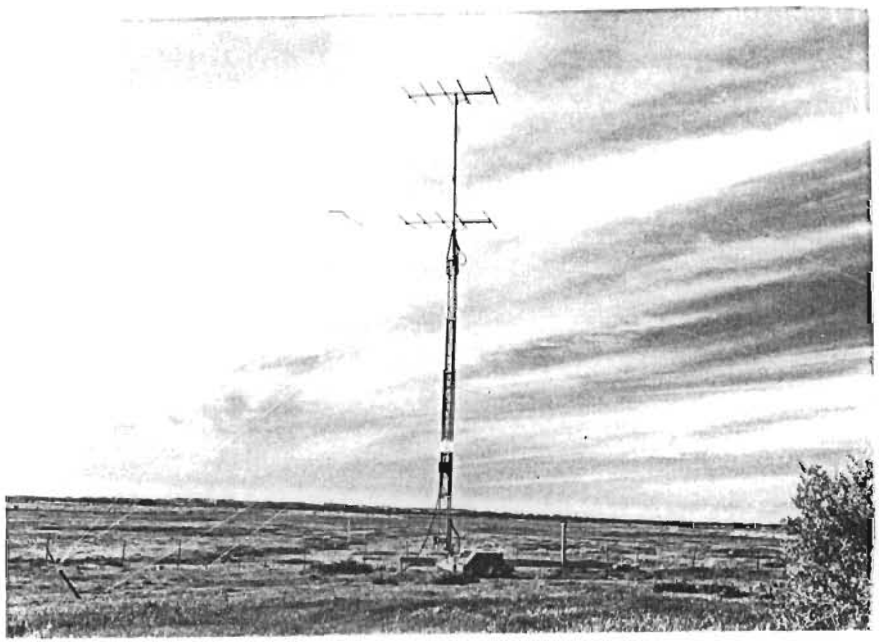

Figure 3-33. Photograph of Receiving Antenna Configuration.

A total of 91647 trails were captured in 212 hours of data from 28-August-1987 to 7-September-1987. The diurnal cycle for this measurement is shown in figure 3-34. The overall peak signal and duration distributions are shown in figures 3-35 and 3-36. The exponential shape of the peak signal and duration distribution are as expected by theory.

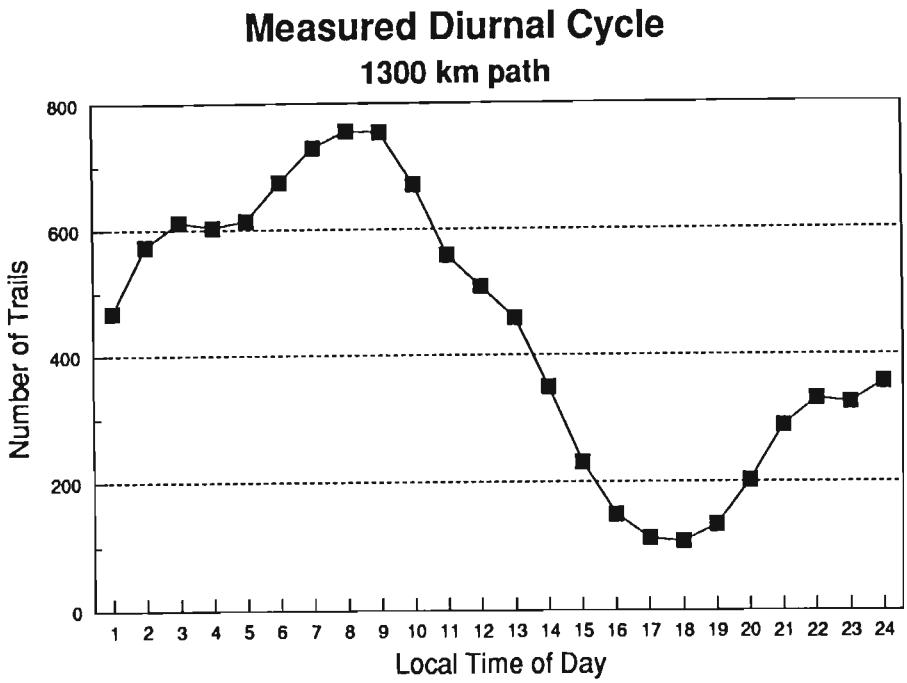

Figure 3-34. Measured Diurnal Cycle for Remote Experiment.

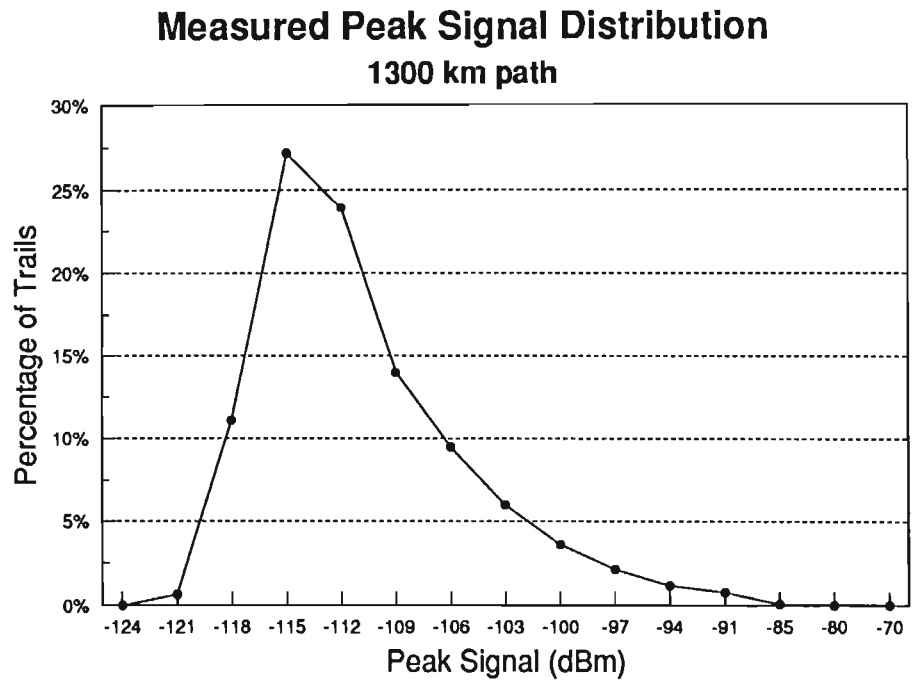

Figure 3-35. Measured Peak Signal Distribution for Remote Experiment.

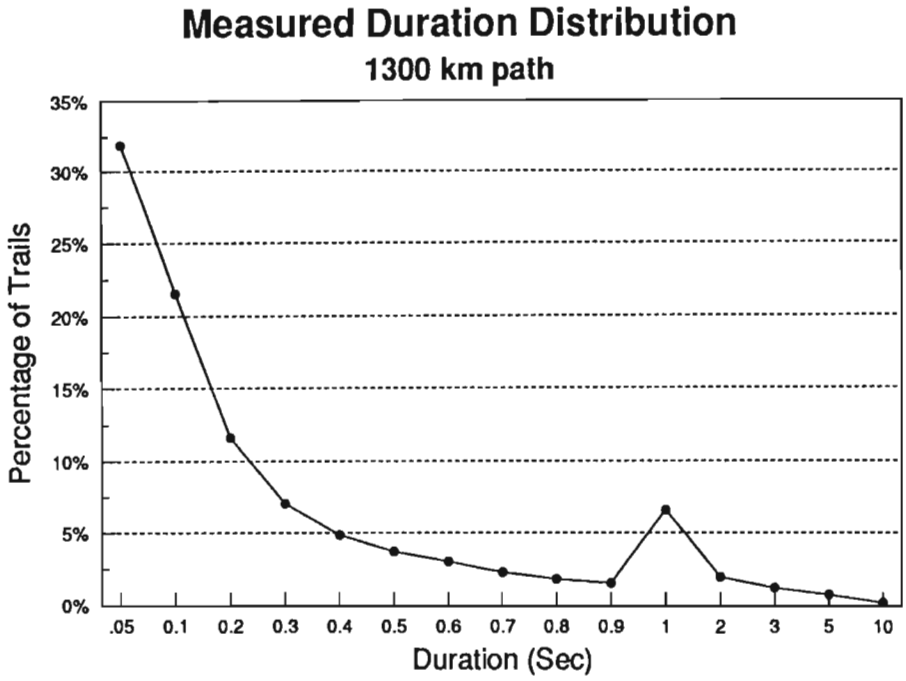

Figure 3-36. Measured Duration Distribution for Remote Experiment.

Subsequent to the remote experiment, permission was obtained to use the sports field of an adjacent school as an antenna range. This site was within cable range of the converted container and had a marginally acceptable first Fresnel zone[1]. The antenna configuration and converted container are shown in figures 3-37 and 3-38. A total of 24843 trails were captured in 221 hours of data from 5-October-1987 to 16-October-1987. The diurnal cycle for this data is shown in figure 3-39. Subsequent to that experiment, a total of 110061 trails were captured between 4-December-1987 and 31-December-1987.

1 The field was flat for 40 meters in the direction of the transmitter. The first Fresnel zone at 50 MHz for a single antenna 3m above the ground covers an elliptic region from the antenna to 45 meters from the antenna with a maximum width of 15 meters.

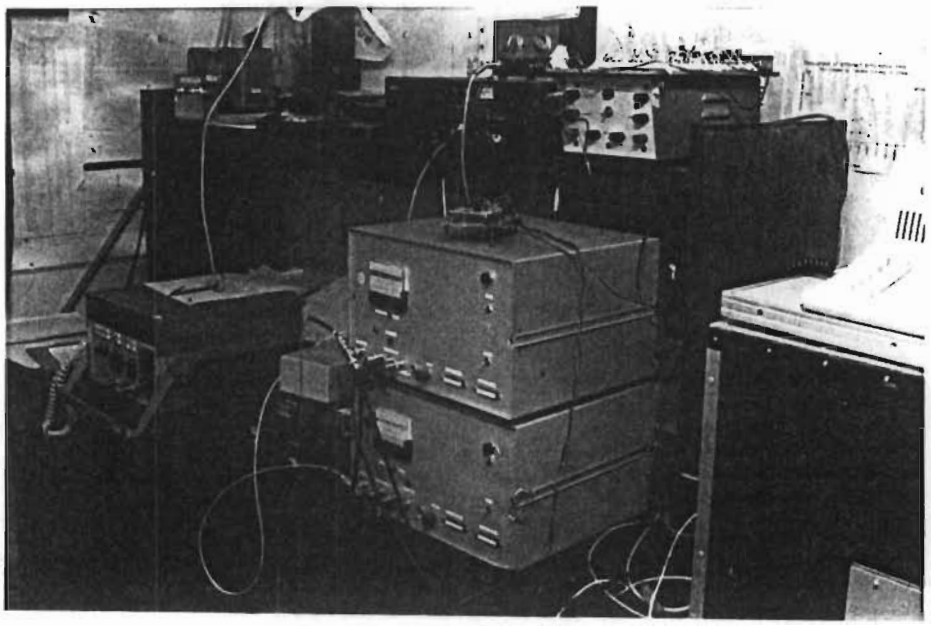

Figure 3-37. Photograph of Durban Monitoring Station.

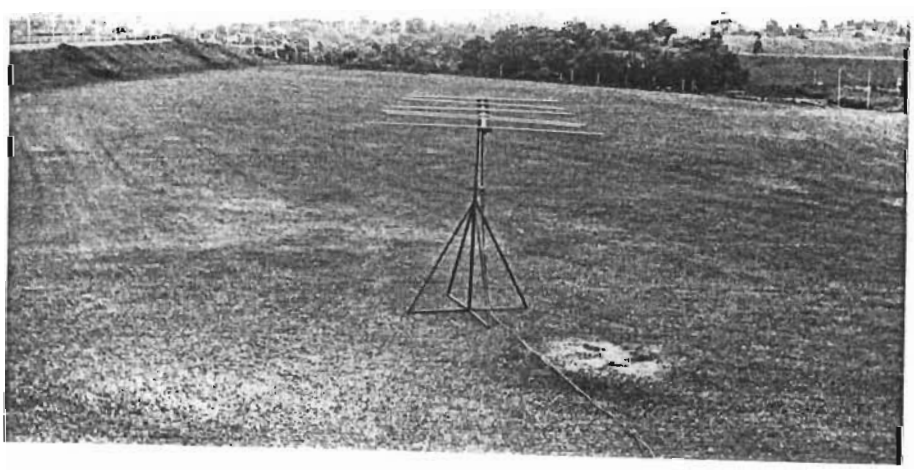

Figure 3-38. Photograph of Durban Antenna Configuration.

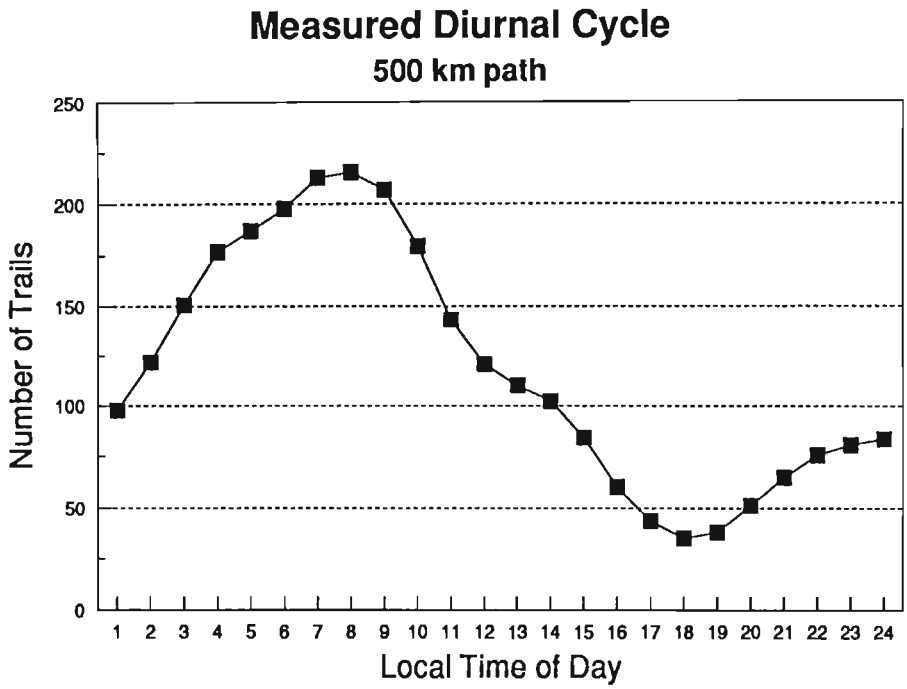

Figure 3-39. Measured Diurnal Cycle for Durban Experiment.

3.7 Comparison of Measured Data to Predicted Duration Distribution

The theoretical investigation used in this thesis only applies to underdense trails. It is therefore necessary to restrict the data analysis to underdense trails. Baggaley [Baggaley, 1981], working with backscatter measurements, specified the following criterion for a trail to be underdense:

a. The rise time (trail formation time) must be less than 0.1 second.

b. There must be no observed body doppler.

c. There must be a linear correlation coefficient greater than 0.90 in the log echo amplitude to time characteristic.

Webb [Webb, 1981], working with simultaneous forward scatter and backscatter, noted that:

d. The first 25% of the trail after the initial peak must be ignored in the linear correlation to avoid resonance effects.

e. Any envelope after 0.3 seconds must be ignored in the linear correlation to avoid confusion due to the formation of multiple reflection points.

The measurement system used for this experiment recorded the log of the amplitude but not frequency or phase. Therefore, it is not possible to determine whether or not any body doppler was present. The selection criterion used in this analysis is:

1. Linear correlation coefficient greater than 0.90 in the log amplitude to time characteristic for the portion of the trail from 25 mSec past the initial peak to 0.3 seconds or the end of the trail whichever is less.

2. Trail duration greater than 0.1 second.

3. Ratio of trail formation time to time constant less than 0.8.

4. Trail formation time less than 0.2 second.

A maximum trail formation time of 0.2 second was used in this analysis instead of the 0.1 second limit used by Baggaley because of the longer trail formation time for forward scatter. The trail formation time is proportional to the length of the first Fresnel zone of the reflecting ionized column as described in section 3.4.4 which is proportional to $\sec\phi$. For radar (or backscatter), $\sec\phi = 1$. For a 500 km path, $\sec\phi$ has a maximum of about 2.7 at the center of the path, but for a 1300 km path, $\sec\phi$ has a maximum of about

6 at the center of the path. In the region of interest for the 1300 km path, the trail formation time varies between 0.1 second and 0.33 second. Thus the measurement of the time constant in the central region will be difficult due to the length of the trail formation time compared to the duration past which multiple path reflections become a problem. An additional problem is the measurement of the trail formation time. Although the end of the trail formation time is easily detected, the beginning is not. For this analysis, the interval from the time the signal exceeds 9 dB above the background noise level until the peak amplitude is achieved is taken to be the trail formation time. The true trail formation time will be larger.

For each trail selected, the time constant was computed by determining the slope (m) of a least squares line through the log amplitude to time data. The same restrictions on which portions of the envelope were to be used were placed on the slope determination as were placed on the linear correlation computation. From the slope of the regression line, the time constant was found by differentiating the dB value of equation (3.8) with respect to time and solving for the time constant

$$m = \frac{d}{dt} 10 \log P_R(t) = \frac{d}{dt} 10 \log \left[A \cdot \exp \frac{-2t}{\tau} \right] \approx \frac{-8.343}{\tau} \tag{3.37}$$

hence

$$\tau = \frac{-8.343}{m} \tag{3.38}$$

A three day sample was used for the verification process. Of the 25349 envelopes recorded during the sample period, one was rejected as a noise spike, an additional 15449 were rejected because the linear correlation coefficient was less than 0.90, an additional 2285 were rejected because their duration was less than 0.1 second, an additional 2806 were rejected because the ratio of the trail formation period to time constant was greater than 0.8 and a further 4 were rejected because their trail formation was greater than 0.2 second. This left a sample set of 4804 typical underdense trails. Although only 19% of the trails were accepted as typical underdense trails, the stringent selection criterion applied rejected many non-perfect underdense trails.

This 19% compares favorably with early work by Hawkins [Hawkins and Brown, 1967] where only 15% of the trails recorded were classified as having near ideal rise shapes and ideal middle shapes. More sophisticated classification techniques [Weitzen and Tolman, 1986] could be used to identify the other types of propagation recorded by the measurement system. Audio observation of the received signal observed periods of slow, periodic fading typical of ionospheric scatter propagation. These events would be recorded by the measurement system, but would not be classified as underdense trails due to their rounded shape.

Sample envelopes of underdense trails are shown in figure 3-40. The regression line is included to show the slope determined by this technique. Note that resonance effects and multiple reflections occur in some trails and the regression line plots a good fit to the extrapolated slope.

The distribution of time constants for the underdense trails was computed and is shown in figure 3-41. The diurnal variation in the number of underdense trails and the diurnal variation in the average time constant are shown in figures 3-42 and 3-43. The diurnal variation in the number of underdense trails follows the same shape as the diurnal cycle for all trails shown in section 3.6.3. The diurnal cycle in time constants peaks at 6 PM local time as expected, however the minimum occurs several hours later than predicted by simple theory. This could be explained as the result of taking all the data from one time of year.

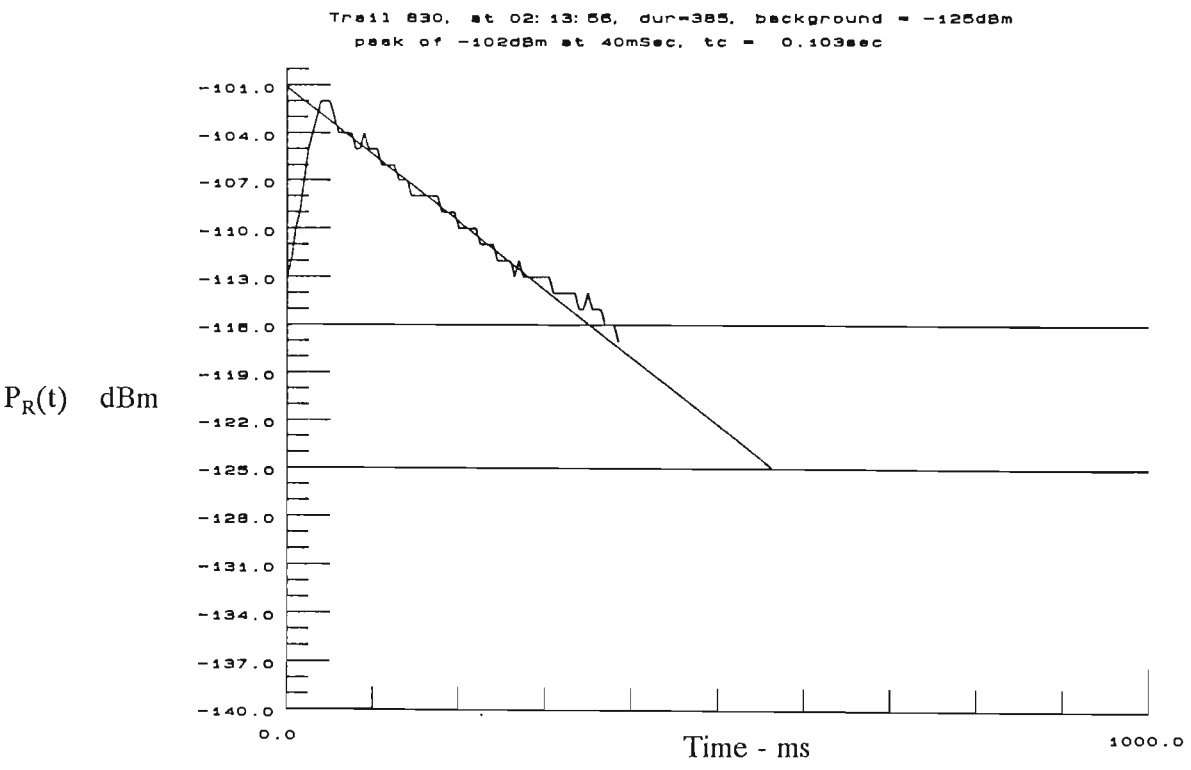

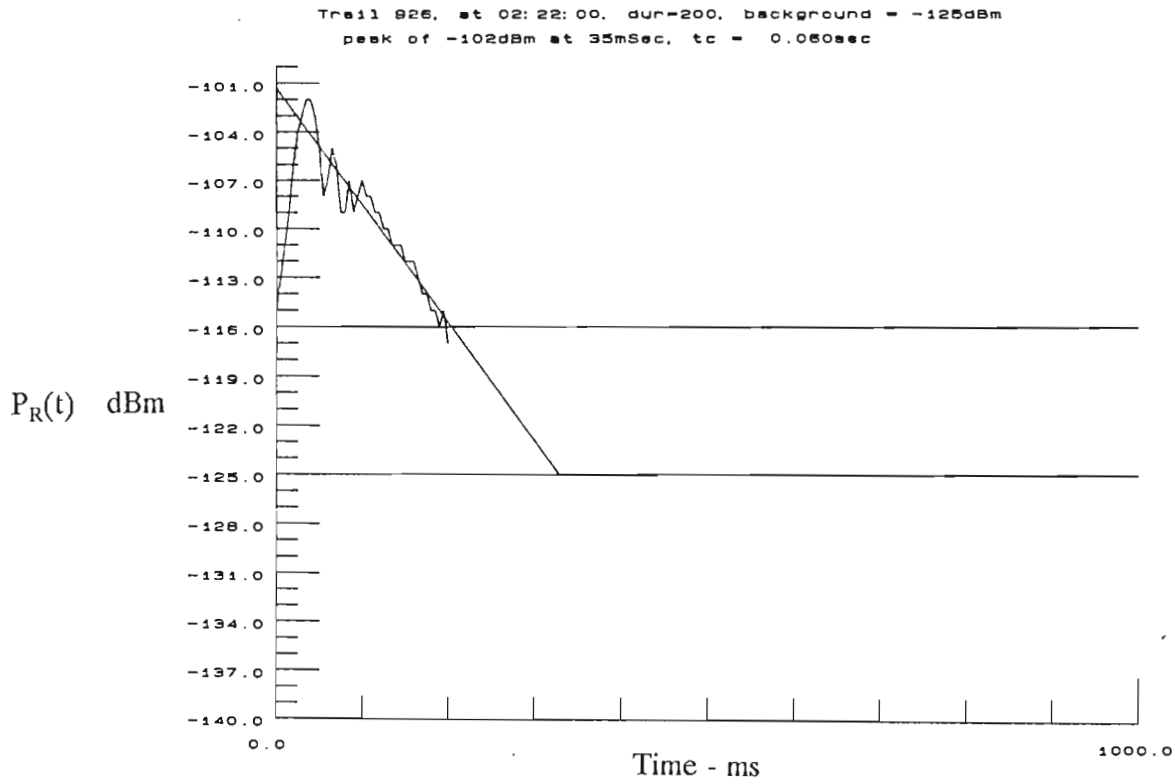

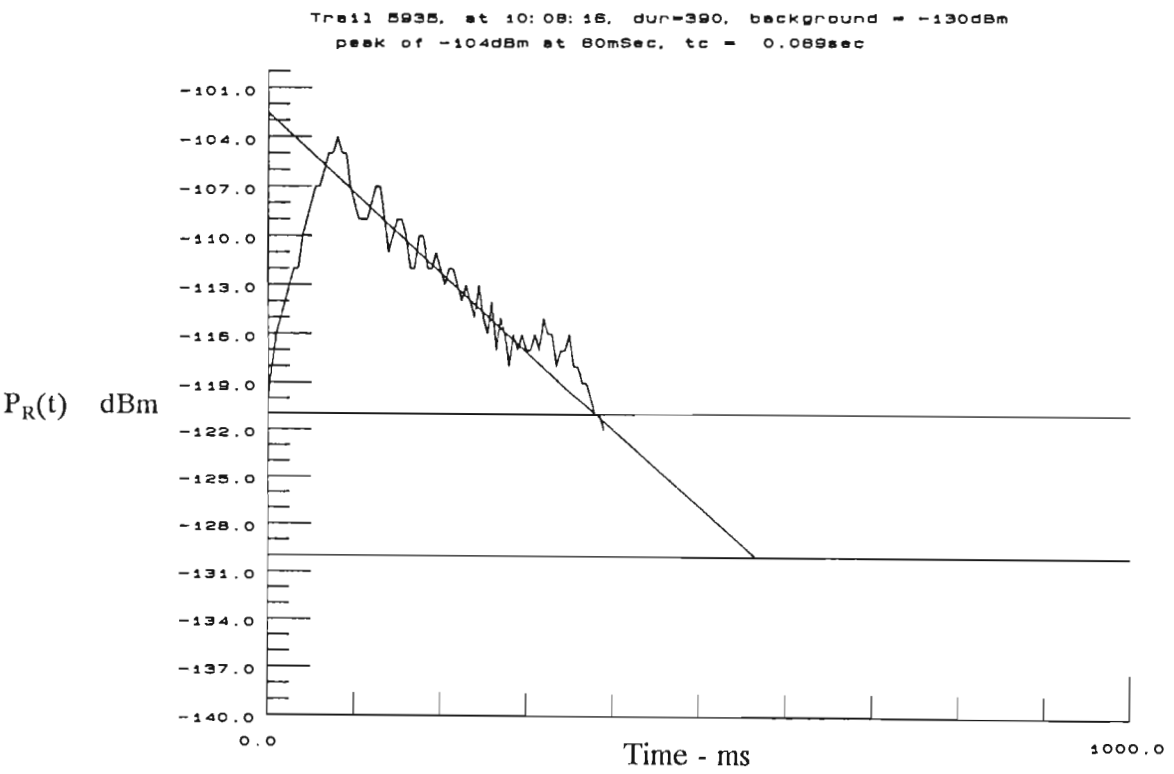

Figure 3-40. Sample Underdense Trails Recorded By Measurement System with Regression Line Plotted

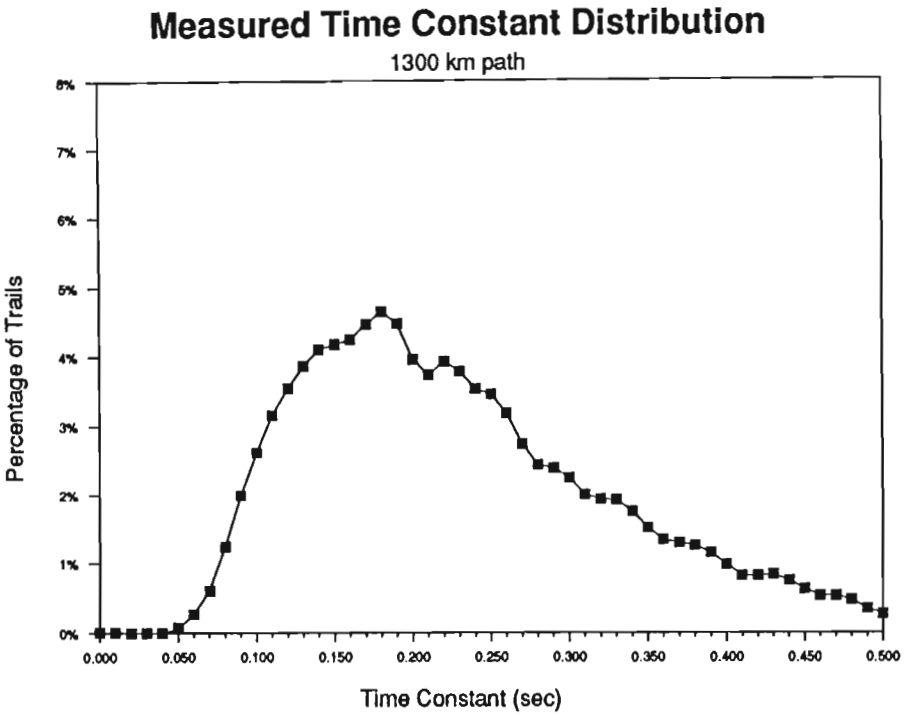

Figure 3-41. Measured Time Constant Distribution for Underdense Trails

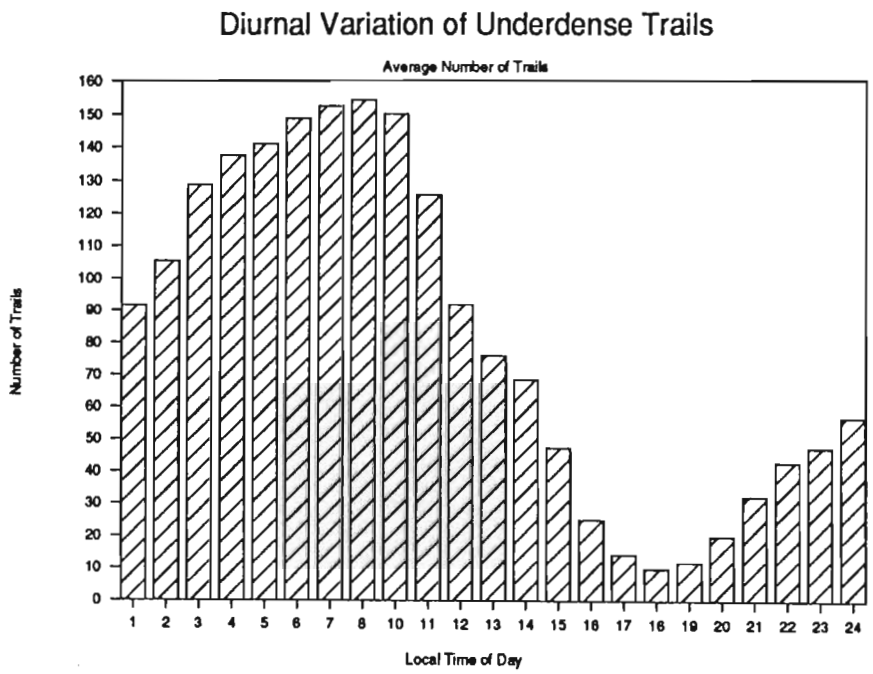

Figure 3-42. Diurnal Variation in Number of Underdense Trails

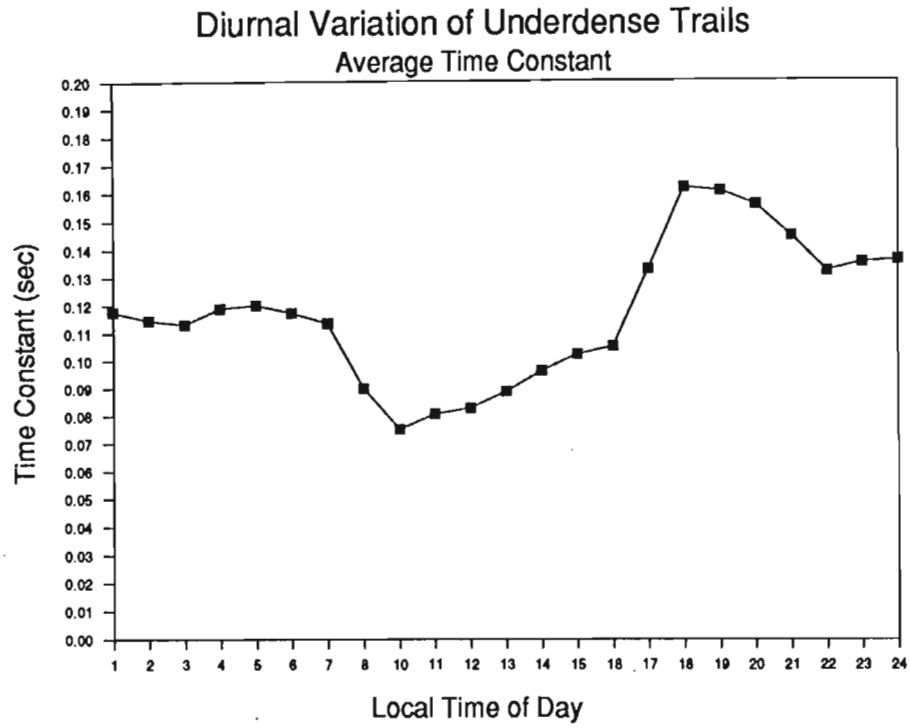

Figure 3-43. Diurnal Variation in Time Constants for Underdense Trails

3.7.1 Verification of Independence of Time Constant and Initial Amplitude

The derivations made in earlier sections assume that the time constant of an underdense trail is independent of the initial amplitude. The assumption will be verified using statistical methods.

The sample correlation coefficient will be used to demonstrate the statistical independence of the time constant distribution and the duration distributions. The sample correlation coefficient indicates what proportion of the variation of the time constant can be attributed to a linear relationship with the duration [Miller and Freund, 1985].

The sample correlation coefficient (r^2) is given by

$$r = \frac{S_{xy}}{\sqrt{S_{xx} \cdot S_{yy}}} \tag{3.39}$$

where

$$S_{xx} = n \sum_{i=1}^{n} x_i^2 - \left(\sum_{i=1}^{n} x_i \right)^2 \tag{3.40}$$

$$S_{yy} = n \sum_{i=1}^{n} y_i^2 - \left(\sum_{i=1}^{n} y_i \right)^2 \tag{3.41}$$

$$S_{xy} = n \sum_{i=1}^{n} x_i y_i - \left(\sum_{i=1}^{n} x_i \right) \left(\sum_{i=1}^{n} y_i \right) \tag{3.42}$$

The three day sample set selected in section 3.7 was analyzed and the sample correlation coefficient between the time constant and the initial amplitude was found to be less than 10^{-5} for the 1300 km path. The sample correlation coefficient for the 500 km path was found to be less than 10^{-3}. This low correlation coefficient confirms there is no linear correlation between the time constant and the log of the initial amplitude. This lack of correlation is displayed graphically in the scatter charts with the regression line drawn in figures 3-44 and 3-45.

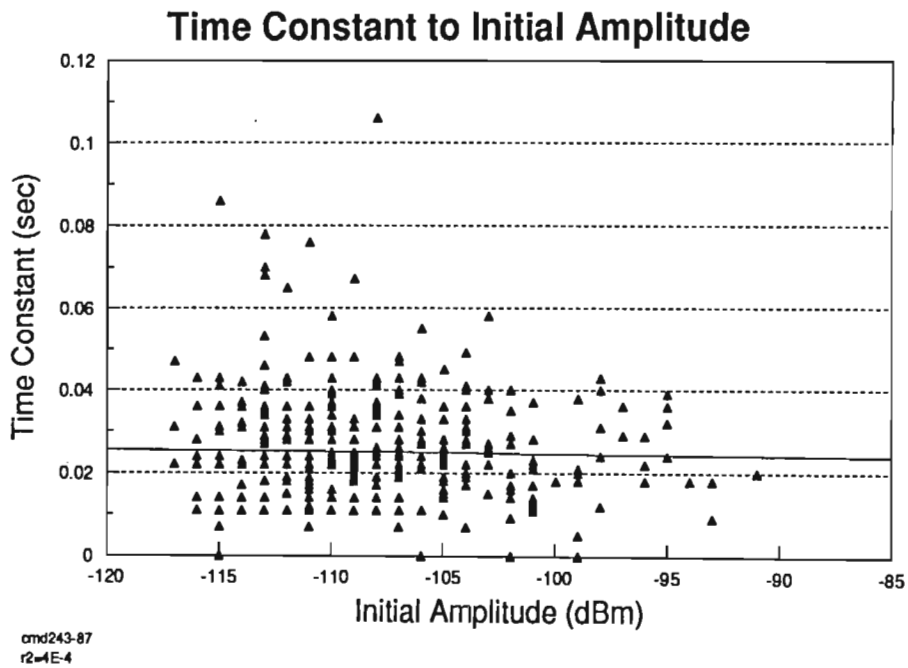

Figure 3-44. Time Constant to Initial Amplitude Scatter Chart for the 1300 km path.

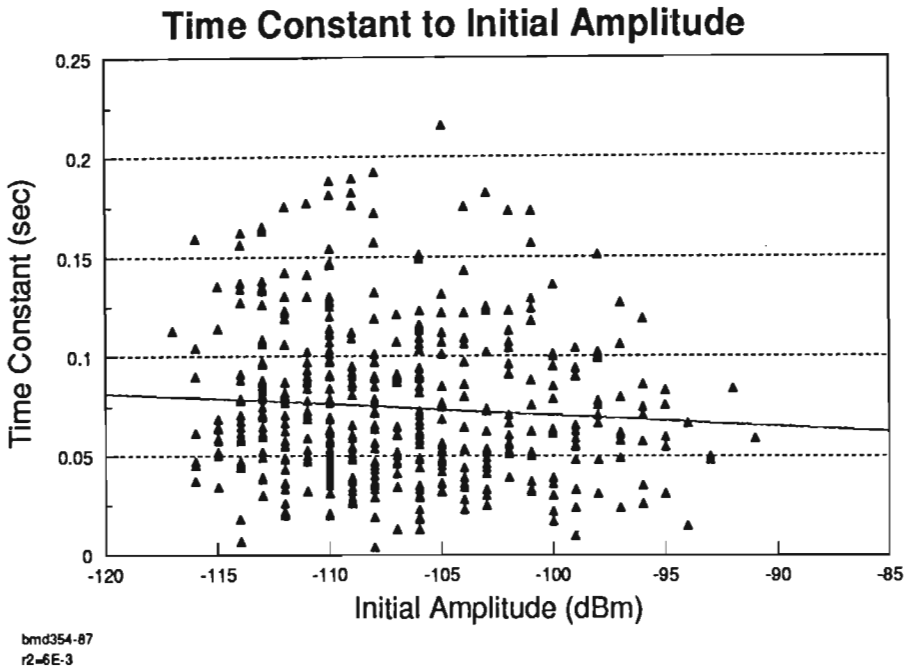

Figure 3-45. Time Constant to Initial Amplitude Scatter Chart for the 500 km path.

3.7.2 Verification of Dependance of Duration and Initial Amplitude

The correlation coefficient between the duration and the initial amplitude was computed to verify the dependance. The correlation coefficient (r^2) between the duration and the initial amplitude for the 1300 km path was found to be 0.13 over the sample period. The correlation coefficient for the 500 km path was found to be 0.21. The scatter charts demonstrating the correlation between the duration and the initial amplitude are shown in figures 3-46 and 3.47.

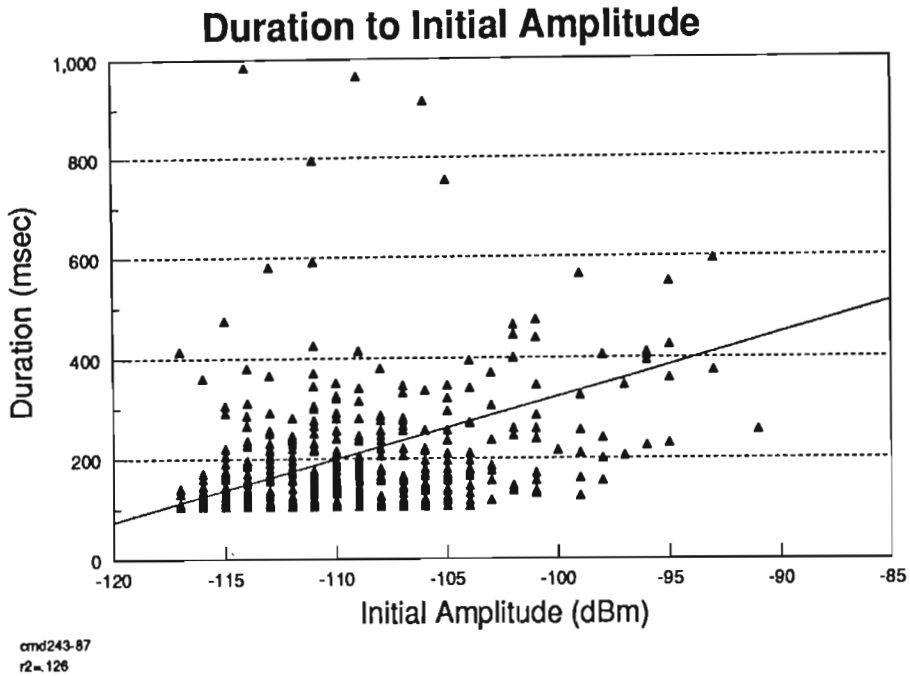

Figure 3-46. Duration to Initial Amplitude Scatter Chart for the 1300 km path.

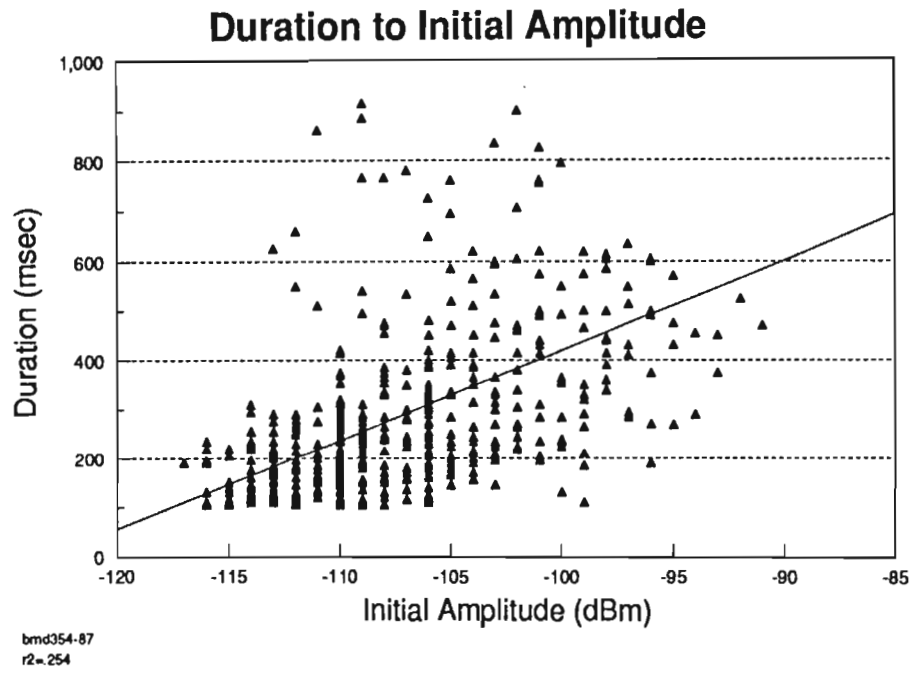

Figure 3-47. Duration to Initial Amplitude Scatter Chart for the 1300 km path.

It is also interesting to note the dependance of duration to initial amplitude for the full sample set is 0.21 for the 1300 km path but was less than 10^{-3} for the 500 km path. This might suggest that more of the trails recorded for the 1300 km path are underdense than are accepted by the selection criterion. An alternate interpretation is that many of the

reflections recorded for the 1300 km path were the result of other modes of propagation (such as ionospheric scatter) which the duration is also linearly related to the log of the initial amplitude.

3.7.3 Comparison of Predicted Time Constant Distribution to Measured Data

The measured time constant distribution was compared to the distribution predicted in section 3.5.6 using the normal height distribution and the results shown in figure 3-48. From this figure, there are far fewer trails with long time constants than predicted by the model. There are several explanations for this observation. Firstly, for a trail to have a long time constant, it must occur near the center of the path, and the point of reflection must occur at a lower altitude. Trails that occur near the center of the path for the 1300 km path would have trail formation times that would cause them to be discarded by the selection criterion.

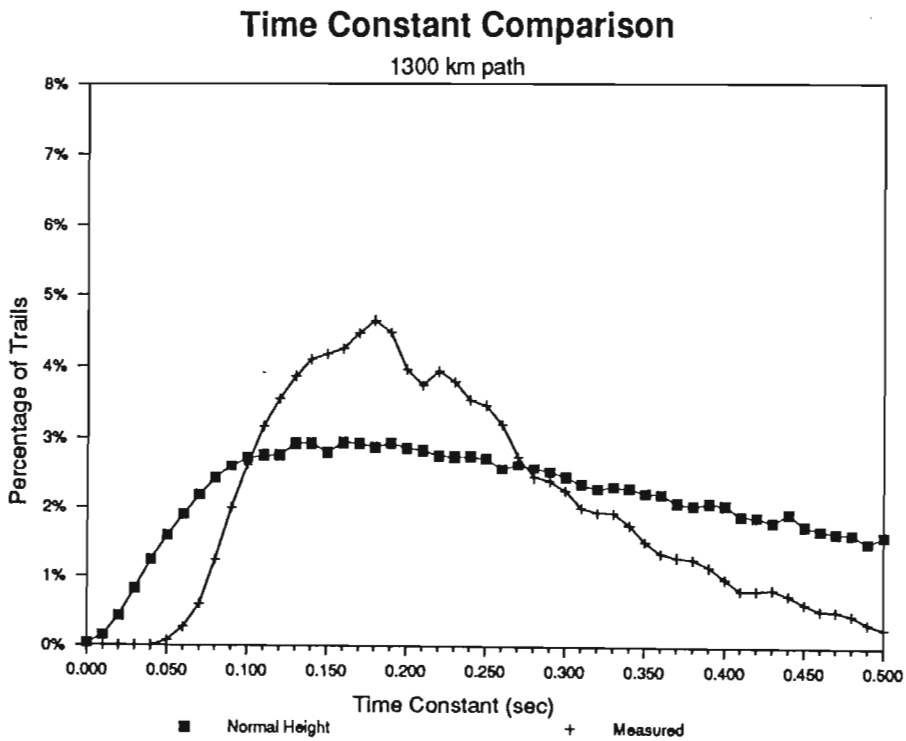

Figure 3-48. Comparison Of Measured Time Constant Distribution To Predicted Value With The Normal Height Distribution for the 1300 km path.

Assuming the selection criterion to be at fault, a manual scan was performed on several hours trail envelopes. This manual scan failed to locate the missing trails. Therefore another factor must be the cause. In figure 3-49, the measured time constant distribution

is compared to the predicted time constant distribution at several fixed heights. The close correlation between the predicted time constant distribution and the measured time constant distribution for a fixed trail height of 98 km leads to a hypothesis that the height distribution of Baggaley [Baggaley and Webb, 1980] may not be applicable to the forward scatter configuration.

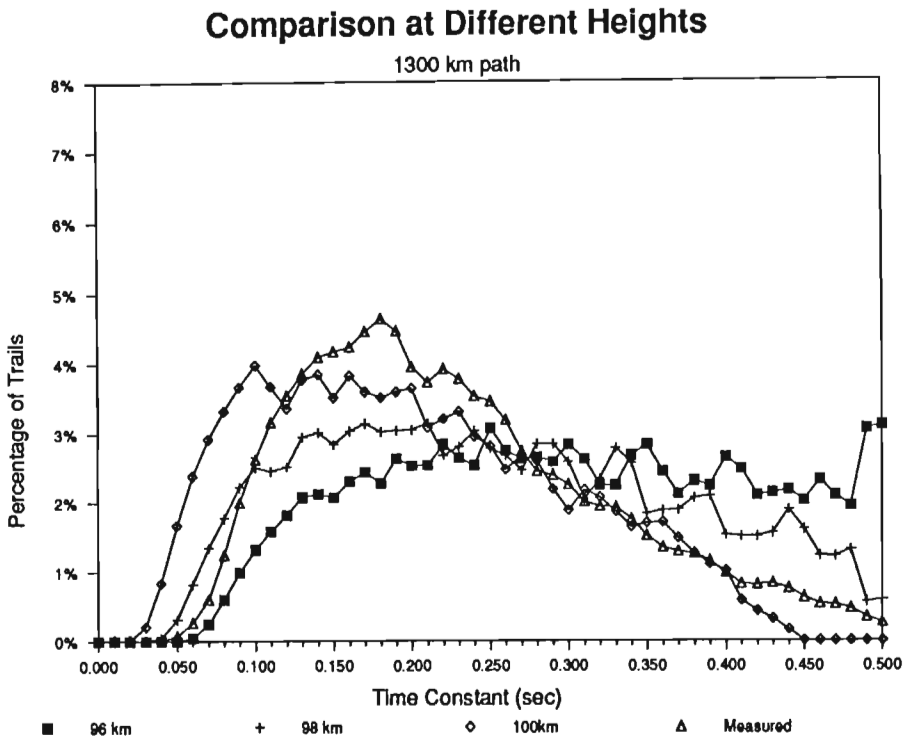

Figure 3-49. Comparison Of Measured Time Constant Distribution To Predicted Value At Various Heights for the 1300 km path.

The height distribution presented by Baggaley and Webb was measured using backscatter techniques. Meteor trails detected by backscatter techniques must be in a plane perpendicular to the transmitted wave. On the other hand, meteor trails oriented to produce a forward scatter reflection must be in the tangent plane as discussed in section 3.4.3. The differences in geometry between the two systems could explain the differences observed. For a forward scatter system, a trail near the center of the path must be in a plane nearly parallel to the surface of the earth to produce a specular reflection. Such trails must travel a long distance through the earth upper atmosphere to reach the center of the path. Because trails start to ionize when they enter the relatively dense atmosphere approximately 110 km above the earth, few meteors are likely to survive long enough to produce a usable trail near the center of the path at heights below about 100 km. A meteor must create a trail longer than 500 km to produce a reflection at a height of 80 km near the center of the path as shown in figure 3-50. With an average trail length of 25 km

[Manning *et al*, 1953], such trails are likely to be very rare. Trails formed with similar elevation angles to those recorded by backscatter systems must be at least 200 to 300 km from the center of the path to form a forward scatter reflection [Hines, 1958].

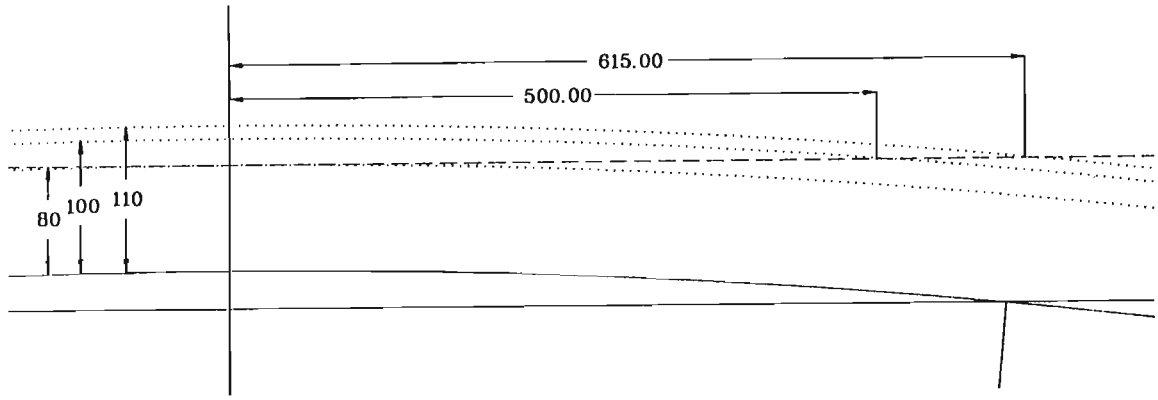

Figure 3-50. Trail Length Requirements at The Center of the Path.

This hypothesis gets some support from measurements taken over the 500 km path from Pretoria to Durban. The measured time constant distribution compared to the predicted distribution using the normal height distribution is shown in figure 3-51 whilst the measured time constant distribution compared at various fixed heights is shown in figure 3-52. For the 500 km path, more of the long time constant trails were observed thus providing a better match to the normal height distribution. A closer correlation with predictions using the normal height distribution would be expected because the geometry for the shorter paths is closer to the geometry of back scatter than it is for the longer paths.

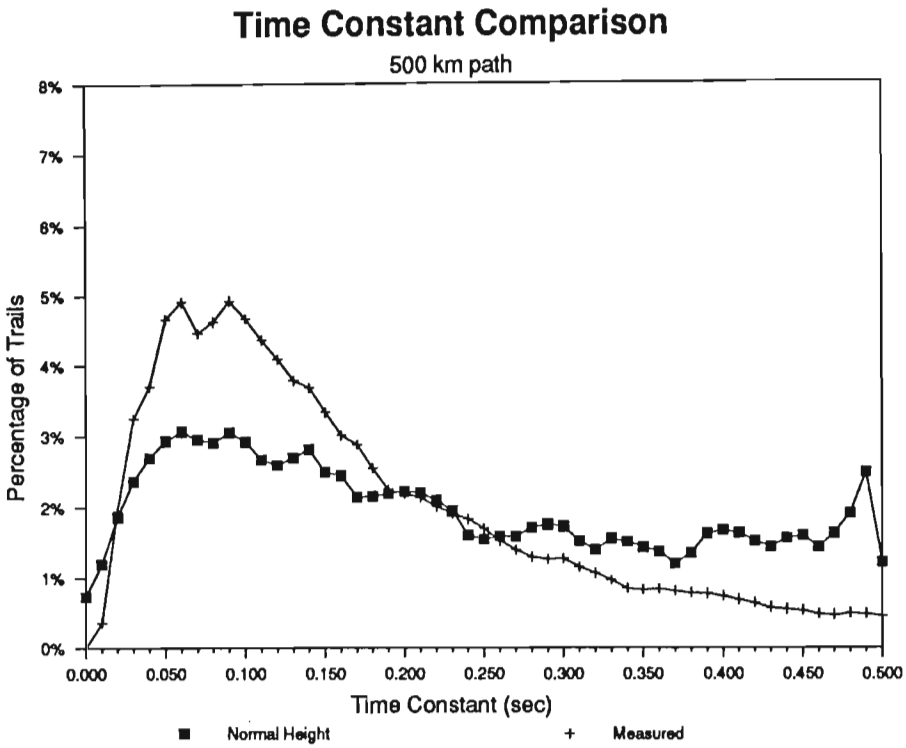

Figure 3-51. Comparison of Measured Time Constant Distribution To Predicted Value With the Normal Height Distribution for the 500 km path.

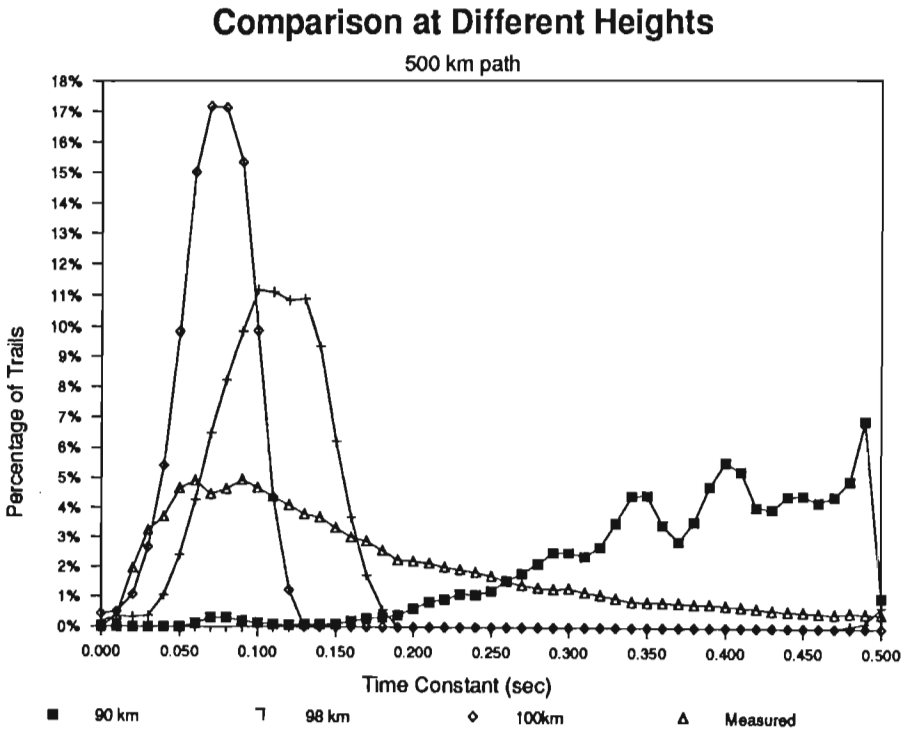

Figure 3-52. Comparison of Measured Time Constant Distribution To Predicted Value At Various Heights for the 500 km path.

Chapter 4

Adaptive Protocols

Most protocols are designed to operate in an environment where the signal to noise ratio remains constant as would be found in line of site or telephone systems. Other protocols are designed for periodic cycles in the signal to noise ratio that are found in HF radio systems. With meteor burst communications, the signal to noise level varies over the duration of the trail and the envelope of this variation changes from trail to trail. This makes the calculation of basic system parameters difficult. Some investigators avoid this difficulty by defining a standard echo and specifying the system parameters for this standard echo [Milstein *et al*, 1986]. If the duration of a trail is much shorter than the standard echo, a block protocol will not get a complete block through which will result in zero utilization. On the other hand, if the duration is longer than the standard echo, the trail will not be used to its full potential. It is therefore desirable to change some of the system parameters to better use the link as conditions change. A protocol that does this is called an adaptive protocol.

4.1 When Parameters Can be Adapted

There are several methods of altering these basic system parameters. The major differences between these methods on how often the parameters are changed, and what relationship these changes have the nature of the channel. Several adaption strategies are discussed below.

4.1.1 Manual Adaption

In a manually adaptive system, all the system parameters are set at configuration time, although some of the system parameters may be altered by the operator. This would allow the operator to tune the system for the time of day or season of year.

4.1.2 Periodic Adaption

A simple adaptive system would allow the controller periodically alter the system parameters to better utilize the expected rate and class of meteors for the next interval. This could, for example, automatically adjust the protocol for the daily cycle. Using high gain antennas, the controller could redirect the beam patterns to follow the 'hot spots' if the radiant distribution was known.

4.1.3 Event Adaption

The next level of adaptive system would be to adapt on a meteor to meteor basis. In this configuration the system controller would be required to identify the class of meteor during trail formation and reconfigure the system parameters to best utilize that class of trail. A very simple implementation would treat underdense trails differently than overdense trails. This could be extended to identify different classes of underdense and overdense trails based on the attack time of the envelope, the peak signal to noise ratio, the current background noise level and perhaps information stored on previous meteor events. This level of adaption could be used in conjunction with periodic reconfiguration of the slow changing system parameters.

4.1.4 Frame Adaption

In event adaption, once the characteristics of a meteor event have been chosen, they are fixed for the duration of the meteor trail. The next logical step would be to change some

of the system parameters as the characteristics of the link change. In order reduce the number of changes that will take place, and therefore the overhead in the protocol, changes can be limited to frame boundaries. To change on a frame to frame basis could allow the controller to monitor the condition of the link in a full duplex environment and perhaps alter the parameters from the ones initially selected when the meteor was initially selected. Alternately, in a half duplex environment, the parameters of the system could be changed in a pre-defined order as the meteor event progresses. In this case, the class of meteor must be identified and communicated to the remote station during the initial handshake.

4.1.5 Character adaption

Logically, the reduction from event adaption to frame adaption can be taken further. One possible reduction would be to adapt on a character to character basis. At this point it is not necessary to specify whether a character is defined to be an eight bit ASCII character, a five bit BAUDOT character or some other code. It is sufficient to say that the adaption can take place on some specified sub-portions of a frame boundary. The same considerations for frame adaption also apply to character adaption.

4.1.6 Continuous adaption

The only level of adaption left after reducing the boundary of adaption down past the smallest divisible portion of a frame, the bit, is continuous adaption. In continuous adaption, selected parameters are altered asynchronously to the transmission of data.

Once the interval of adaption has been chosen, the basic system parameters to alter must be selected. In addition, an algorithm must be developed to adapt these parameters for the varying link conditions.

4.2 Protocol Parameters That Can be Adapted

There are several basic system parameters that can be changed to adapt the meteor burst communications system to the channel conditions. The parameters considered in this section are:

1. Transmission rate.
2. Transmitter power.
3. Antenna position.
4. Block length.

4.2.1 Data Rate Adaptive

It is possible to adapt the data rate, and hence the bandwidth, to maintain a constant signal to noise ratio throughout a meteor burst. The bit error rate can be controlled by setting the signal to noise ratio to be maintained. The subject of data rate adaption has been covered in the literature [Weitzen, 1983, Weitzen *et al*, 1984]. A summary determined that a data rate adaptive system can achieve a two to three times throughput improvement over a system operating at the optimal fixed data rate for an idealized meteor scatter link [Abel, 1986]. Although considering the idealized meteor scatter link yields an upper bound on performance, a real link is not as well behaved.

4.2.2 Power Adaptive

In a power adaptive system, the desired signal to noise ratio is maintained by controlling the transmitter power. A power adaptive system can not yield any greater throughput than a system operating at the maximum output power. The benefits of a power adaptive system could include longer battery life, lower probability of detection and possibly a higher peak output power due to lower duty cycle at maximum output.

Because power adaptive systems do not offer any throughput improvement, they will not be considered further. They are mentioned as they may be used in conjunction with other techniques.

4.2.3 Antenna Adaptive

The variation in the contribution of the various sky regions due to the meteor radiant distribution gives way to another form of adaption. An antenna adaptive system could alter the position or polarization of the antenna system to optimize performance. The antenna aspects of an adaptive system are likely to be adapted on a periodic basis, although a phased array might be electrically steered to improve reception on a trail by trail basis.

4.2.4 Block Adaptive

In a block adaptive protocol, the blocking characteristics of a protocol are adapted to better utilize the channel. Both frame size and window size can be changed. Because of the tradeoff between the probability of successful reception and protocol efficiency, block adaptive protocols can offer significant improvements.

Chapter 5

Modeling of Protocols

One way to develop an efficient protocol for use over half duplex meteor scatter channels would be to implement various protocols and measure their efficiency. To do this, every possible configuration would have to be implemented and tested. Although costly and time consuming, this method would yield an accurate measure of the performance of a protocol for the test system. Another way to develop an efficient protocol would be to record the characteristics of trails received over a meteor scatter link and model the performance of various protocols based on this data. This would allow a wider variety of protocols to be evaluated in a limited time, but could not be relied upon to provide an absolute measure of a protocols efficiency. All that could hoped from such an analysis is a relative measure of the performances of various protocols for the test link. Modeling was selected for this investigation because relative measures are sufficient for this work.

Methods exist for choosing the optimum data rate and frame size if the trail parameters are known [Stone, 1976; Weitzen, 1983; Abel, 1986]. However, some of these models assume a simplified geometry which is not found in practical systems. None of the existing models take protocol blocking into consideration.

In this chapter, a simple model is derived to compute the efficiency of block protocols for trails with a known duration distribution or known initial amplitude and time constant distributions.

The performance of a protocol can be expressed in terms of various measures:

1 Total Throughput

The total throughput indicates how many bits of information were accurately transmitted over the link taking into account protocol overheads and retransmissions for damaged frames. This thoughput is often expressed in bits per second or bits per trail.

2 Number of usable trails.

The number of usable trails gives an indication of the minimum waiting time. When considered in conjunction with the average trail duration, an estimate of the minimum time to pass specific size messages can be computed. To compute the actual waiting time, the system buffering scheme would have to be considered.

3 Transmitter efficiency.

The transmitter efficiency gives an indication of what portion of the time the transmitter is turned on is actually being used to transmit data. The efficiency of the transmitter is crucial in battery powered portable applications and when low probability of intercept is desired.

In all network applications, there is a tradeoff between throughput and delay time. According to Tanenbaum [Tanenbaum, 1981], "to achieve the maximum theoretical flow, we must tolerate an infinite delay. In fact, to even achieve a flow close (say within 20%) of the theoretical limit, we must tolerate a queuing delay several times the delay of the unloaded network." Further, in meteor scatter applications, there is a tradeoff between throughput and transmitter efficiency. These tradeoffs must be considered within the network goals when a meteor scatter protocol is specified.

5.1 Model Specification

On average, the throughput per frame is equal to the number of data bits times the probability the frame was successfully received[1]. Although frames must be received with zero uncorrectable errors for any data to be used, for a large sample this approximation is validated by the law of large numbers [Scheaffer and Mendenhall, 1975]. To determine the probability of a frame being successfully received, the equation presented in section 2.3.4 could be used if the bit error rate was constant.

Because the bit error rate is not constant for propagation by meteor reflection, this probability of successful reception is more difficult to compute. It is possible to compute the instantaneous signal to noise ratio at all bit times in the trail and thereby accurately compute the probability of error over each trail if the amplitude is known at all times in the trail. A simulation of this sort could provide an accurate estimation of the throughput of a link under various operating conditions although these simulations would be time consuming to perform. An alternative to simulation is modeling. A channel based model considers the error rate of the modulation technique under consideration to predict the probability of error over a frame. An approach similar to this was used by Stone [Stone, 1976] to compute the optimum length of time to transmit for a given system configuration and included the ability to incorporate the effects of error correction codes. A simpler technique is to use the predictable fading characteristic of meteor trails can and assumes the probability of error is zero when the signal to noise ratio (SNR) is above some threshold and one when the signal is below the threshold. Because the time amplitude characteristic of an underdense meteor reflection is always decreasing no additional throughput can be achieved by further transmission once this threshold is reached. A block model of this sort will be used in this investigation rather than a channel based model such as derived by Stone.

Using this model, the average throughput per frame (I_F) is

$$I_F = N_D \cdot P(T_u \geq t_e) \tag{5.1}$$

where T_u is the usable time and is equal to the time from the beginning of the trail to the time the signal to noise ratio is less than the threshold and t_e is the time from the beginning of the trail to the end of the current frame and t_s is the time from the beginning of the trail to the start of the current frame.

---

1 This model is only concerned with the low level delivery of frames of data. Overall throughput is limited by the ability of higher protocol layers to use all the data delivered.

$$t_e = t_s + T \tag{5.2}$$

For a stop and wait protocol,

$$t_s = (n_w - 1) \cdot (T + T_t) \tag{5.3}$$

For a sliding window protocol,

$$t_s = (n_w - 1) \cdot (N_f \cdot T + T_t) + (n_f - 1)T \tag{5.4}$$

which reduces to equation (5.3) for $N_f = 1$.

where

N_D Number of data bits per frame.

N_f number of frames per window.

n_f number of frame being sent.

N_O number of overhead bits per frame.

n_w number of window being sent.

T Time to transmit one frame = $R(N_D+N_O)$.

T_t Turnaround time = $2T_p + 2T_x + 2T_l + T_{ack}$.
T_p is the one way propagation time.
T_x is the transmitter turn on time.
T_l is the system locking time.
T_{ack} is the time to transmit an acknowledgment.

5.2 Fixed Block Protocol Model

For a fixed block protocol, the average one way throughput per frame is given by equation (5.1). The average throughput per window (I_W) is

$$I_W = \sum_{n_f=1}^{N_f} I_F = \sum_{n_f=1}^{N_f} N_D \cdot P_D(T_u \geq t_e) \tag{5.6}$$

and the average throughput per trail (I_T) is

$$I_T = \sum_{n_w=1}^{\infty} I_W = \sum_{n_w=1}^{\infty} \sum_{n_f=1}^{N_f} N_D \cdot P_D(T_u \geq t_e) \tag{5.7}$$

when throughput is maximized. An alternate protocol presented by Milstein [Milstein *et al*, 1986] only transmits one frame per trail. Although this protocol will achieve less throughput, better transmitter efficiency should be achieved.

The summation to infinity in equation (5.7) can be approximated by a series terminated when the probability of success for the last frame is less than an arbitrarily small constant. For this model, the series is terminated when the probability of success for the last frame in a window is less than two percent. By increasing the threshold, a larger transmitter efficiency can be achieved at a cost of reduced throughput.

The relative number of usable trails is taken to be the probability that at least one frame is successfully transmitted on each trail. Because of the amplitude-time characteristic of underdense trails, the first frame has the highest probability of being successfully transmitted. Hence the relative number of usable trails is taken to be the probability that the first frame of the first window was successfully transmitted.

By multiplying the relative number of usable trails (N_T) times the average throughput per trail, an estimate of the average relative throughput (R) can be determined.

$$R = N_T \times I_T \tag{5.8}$$

For a non adaptive protocol, $p_t(D)$ is the duration distribution. The duration distribution for the 1300 km reference system presented in section 3.6.3 was used to evaluate the effects of frame size and window size. Table 5-1 shows the effect of different frame sizes and window sizes for a data rate of 2000 b/s, a protocol overhead of 48 bits per frame and a turnaround time of 0.050 second. Although both the protocol overhead and turnaround time are dependant on the data rate and the window size, they are assumed constant for this analysis. This data is plotted in figure 5-1 to show the link efficiency,

in figure 5-2 to show the relative number of usable trails and in figure 5-3 to show the transmitter efficiency. The maximum protocol efficiency due to overheads is also plotted in figure 5-1 to emphasize the inherent inefficiencies of short frame sizes.

Table 5-1. Results of Fixed Block Protocol Simulation

Window size	Frame size (bits)	Average Through (bit/tr)	Link Effic (%)	Usable Trails (%)	Tx Effic (%)
1	25	116.1	11.0%	90.6%	4.5%
1	50	193.9	18.3%	87.7%	6.6%
1	75	246.7	23.3%	84.9%	7.9%
1	100	283.5	26.7%	82.3%	8.6%
1	125	310.5	29.3%	79.9%	9.0%
1	**150**	**328.9**	**31.0%**	**77.6%**	**9.3%**
1	175	300.9	28.4%	68.5%	9.4%
1	200	300.5	28.4%	65.3%	9.3%
1	225	294.4	27.8%	62.2%	9.6%
1	250	288.0	27.2%	59.3%	9.6%
1	275	279.6	26.4%	56.5%	9.6%

Table 5-1. (Continued)

Window size	Frame size (bits)	Average Through (bit/tr)	Link Effic (%)	Usable Trails (%)	Tx Effic (%)
2	25	164.3	15.5%	90.6%	4.4%
2	50	261.6	24.7%	87.7%	6.6%
2	75	318.8	30.1%	84.9%	7.6%
2	100	354.3	33.4%	82.3%	8.6%
2	125	376.5	35.5%	79.9%	9.1%
2	**150**	**392.7**	**37.0%**	**77.6%**	**9.1%**
2	175	356.7	33.6%	68.5%	9.0%
2	200	350.8	33.1%	65.3%	9.0%
2	225	341.2	32.2%	62.2%	9.1%
2	250	328.9	31.0%	59.3%	9.3%
2	275	315.0	29.7%	56.5%	9.6%

Window size	Frame size (bits)	Average Through (bit/tr)	Link Effic (%)	Usable Trails (%)	Tx Effic (%)
4	25	206.4	19.5%	90.6%	4.3%
4	50	313.6	29.6%	87.7%	6.5%
4	75	372.0	35.1%	84.9%	7.4%
4	100	404.1	38.1%	82.3%	8.3%
4	125	424.9	40.1%	79.9%	8.5%
4	**150**	**434.3**	**41.0%**	**77.6%**	**8.8%**
4	175	388.4	36.6%	68.5%	9.1%
4	200	383.8	36.2%	65.3%	8.5%
4	225	367.3	34.7%	62.2%	9.0%
4	250	357.5	33.7%	59.3%	8.4%
4	275	337.2	31.8%	56.5%	9.2%

Table 5-1. (Continued)

Window size	Frame size (bits)	Average Through (bit/tr)	Link Effic (%)	Usable Trails (%)	Tx Effic (%)
8	25	233.9	22.1%	90.6%	4.4%
8	50	347.3	32.8%	87.7%	6.3%
8	75	406.4	38.3%	84.9%	6.9%
8	100	438.2	41.3%	82.3%	7.5%
8	**125**	**451.9**	**42.6%**	**79.9%**	**8.2%**
8	150	451.8	42.6%	77.6%	9.2%
8	175	410.5	38.7%	68.5%	8.4%
8	200	403.7	38.1%	65.3%	7.8%
8	225	377.4	35.6%	62.2%	9.3%
8	250	366.6	34.6%	59.3%	8.6%
8	275	354.7	33.5%	56.5%	8.1%

Window size	Frame size (bits)	Average Through (bit/tr)	Link Effic (%)	Usable Trails (%)	Tx Effic (%)
16	25	253.7	23.9%	90.6%	4.0%
16	50	372.8	35.2%	87.7%	5.4%
16	75	426.9	40.3%	84.9%	6.4%
16	100	449.1	42.4%	82.3%	7.7%
16	125	472.6	44.6%	79.9%	7.1%
16	**150**	**485.7**	**45.8%**	**77.6%**	**6.6%**
16	175	416.2	39.3%	68.5%	8.5%
16	200	408.6	38.5%	65.3%	7.9%
16	225	397.9	37.5%	62.2%	7.3%
16	250	385.4	36.4%	59.3%	6.8%
16	275	368.8	34.8%	56.5%	6.3%

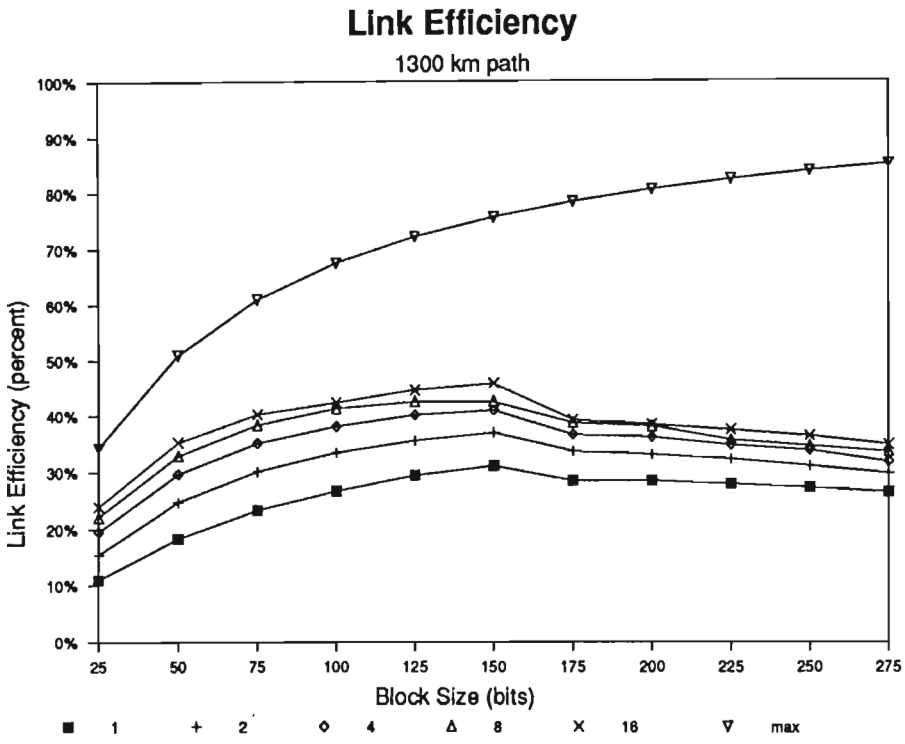

Figure 5-1. Link Efficiency as a Function of Frame Size and Window Size.

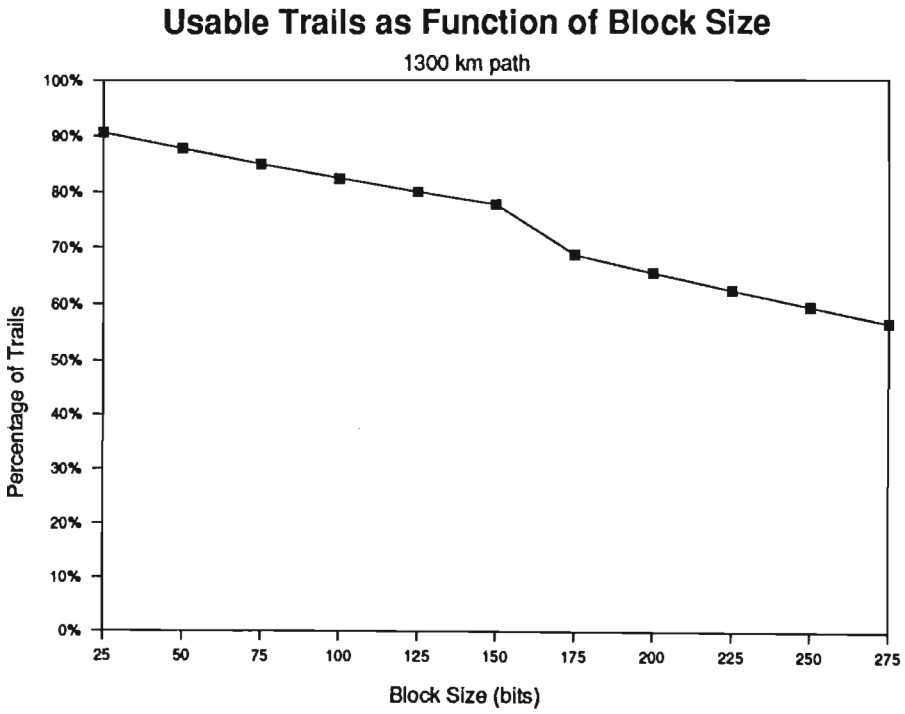

Figure 5-2. Number of Usable Trails as a Function of Frame Size.

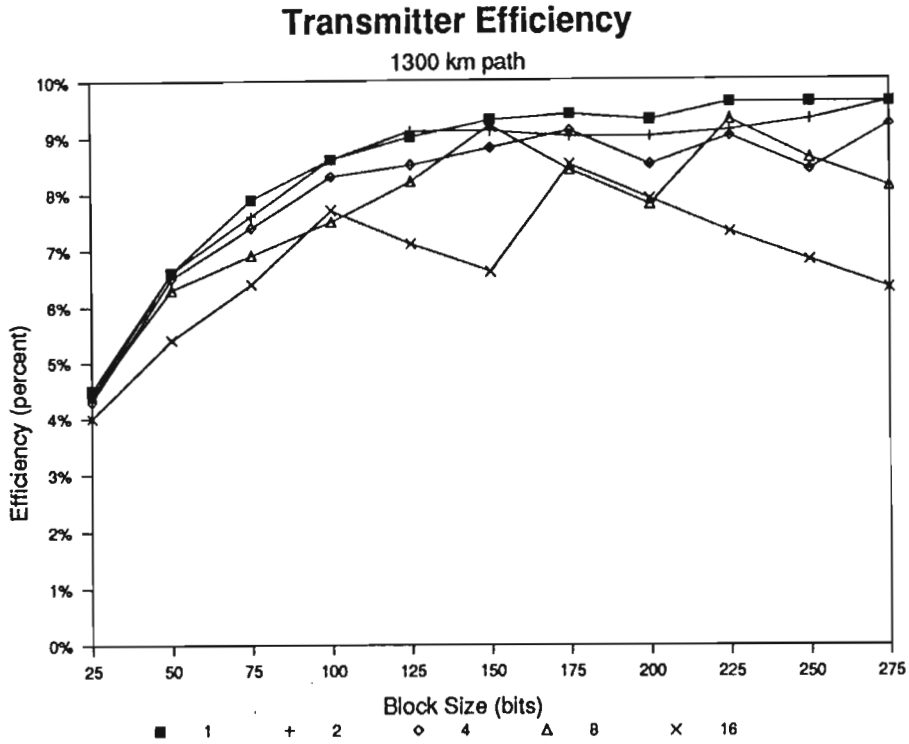

Figure 5-3. Transmitter Efficiency as a Function of Frame Size and Window Size.

It is worth noting that the advantage of using a 16 frame sliding window over a stop and wait protocol is a throughput improvement of 1.48 times. Caution must be used as this improvement assumes that all frames successfully received are used. This assumption requires a powerful selective retransmission error control scheme and is rarely true in practice, hence the improvement is likely to be somewhat less than predicted.

To convert from the average relative throughput to absolute throughput, the number of trails per unit time must be known. Thus the total throughput for a non-adaptive fixed block protocol on a system with 450 trails per hour using eight, 125 bit frames is 450 (trails/hour) * 451.9 (bits/trail) = 203,355 bits per hour or a 24 hour average of 56 bits per second. A stop and wait protocol on the same system only offers an average throughput of 41 bits per second.

The expected throughput for a sliding window protocol that only transmits one window per trail is shown in table 5-2 for different window sizes. Such a protocol with eight frames per window achieves more than three times the transmitter efficiency with a reduction in throughput of 30% compared to a protocol that optimizes the throughput per trail. In battery powered operations, this reduction in throughput per trail may be more than compensated for by the additional transmit time available.

Table 5-2. Throughput at Different Window Sizes for a Single Window per Trail Protocol.

Window size	Frame size (bits)	Average Through (bit/tr)	Link Effic (%)	Usable Trails (%)	Tx Effic (%)
1	150	90.4	13.4%	77.6%	58.8%
2	150	147.9	21.9%	77.6%	48.1%
4	150	225.5	33.4%	77.6%	36.7%
8	150	314.7	46.5%	77.6%	25.6%
16	150	397.1	58.7%	77.6%	16.1%

5.3 Adaptive Block Protocols Model

For an adaptive protocol, T_u is dependant on τ as given in equation (3.12). The time constant distribution for the 1300 km path reference system presented in section 3.7 was used to evaluate the effects of different frame sizes at different signal to noise ratios. The signal to noise ratio distribution was extracted from the measured data and is presented in table 5-3 with the maximum link utilization selected for each value. The average throughput for this protocol is 664 bits per trail which is twice the throughput of the stop and wait protocol. Furthermore, the adaptive protocol effectively uses almost all the trails thus reducing waiting times.

Table 5-3. Throughput Analysis of Adaptive Block Protocol.

SNR (dB)	Number Trails	Frame Size	Usable (bits)	Link Effic	Usable Trails	Tx Effic
3	0.0%	50	41.4	26.6%	77.7%	6.8%
6	0.0%	75	144.4	46.4%	96.0%	15.3%
9	0.0%	125	264.0	56.5%	97.2%	19.6%
12	15.2%	150	387.9	62.2%	98.9%	24.8%
15	25.4%	200	515.9	66.2%	98.9%	26.3%
18	23.9%	225	644.2	68.9%	99.4%	29.7%
21	16.5%	250	775.2	71.1%	99.6%	32.7%
24	10.1%	275	908.8	72.9%	99.7%	35.3%
27	4.9%	300	1042.4	74.4%	99.8%	18.8%
30	2.9%	325	1176.5	75.5%	99.8%	19.7%
33	0.9%	350	1312.2	76.6%	99.9%	20.6%
36	0.2%	375	1447.0	77.4%	99.9%	21.4%
39	0.0%	425	1583.6	78.2%	99.9%	21.0%
42	0.0%	450	1719.6	78.9%	99.9%	21.6%
45	0.0%	475	1855.3	79.4%	99.9%	22.2%
totals	100.0%		664	68.5%	99.3%	28.2%

For example, when computing the 18 dB SNR values, all trails between 18 dB and 21 dB were used. The measured signal to noise ratio distribution is shown in the first two columns. The measured duration distribution for each SNR value was used in equation (5.7) to compute the average throughput per trail at a data rate of 2000 bps and with a protocol overhead of 48 bits/frame. The frame size (N_D) was varied from 0 to 1000 in steps of 25 bits. The value that maximized throughput (I_T) is shown in table 5-3 for each SNR value.

Chapter 6

Protocol Specification

It is important to recognize the role of meteor scatter communications in a network configuration before details of the communication subnet can be discussed. Whilst the use of trails of ionized particles created when a meteor burns up when entering the earth's atmosphere to propagate radio waves beyond the horizon should only affect the first two layers of the OSI reference model, there are characteristics of meteor scatter communications that must be taken into account by higher layers. For example, if layer two knows that a message is confidential, it can transmit that message using only underdense trails to minimize the change of interception. Likewise, if a message is very urgent, layer two might attempt to utilize meteor reflections that would normally be considered too small to use efficiently, but could be used to transmit a small amount of data. Perhaps more importantly, the routing algorithms might wish to take advantage of the diurnal cycle to use different paths to a station at different times of the day. This might mean that it would be 'better' to leave the meteor scatter network and use alternate communication techniques to get to the desired location. Any network using meteor scatter links must take advantage of all available methods of communication in addition to meteor scatter.

Protocols used in early full duplex meteor scatter systems relied on reciprocity to determine when link conditions were suitable for the transmission of data. There was no error detection or correction. Data was only transmitted when a sufficiently good channel existed to exchange data with an acceptable error rate. As soon as the signal to noise ratio dropped below a specified threshold, data transmission was terminated and a code was sent to disable the remote receiver [Carpenter and Ochs, 1959].

In a half duplex environment, the signal to noise ratio is not always known, so the frame size must be selected in advance. In this chapter, the effects of system gain and bandwidth are considered in conjunction with blocking. This leads to the specification of a fixed data rate, frame adaptive protocol to provide a communications subnet in the half duplex meteor scatter environment.

6.1 Effects of System Configuration on Performance

Modeling the effect of different data rates is a two fold process. In addition to changing the times required to transmit a frame and to exchange a handshake, the change in bandwidth affects the relative number of usable trails. Increasing the data rate requires a corresponding increase in bandwidth. If the channel is assumed to be an additive Gaussian white noise channel, an increase in bandwidth produces a corresponding increase in average noise level. Because the model used in this evaluation is based on a measured signal to noise ratio distribution, it is only possible to model the effect of increasing the noise level. It is not possible to improve the signal to noise ratio of the measured data due to the lack of information at signal levels approaching the noise level. By increasing the average noise level, the signal to noise ratio distribution is shifted with those trails with a signal to noise ratio less than the threshold (9dB in this case) discarded.

The adaptive block protocol model from section 5.3 was used to estimate the effect of increasing the data rate for the measurement system. For each data rate, the blocking configuration that yielded the maximum throughput was selected using the default window size, overhead and turnaround times from section 3.2. From table 6-1, it can be seen that above the optimum data rate, throughput falls off due to a reduction in the number of usable trails.

Table 6-1. Throughput as a Function of Data Rate

Data Rate (bits/sec)	Usable Trails	Throughput (bits/trail)
2000	1.0	664
4000	.85	1116
8000	.59	1556
16000	.36	1850
32000	.19	1945
64000	.09	1792
128000	.04	1515
256000	.01	808

To consider the effect of system gain in the general case is beyond the capability of the model used in this analysis. For example, to consider altering the gain of the antenna systems would alter the polar patterns and therefore the regions of sky illuminated. As was demonstrated in Chapter three, predicting the effects of different antennas on the duration distribution is difficult. For this reason, this section will only be concerned with the effect of changing the transmitter power.

The effect of changing transmitter power can be modeled by shifting the signal to noise ratio distribution by the corresponding amount. Thus it can be seen that the effect of doubling the transmitter power and doubling the data rate cancel as far as the signal to noise ratio distribution is concerned. As with the data rate modeling, it is not possible to increase the signal to noise ratio distribution above the level measured. In order to model larger transmitter power levels, higher data rates must be selected to maintain the same (or lower) signal to noise ratio distribution.

Extending the adaptive block protocol model to allow different transmitter power levels, a data rate to throughput relationship can be established at different power levels. This relationship is shown in figure 6-1 for the 1300 km path and in figure 6-2 for the 500 km path and displays several interesting characteristics. Firstly, the optimum data rate to power ratio remains constant and secondly, the throughput is proportional to the transmitter power if data is transmitted at the optimum data rate for that power level. Brown [Brown and Williams, 1977] predicts that the throughput is related to power by

$$I \propto P_T^{0.6}$$

assuming a fixed bandwidth, non adaptive protocol. Stone [Stone, 1976] predicts throughput is related to power by

$$I \propto P_T^{0.5}$$

for a non adaptive protocol. Thus, by using a block adaptive protocol, throughput can be doubled by doubling the power instead of only one and a half times without adaptive block protocols.

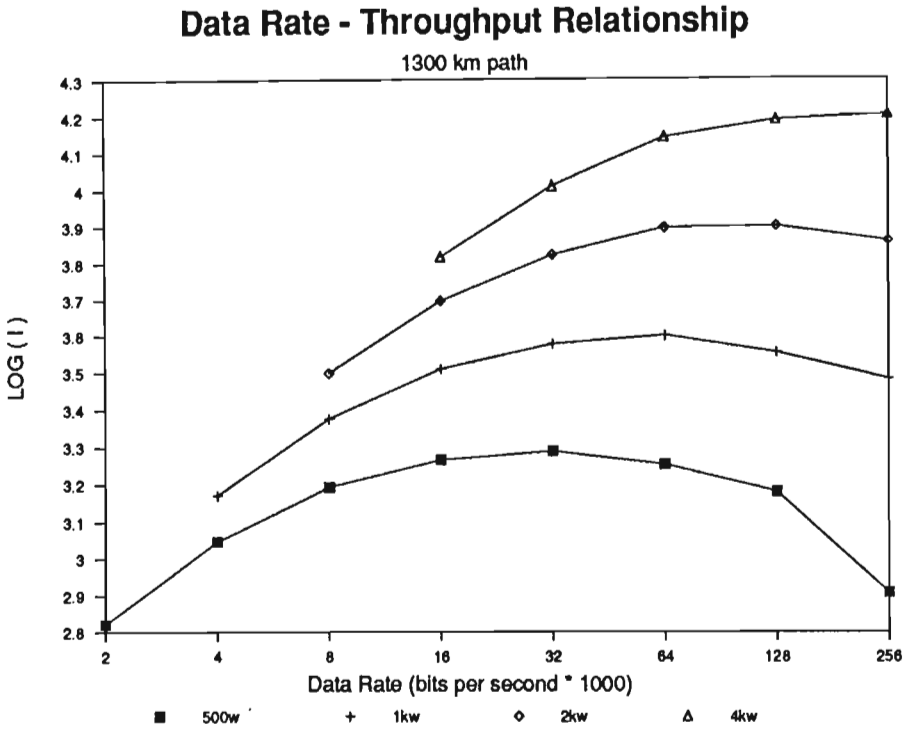

Figure 6-1. Effect of Data Rate and Transmitter Power on Throughput for the 1300 km path.

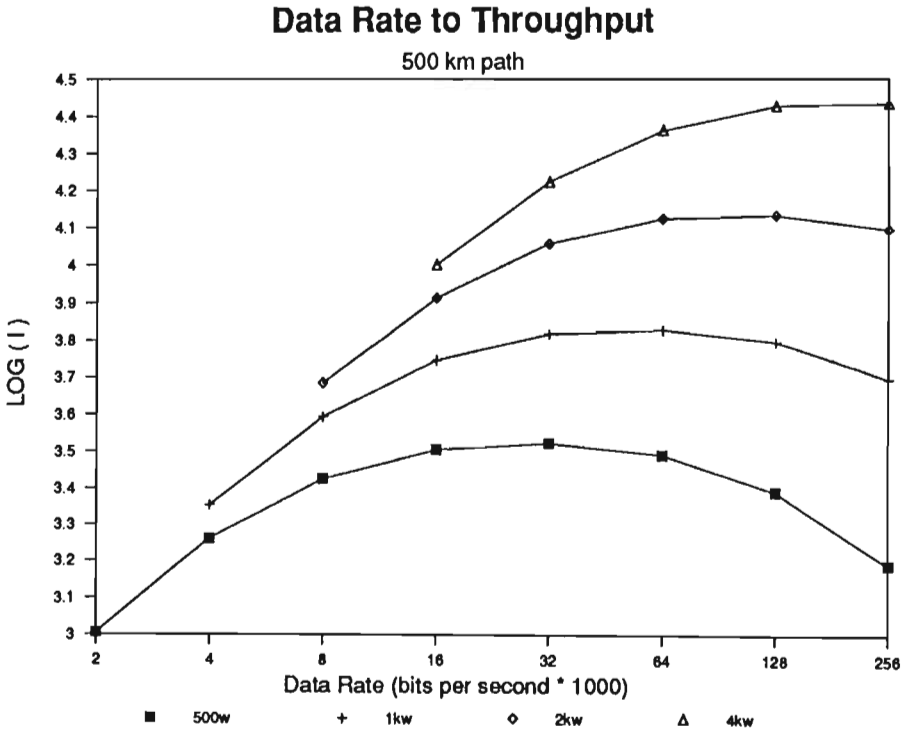

Figure 6-2. Effect of Data Rate and Transmitter Power on Throughput for the 500 km path.

6.2 Specification of Protocol

A block adaptive protocol can now be presented using the results from the previous section. A functional specification addressing a communication subnet protocol will be presented for the two measured configurations. The communication subnet described in this thesis comprise layer one and parts of layer two of the ISO-OSI reference model. Neither the higher layers, nor the interface between the layers will be discussed. Further, the communication subnet is providing an unsequenced datagram level of service. It is the responsibility of higher layers to efficiently use the error prone communication subnet.

The communication subnet protocol used in this thesis is a block oriented synchronous protocol such as X.25 or Bi-sync. The following parameters are assumed for the protocol.

a. A transmitter turnaround time of 0.050 second can be achieved including modem locking times.

b. The modem used is capable of virtually error free operation with a signal to noise ratio of 9dB or greater[1].

c. A maximum window size of eight frames per window will be used.

d. A transmitter operating at 2000 watts.

e. Unlimited bandwidth is available and maximum throughput is desired.

---

1 This assumption excludes the effects of modulation technique and error correction techniques. A more general model would consider these factors.

Case 1 - 1300 km path

For the 1300 km link, the optimum data rate of 128000 bits per second is selected from figure 6-1. The frame size the protocol will select based on the initial signal to noise ratio is shown in table 6-2. The 7923 bits per trail average throughput with an average of 450 trails per hour produces an average 24 hour rate of 990 bits per second. This is a twelve times improvement over the 500W protocol specified in section 5.3. Because of the diurnal cycle, the throughput varies from 1760 bits per second in the morning to 220 bits per second in the evening.

Table 6-2. Adaptive Protocol Specification for the 1300 km path.

SNR (dB)	Number Trails	Frame Size	Usable (bits)	Link Util	Usable trails	Tx Eff
3	0.0%	2100	8499.4	85.3%	99.9%	24.7%
6	0.0%	4000	17216.0	86.3%	100.0%	26.6%
9	0.0%	5500	26048.7	87.1%	100.0%	29.3%
12	10.1%	7000	34956.6	87.7%	100.0%	31.0%
15	4.9%	7700	43944.0	88.2%	100.0%	35.5%
18	2.9%	9100	53001.7	88.6%	100.0%	36.2%
21	0.9%	9200	62126.4	89.0%	100.0%	42.0%
24	0.2%	10400	71304.6	89.4%	100.0%	42.7%
27	0.0%	11600	80489.5	89.7%	100.0%	43.2%
30	0.0%	12900	89678.4	90.0%	100.0%	43.3%
totals	19.0%		7923	16.7%	19.0%	6.4%

Case 2 - 500 km path

For the 500 km path, the optimum data rate of 128000 bits per second is selected from figure 6-2. The frame size the protocol will select based on the initial signal to noise ratio is shown in table 6-3. The 6480 bits per trail average throughput with an average of 110 trails per hour produces an average 24 hour rate of 198 bits per second. Comparing the throughput for the two paths shows that the 1300 km path offers five times the capacity of the 500 km path. Most of this improvement is achieved by the increase in the number of usable trails.

Table 6-3. Adaptive Protocol Specification for the 500 km path.

SNR (db)	Number Trails	Frame Size	Usable (bits)	Link Util	Usable trails	Tx Eff
3	0.0%	1600	5298.7	61.8%	91.9%	21.9%
6	0.0%	2400	11176.3	65.2%	95.2%	30.0%
9	0.0%	3400	17364.3	67.5%	95.8%	32.9%
12	11.9%	4300	23600.7	68.8%	96.3%	23.5%
15	6.4%	4500	29978.0	69.9%	97.5%	28.2%
18	3.0%	5200	36470.1	70.9%	97.8%	29.6%
21	1.3%	5700	43022.1	71.7%	98.1%	31.8%
24	0.2%	6500	49601.1	72.3%	98.1%	32.2%
27	0.0%	7300	56186.3	72.8%	98.1%	32.5%
30	0.0%	8100	62776.1	73.2%	98.1%	32.7%
totals	22.8%		6480	15.9%	22.1%	6.0%

Chapter 7

Conclusions

This thesis set out to show that a relationship exists between the initial amplitude of a trail and the duration for underdense trails and that this relationship can be used to develop block adaptive protocols that more efficiently use underdense trails in the half duplex, forward scatter, meteor scatter environment. After brief introductions into digital communications and meteor scatter, the literature relevant to the derivation of a sky region model was reviewed. From this review, a model was adopted and the time constant distribution was computed for two different paths. The time constant distribution for the two paths was measured and compared to the predicted values. From the comparison of the predicted values to the measured values, it is proposed that the height distribution of meteor trails measured by backscatter techniques is not applicable to long distance forward scatter systems. The geometry at shorter paths is closer to the geometry of the backscatter systems and therefore correlates better to the backscatter predictions. Although more research is required into the height distribution of usable meteors for forward scatter communications to accurately model the link, a time constant distribution was determined experimentally and the peak signal to duration distribution was demonstrated.

Adaptive protocols were then discussed that could use the peak signal to duration distribution. In this thesis, only the blocking characteristics were selected for adaption. This thesis then demonstrated how to specify an adaptive protocol to more effectively use a meteor scatter link. More effective both in terms of data throughput and wait time reduction. Block adaptive protocols provide a two times improvement in throughput over stop and wait protocols and over three times improvement in transmitter efficiency. Block adaptive protocols that are optimized for throughput make more efficient use of the transmitter than single window per trail protocols. Single window per trail protocols using block adaptive techniques should be even more efficient.

Modeling demonstrated that there is an optimum data rate for each power level when protocol overheads are included. Transmitting at higher data rates than the power level

allows results in reduced throughput. This is an important consideration when designing fixed data rate systems. Finally, it was found that throughput is directly proportional to transmitter power when the optimum data rate is used.

The techniques developed in this thesis are applied to the half duplex, fixed data rate configuration. These techniques can be applied to possible future work that included data rate adaption and full duplex operations.

References Cited

Abel, M.W., "Meteor Burst Communications: Bits per Burst Performance Bounds," *IEEE Transactions on Communications*, Volume COM-34, Number 9, September 1986, Pages 927-936.

Abramson, N., "THE ALOHA SYSTEM-Another alternative for computer communications," in *Proceedings of Fall Joint Computer Conference*, 1970, Pages 281-285.

Baggaley, W.J., "Single Wavelength Measurements of the Initial Radii of Radio Meteor Ionization Columns," *Bull. Astron. Inst. Czech.*, Volume 32, Number 6, 1981, Pages 345-349.

Baggaley, W.J. and Webb, T.H., "Measurements of the Ionization Heights of Sporadic Radio-Meteors," *Royal Astronomical Society, Monthly Notices*, Volume 191, Number 3, 1980, Pages 829-839.

Bokhari, S.H., Javed, A. and Grossi, M.D., "Data Storage for Adaptive Meteor Scatter Communication," *IEEE Transactions on Communications Technology*, Volume COM-23, Number 3, 1975, Pages 397-399.

Brown, D.W. and Williams, H.P., "The Performance of Meteor-Burst Communications at Different Frequencies," in *AGARD Conference Proceedings, Aspects of Electromagnetic Wave Scattering in Radio Communications*, Number 224, October 1978, Pages 24.1 - 24.26.

Bylanski, P. and Ingram, D.G.W, *Digital Transmission Systems*, Peter Pereginus, Ltd, Stevenage, England, 1976.

Capetanakis, J.I., "Generalized TDMA: The Multi-Accessing Tree Protocol," *IEEE Transactions on Communications*, Volume COM-27, Number 10, October 1979, Pages 1476-1484.

Carpenter, R.J. and Ochs, G.R., "The NBS Meteor Burst Communication System," *IRE Transactions on Communications Systems*, 1959, Pages 263-271.

Collin, R.E., *Antennas and Radiowave Propagation*, McGraw-Hill Book Company, New York, 1985.

Connor, F.R., *Antennas*, Edward Arnold (Publishers) Ltd, London, 1972.

Day, W.E., "Meteor-Burst Communications Bounce Signals Between Remote Sites," *Electronics*, Volume 55, Number 26, 1982, Pages 71-75.

Eshleman, Von R. and Manning, L.A., "Radio Communication by Scattering from Meteoric Ionization," *Proceedings of the IRE*, Volume 42, 1954, Pages 530-536.

Felber, F., Davis, H., Stahl, R., Wheeler, R. and Wright, D., "Concepts for Near Continuous Reception of VHF (Very High Frequency) Signals Using Meteor Burst Propagation," Report No. JAYCOR-J200-85-875/2393, JAYCOR, San Diego, CA., 1985.

Green, P.E., "An Introduction to Network Architectures and Protocols," *IEEE Transactions on Communications*, Volume COM-28, Number 4, April 1980, Pages 413-424.

Greenhow, J.S. and Hall, J.E., "The Variation of Meteor Heights with Velocity and Magnitude," *Royal Astronomical Society, Monthly Notices*, Volume 121, Number 2, 1960, Pages 174-182.

Greenhow, J.S. and Nufeld, E.L., "Turbulence at Altitudes of 80-100 km and its Effects on Long Duration Meteor Echoes", *Journal of Atmospheric and Terrestrial Physics*, Volume 16, 1959, Pages 384-392.

Hawkins, G.S., "A Radio Echo Survey of Sporadic Meteor Radiants," *Royal Astronomical Society Monthly Notices*, Volume 116, Number 1, 1956, Pages 92-104.

Hawkins, G.S. and Brown, J.C., "A Comprehensive Study of the Characteristics of Meteor Echoes - I," Smithsonian Astrophysical Observatory, Cambridge Mass., Special Report, Volume 254, 1967.

Hines, C.O., "Diurnal Variations in the Number of Shower Meteors Detected by the Forward Scattering of Radio waves. Part III. Ellipsoidal Theory," *Canadian Journal of Physics*, Volume 36, 1958, Pages 117-126.

James, J.C., "The Influence of Meteor Radiant Distributions on Radio Echo Rates," Ph.D. Thesis, Georgia Institute of Technology, Atlanta, Georgia, 1958.

James, J.C. and Meeks, M.L., "On the Relative Contributions of Various Sky Regions to Meteor-Trail Communications," Georgia Institute of Technology, Atlanta, Georgia, Engineering Experiment Station, Technical Report No. 1, Naval Research Contract No. NOnr-991(02), 1956.

Keary, T.J. and Wirth, H.J., "Statistical Characteristics of Forward Scattered Radio Echoes from Meteor Trails," in "Electro-Magnetic Wave Propagation," Academic Press, New York, 1960, Pages 277-289.

Kleinrock, L. and Tobagi, F.A., "Packet Switching in Radio Channels: Part I - Carrier Sense Multiple-Access Modes and Their Throughput-Delay Characteristics," *IEEE Transactions on Communications*, Volume COM-23, 1975, Pages 1400-1416.

Larsen, J.D, "The Feasibility of End-path Illumination in Meteor Scatter Networks," Ph.D Thesis, University of Natal, Durban, to be published.

Lathi, B.P., *Signals, Systems and Communication*, John Wiley and Sons, New York, 1965.

Lawson, J.L., *Yagi Antenna Design*, American Radio Relay League, Newington, CT, 1986.

Lin, S. and Costello, D.J., *Error Control Coding: Fundamentals and Applications*, Prentice-Hall Inc, Englewood Cliffs, New Jersey, 1983.

Manning, L.A. and Eshleman, Von R., "Meteors in the Ionosphere," *Proceeding of the IRE*, Volume 47, 1959, Pages 186-199.

Manning, L.A., Villard, O.G. and Peterson, A.M., "The Length of Ionized Meteor Trails," *Trans. Am. Geophys. Union*, Volume 43, 1953, Pages 16-21.

Mawrey, R.S., "A Meteor Monitoring System," M.Sc Thesis, University of Natal, Durban, 1988.

McKinley, D.W.R., *Meteor Science and Engineering*, McGraw-Hill, Toronto, Canada, 1961.

Meeks, M.L. and James, J.C., "Meteor Radiant Distributions and the Radio-echo Rates Observed by Forward Scatter," *Journal of Atmospheric and Terrestrial Physics*, Volume 16, 1959, Pages 228-235.

Meeks, M.L. and James, J.C., "On the Influence of Meteor-Radiant Distributions in Meteor-Scatter Communication," *Proceedings of the IRE*, Volume 45, 1957, Pages 1724-1733.

Meyer, J.A., Digital Meteorburst Communications, paper presented during Horizon House's sixth International Telecommunication and Computer Exposition, Los Angeles, California, 10-13 November 1980, Pages 453-458.

Miller, I., Freund, J.E., *Probability and Statistics for Engineers*, Prentice-Hall, Inc., Englewood Cliffs, New Jersey, 1985.

Milstein, L.B., Schilling, D.L., Pickholtz, R.L., Sellman, J., Davidovici, S., Pavelchek, A., Schneider, A. and Eichmann, G., "Analysis of Two Protocols for Meteor-Burst Communications," in *IEEE Conference Proceedings*, 1986, Pages 19.6.1-19.6.5.

Papoulis, A., *Probability, Random Variables, and Stochastic Processes*, McGraw-Hill Book Company, New York, 1984.

Ples, V., *Introduction to the Theory of Error-Correcting Codes*, John Wiley and Sons, New York, 1982.

Roberts, L.G., "The Evolution of Packet Switching," *Proceedings of the IEEE*, Volume 66, Number 11, November 1978, Pages 1307-1313.

Rudie, N.J., "The Relative Distribution of Observable Meteor Trails in Forward-Scatter Meteor Communications," Ph.D. Thesis, Montana State University, August 1967.

Scheaffer, R. and Mendenhall, W., *Introduction to Probability: Theory and Applications*, Duxbury Press, North Scituate, Massachusetts, 1975.

Schwartz, M., *Information Transmission, Modulation and Noise*, McGraw-Hill Book Company, New York, 1980.

Sites, F.J., "Communications via Meteor Trails", in *Conference. Rec. 23rd Symp. Aspects of EM Wave Scattering Radio Communications*, 3-7 October, 1977, Number 244, 1978, Pages 25.1-25.21.

Stone, R.R., "Basic Analysis and Design for Optimizing Transmission via Meteor Trails," M.Sc Thesis, Montana State University, December 1976.

Sugar, G.R., "Radio Propagation by Reflection from Meteor Trails," *Proceedings of the IEEE*, Volume 52, 1964, Pages 116-136.

Tanenbaum, A.S., *Computer Networks*, Prentice-Hall, Englewood Cliffs, New Jersey, 1981.

Tobagi, F.A. and Kleinrock, L., "Packet Switching in Radio Channels: Part II - The Hidden Terminal Problem and the Busy-Tone Solution," *IEEE Transactions on Communications*, Volume COM-23, 1975, Pages 1417-1433.

Townsley, D, "Error Detection and Retransmission Schemes in Computer Computer Networks," in *Proceedings, COMPCON 78 Fall*, 1978.

Webb, T.H., Geomagnetic Effects on Meteor Train Diffusion, *Planet. and Space Science*, Volume 29, Number 4, 1981, Pages 415-424.

Weiss, A.A., "The Temporal Variation of the Heights of Reflection Points of Meteor Trails," *Australian Journal of Physics*, Volume 12, 1958, Pages 116-126.

Weitzen, J.A., "Feasibility of High Speed Digital Communications on the Meteor Scatter Channel," Ph.D. Thesis, University of Wisconsin-Madison, 1983.

Weitzen, J.A., "Predicting the Arrival of Meteors Useful for Meteor Burst Communication," *Radio Science (USA)*, Volume 21, Number 6, November-December 1986, Pages 1009-1020.

Weitzen, J.A., "A Data Base Approach to Analysis of Meteor Burst Data," *Radio Science (USA)*, Volume 22, Number 1, January-February, 1987, pages 133-140.

Weitzen, J.A. and Tolman, S., "A technique for automatic classification of meteor trails and other propagation mechanisms for the Air Force high latitude meteor burst test bed," Technical Report RADC-TR-86-117, Rome Air Development Center, Rome, N.Y., July 1986.

Weitzen, J.A., Birkemeier, W.P. and Grossi, M.D., "An Estimate of the Capacity of the Meteor Burst Channel," *IEEE Transactions on Communications*, Volume COM-32, Number 8, 1984, Pages 972-974.

Zimmermann, H., "OSI Reference Model - The ISO Model of Architecture for Open Systems Interconnection," *IEEE Transactions on Communications*, Volume COM-28, Number 4, April 1980, Pages 425-432.

Glossary Of Symbols

d	Is half the straight line distance from T to R (meters). $d = R_E \sin\frac{s}{2R_E}$
D	Is the diffusion coefficient (meters^2/second). The assumed height diffusion relation given by Greenhow [Greenhow and Nufeld 1959] as $\log_{10} D(h) = 6.7 \times 10^{-5} h - 5.6$
f	Is the frequency of operation.
G_R	Is the gain of the receive antenna.
G_T	Is the gain of the transmit antenna.
h	Is the height of the point of reflection above the surface of the earth (meters).
I	Average throughput (bits/second).
I_F	Average number of information bits throughput per frame.
I_W	Average number of information bits throughput per window.
I_T	Average number of information bits throughput per trail.
L	Is the half the length of the first Fresnel zone of the trail (meters) and is given by Eshleman [Eshleman and Manning 1954] as $L = \sqrt{\frac{\lambda R_T R_R}{(R_T + R_R)(1 - \sin^2\phi \cos^2\beta)}}$
m	Is the slope of the regression line of the decay phase of the measured log amplitude to time data.
N	Number of bits per frame. $N = N_D + N_O$
N_D	Number of data bits per frame.
N_O	Number of bits of overhead per frame.
P_{max}	Is the initial peak received power of the meteor reflection.
P_{min}	Is the minimum usable signal.
$P_R(t)$	Is the power received from a meteor reflection as a function of time

P_T Is the transmitter power (watts).

q Is the electron line density of the trail (electrons/meter).

R Is the location of the receiver in the reference system.
R = (-d,0,0)

r_0 Is the initial radius of the ionized trail and is given by Brown [Brown and Williams 1977] as

$$\log_{10} r_0 = 3.5 \times 10^{-5} h - 3.45$$

R_E Is the radius of the earth (meters).

$$R_E = 6.37 \times 10^6$$

R_R Is the distance from the receiver to point of reflection (meters).

$$R_R = \sqrt{(x-d)^2 + y^2 + z^2}$$

R_T Is the distance from the transmitter to point of reflection (meters).

$$R_T = \sqrt{(x+d)^2 + y^2 + z^2}$$

s Is the great circle path from T to R (meters).

S A polarization factor which is the dot product of a unit incident electric vector and a unit vector of the reflected wave in the direction of the polarization of the receiving antenna. When both antennas are adjusted for maximum receptions, S=1. When both antennas are horizontally polarized, S = cos (η_h) where cos (η_h) was derived by Rudie [Rudie, 1978] as

$$\cos(\eta_h) = \frac{y^2 - (y\tan\alpha)^2 - (z\tan\alpha + d - x)(z\tan\alpha + d + x)}{C'C''}$$

where

$$C' = \sqrt{(y\sec\alpha)^2 + (z\tan\alpha)^2 + (x-d)^2 - 2z(x-d)\tan\alpha}$$

and

$$C'' = \sqrt{(y\sec\alpha)^2 + (z\tan\alpha)^2 + (x+d)^2 - 2z(x+d)\tan\alpha}$$

t Is the time since formation of the trail (seconds).

t_0 Is the trail formation time.

$$t_0 = \frac{2L}{V}$$

T Is the location of the transmitter in the reference system.
T = (-d,0,0)

T_u Is the usable duration of a trail. For an underdense trail,

$$T_u = \frac{\tau}{2} \ln\left(\frac{A}{P_{min}}\right)$$

V Is the velocity of the meteor.

x,y and z Are the coordinates in the cartesian coordinate system with the origin at the midpoint of the straight line between the transmitter and the receiver with the X axis along the line between the transmitter and the receiver and the Z axis being vertical (meters).

A useful conversion from the earth based (x,y,h) system to the reference system (x,y,z) is

$$z = \sqrt{(R_E + h)^2 - x^2 - y^2} - R_E \cdot \cos\left(\frac{s}{2R_E}\right)$$

β Is the angle between the axis of the meteor and the plane defined by the R, T and M.

ε Is the angle between the intersection of the M-plane with the h-surface and the intersection of the M-plane with the plane containing R, T and M and is given by James [James, 1958] as

$$\varepsilon = \cos^{-1}\left[\frac{y}{\sqrt{y^2 + z^2 \sin^2(\phi - \lambda_1)}}\right]$$

where

$$\lambda_1 = \cos^{-1}\left[\frac{\sqrt{z^2 - y^2}}{R_R}\right]$$

γ Is the angle between a vertical line and the M-plane and is given by James [James, 1958] as

$$\gamma = \sin^{-1}\sqrt{\frac{z^2(R_T + R_R)^2}{R_T R_R (R_T + R_R)^2 - 4R_T R_R d^2}}$$

K Is the ground permittivity.

λ Is the wavelength of the transmitted signal (meters).

ϕ Is half the angle between the vector from the transmitter to the trail and the vector from the trail to the receiver.

$$\phi = \frac{1}{2}\cos^{-1}\left[\frac{x^2 + y^2 + z^2 - d^2}{R_T R_R}\right]$$

ψ Is the elevation angle above the horizon for antenna polar pattern and ground reflection calculations.

ψ_m Is the width of the narrow band on the celestrial sphere in which a meteor must occur for a specular reflection to occur and is given by Eshleman [Eshleman and Manning, 1954] as

$$\psi_m = \frac{L(R_T + R_R)}{4R_T R_R \cos\phi}(1 - \cos^2\phi \sin^2\beta)$$

σ Is the ground conductivity. σ ranges from about 1 S/m to 10^{-2} S/m.

σ_e Is the classical radius of an electron (meters).
$\sigma_e = 2.8178 \times 10^{-15}$ meters

τ Is the time constant of an underdense trail.

$$\tau = \frac{32\pi^2 D}{\lambda^2 \sec^2\phi}$$

θ Is the azimuth angle off the main beam direction for antenna polar patterns.

ζ Is the angle between a vertical line and the axis of the meteor trail and is given by James [James, 1957] as $\cos\zeta = \cos\gamma \sin(\beta + \varepsilon)$

Index